Failure Analysis Associates

ENGINEERING AND METALLURGICAL CONSULTANTS
2225 EAST BAYSHORE ROAD, P.O. BOX 51470,
PALO ALTO, CALIFORNIA 94303 (415) 856-9400 TELEX 704216

FaAA-PA-R-86-07-21
PA11081

IMPACT OF SLOW STARTS ON THE FATIGUE LIFE OF EMERGENCY DIESEL GENERATOR DSRV-20 CRANKSHAFTS AT SAN ONOFRE NUCLEAR GENERATING STATION UNIT 1

Prepared by

Failure Analysis Associates
2225 East Bayshore Road
Palo Alto, California 94303

Prepared for

Southern California Edison
2244 Walnut Grove Avenue
Rosemead, California 91770

July 1986

TABLE OF CONTENTS

1.0 INTRODUCTION

In a previous report [1], Failure Analysis Associates (FaAA) evaluated the effect of startup and coastdown conditions on the fatigue life of emergency diesel generator crankshafts at San Onofre Nuclear Generating Station. After extensive testing, analysis, and inspections, FaAA concluded that it was safe to operate the engines provided that inspections were performed at outages as outlined in the report. It was also found that cracks would propagate somewhat more slowly if slow starts, of approximately 22 seconds duration, were used rather than fast starts, of approximately 6 seconds duration.

In this report, the impact of using starts of 10 to 15 seconds duration is explored since slower starts cannot be run without disabling an engine start trip. In Section 2.0, a transient torsional analytical model of the crankshaft, used previously to analyze the fast start and coast down events at SONGS [1], is used to examine the effect of duration of start and initial position of the crankshaft on the response of the crankshaft during slow start events. Single cycle pressure curves were developed to adequately represent the pressure during slow start events with durations between 10 and 15 seconds. These curves were used as input to the analytical model. The model is used to determine the time-dependent nominal torsional stress at each main journal.

In Section 3.0, stress levels and number of cycles during worst case and average slow starts, determined in Section 2.0, are compared with the analytical results of fast start and coast down events [1] to assess the relative importance of the slow start events on the adequacy of the crankshaft.

In a previous report [1], the maximum amplitude of vibration in the crankshaft during an engine startup has been found, based on both analysis and testing, to be dependent upon the initial starting position of the crankshaft and the startup duration. The maximum amplitude of vibration occurs as the engine passes through three closely-spaced critical speeds, the five-an-a-half order at 217 rpm, the fifth order at 240 rpm, and the four-and-a-half order at 264 rpm.

It is expected that the startup duration would have a significant effect on the amplitude of vibration, and two competing influences can easily be identified. First, in a fast start there is more cylinder pressure available to excite the crankshaft at the critical speeds compared with a slower start. Second however, the fast start engine spends less time in the speed range of these three criticals giving less time for the amplitude to build and producing fewer high stress cycles.

The influence of the initial starting position of the crankshaft is not so easily identified. Nevertheless, in a six-second fast start the engine spends only a little over one half of a second in the speed range 216 rpm to 264 rpm. This provides only enough time for each cylinder to fire about once in this speed range. Thus, it seems likely that the order in which they fire during this critical time would be important. If starts are repeatable, the order of firing as the engine passes through these criticals is dependent on the initial starting position of the crankshaft.

As the startup duration becomes longer, more and more cylinder firings occur in the speed range of the three criticals. It is therefore expected that the order of these firings, and hence the initial crankshaft position, will become less important for longer startups.

2.0 TORSIONAL ANALYSES OF CRANKSHAFT FOR SLOW START EVENTS

The transient torsional model of the crankshaft used previously to analyze the fast start and coast down events at SONGS [1] is used to examine the effect of duration of start and initial position of the crankshaft on the response of the crankshaft during slow start events. Analyses were performed for slow start events with duration between 10 and 15 seconds at 1-second intervals over this range. Analyses at 6.2 and 22.0† seconds were also performed for comparison with fast and slow starts, for which pressure data was available from earlier testing [1].

2.1 Dynamic Model for Transient Analysis

The dynamic model and pressure loading input used to perform the torsional vibration analyses on the various slow start events are developed in the following sections.

2.1.1 Description of Dynamic Model

STAMS (Shaft Transient Analysis by Modal Superposition), a computer program developed by FaAA, is used to perform transient torsional vibration analyses of the crankshaft. STAMS calculates the torsional natural modes of vibration of an axial system of springs and masses by solving the undamped eigenvalue problem. The response of the system to transient loads is calculated using modal superposition with step-by-step response calculations. The gas pressure, reciprocating inertia and frictional loads, assumed to act on the piston, are converted to torsional loads using geometric relationships between the crank angle and piston location.

The solution obtained using STAMS sums the response of specified harmonic orders for each mode of vibration taking into account the correct

---

† The time required to reach 450 rpm for the slow start event "H" in Reference 1 is approximately 22 seconds, and 430 rpm is reached in approximately 21 seconds. A discussion of the methods used to reduce this test data is provided in Reference 2.

phase angles for all cylinders. This summation is performed for each inertia and stiffness in the model. Time histories and maximum and minimum values of angular vibration and shaft torques are provided in the output for each inertia and shaft section, respectively. Nominal torsional stresses, τ, are calculated from torques, T, by the equation $\tau = Tr/J$ where r is the journal radius and J is its polar moment of inertia. STAMS includes internal modal damping in the analysis.

A 13 degree of freedom idealized lumped inertia and torsional spring model, shown in Figure 2-1, was used for the slow start analyses. The inertias and stiffnesses in Table 2.1 were computed by TDI [3] and have been verified by FaAA using torsiograph testing [1]. Reciprocating inertial loads are calculated using a reciprocating mass of 820 pounds in both left and right bank cylinders. The inertial torques are calculated at each time step and depend on the current angular velocity, ω, and current crank throw orientation, θ, for each cylinder.

The pressure loads for each slow start event were calculated using theoretical pressure curves. A pressure versus crank angle curve for a given cylinder is assumed to be repeated every two crankshaft revolutions. The procedure used to determine the pressure loading for each slow start is discussed in the following section.

2.1.2 Determination of Engine Pressure loading

In order to estimate stress levels in the engine during slow start events with duration between 10 and 15 seconds, it is necessary to develop pressure loading data for each slow start event to be analyzed. Single cycle theoretical pressure curves were developed since test data was not available. Pressure pulses with a uniform amount of energy per cycle were used throughout the duration of a given slow start. Measured pressure data for a typical fast start with a duration of approximately 6.2 seconds, Fast Start Event "D" in Reference 1, and for a slow start with a duration of approximately 22 seconds, Slow Start Event "H" in Reference 1, were used as a basis for developing these single cycle theoretical pressure curves. The method used to obtain these theoretical pressure curves is described in the following paragraphs.

Theoretical Pressure Data. Theoretical pressure curves are calculated at 1-second intervals for startup durations over the 10- to 15-second range, and for 6.2 and 22 seconds utilizing IND, a computer program developed by FaAA. IND calculates the work done in a single compression-expansion cycle by integrating the pressure vs. volume curve as represented by the hatched area in Figure 2-2. The integral is calculated using the following user-specified engine parameters:

Brake horse power per cylinder
Stroke length
Piston diameter
Engine speed
Efficiency factor
Compression ratio
Connecting rod length
Expansion coefficient
Compression coefficient
Maximum cylinder pressure
Intake pressure

The unknown pressure at the end of the expansion cycle is determined by equating the total work to the product of the mean effective pressure and the total displaced volume. Having determined the pressure at the end of the expansion cycle the pressure-volume relationship is known and this is converted to a pressure vs. crank angle curve using the crank angle, connecting rod and piston geometry. The input parameters used to develop the pressure curves for the various startup durations are described in the following paragraphs.

Efficiency and Power Per Cylinder. The amount of work required for the engine to reach rated speed (450 rpm) from the cold condition (0 rpm) can be calculated from simple physics as the change in kinetic energy, ΔKE, using the following equation:

$$\text{Work Required} = \Delta KE_{0\text{-}450rpm} = \frac{1}{2} J (\dot{\theta})^2$$

where J is the polar inertia of the entire system including all cylinders, the flywheel and the generator. The final engine speed is denoted by $\dot{\theta}$. Pressure versus time data obtained during the torsiograph test for the 6.2-second fast start and the 22-second slow start (shown in Figures 2-3 and 2-4), was used to determine the number of pressure cycles between 0 and 450 rpm. The theoretical average energy per pressure cycle for the 6.2-second fast start and the 22-second slow start were determined by dividing the work required by the number of pressure pulses. The theoretical average energy per cycle for the fast start and slow start are summarized in Table 2.2.

Utilizing the pressure test data for the 6.2- and 22-second duration startups, the actual energy per pressure cycle was determined. Comparing the actual and theoretical values of energy per pressure cycle will allow a quantitative assessment of the relative amount of friction per pressure cycle and ultimately of engine efficiency.

The pressure test data from the 6.2- and 22-second startups were used to calculate the torque vs. crank angle time histories for these events. The energy during these starts was calculated utilizing the following equation:

$$\text{Measured energy utilized} = \int T d\theta$$

Knowing the number of pressure cycles from the pressure data, the actual amount of energy per pressure cycle was determined and is summarized in Table 2.2.

The amount of friction per pressure cycle was determined as the difference between the theoretical energy per cycle and the measured energy per cycle. The "efficiency" of the 6.2-second fast start and the 22-second slow start was determined utilizing the following equation:

$$\text{Efficiency} = \left(1 - \frac{\text{friction}}{\Delta KE}\right) \times 100\%$$

These results are summarized in Table 2.2.

These estimates of efficiency are only expected to be sufficiently accurate for a relative comparison of crankshaft response between slow and fast starts. Efficiency values for startups with durations between 10 and 15 seconds were linearly interpolated between these data points. The results are summarized in Table 2.3.

The power per cylinder was calculated from the energy per cycle for an engine speed of 450 rpm using the following equation:

$$\text{Power} = \text{Torque} \times \omega$$

The results for the 6.2- and 22-second duration startups are 498 HP/cylinder and 125.5 HP/cylinder respectively. The values of power per cylinder for startups of durations between 10 and 15 seconds were linearly interpolated between these data points. These results are summarized in Table 2.3.

Peak Pressure. The measured pressure data was used to determine an average peak pressure for the 6.2-second fast start and the 22-second slow start. The average of the peak pressures between 0 and 450 rpm was determined to be 1167 psi for the 6.2-second fast start and 612 psi for the 22-second slow start. Interpolated values for startups with durations between 10 and 15 seconds are summarized in Table 2.3.

Engine Parameters. The following engine parameters were utilized to determine the theoretical pressure curves for engine startups of all durations:

Connecting rod length	46.125 inches
Stroke length	21.0 inches
Piston diameter	17.0 inches
Engine speed	450 rpm
Compression ratio	11.57
Expansion coefficient	1.33
Compression coefficient	1.33
Manifold pressure	15.8 psia

Intake manifold pressures during startup were not available from previous test data. Since the duration of the startup is small, a lower value of intake pressure was assumed. The theoretical pressure curve for a 12-second slow start event is shown as an example in Figure 2-5.

2.2 Analyses of 10- to 15-Second Starts

The analyses of the various slow start events were performed utilizing the theoretical pressure curves for each startup duration. Since no data was available on the engine speed versus time for the different length starts, the pressure curves were timed so that that a linear increase in engine speed from 0 to 450 rpm was obtained. This assumption is based on the results of the torsiograph data which indicate a linear increase in speed throughout a major portion of the duration of the fast start [1]. A damping value of 0.6 percent of critical modal damping in each mode of vibration was used [1]. For each startup duration (6.2, 10, 11, 12, 13, 14, 15, and 22 seconds), the analysis was repeated for 10 initial crankshaft positions, equally spaced throughout 2 revolutions of the crankshaft.

The maximum amplitude of nominal shear stress for each startup duration and for each initial startup position is presented in Table 2.4. These stresses occur in main journal number 11, between cylinder number 10 and the flywheel. The stresses in main journals 8 through 10 are almost equally high. The results indicate that the slow start events with durations between 10 and 15 seconds have stress levels somewhat lower than those attained during a 6.2-second fast start. The maximum amplitudes of free-end vibration for each of the analyses are presented in Table 2.5.

Figure 2-6 summarizes the effect of initial crankshaft position and duration of startup on the response of the crankshafts. The ratio of highest maximum stress amplitude to lowest maximum stress amplitude for each startup duration is presented in Figure 2-7. This figure indicates that the maximum variation in stress as the initial crankshaft starting position is varied occurs for the 6.2-second duration startup where the ratio equals 2.3. Over the range of 10 to 15 seconds the ratio varies between 1.3 and 1.8. These results show that the effect of initial crankshaft position on maximum stress

amplitude is reduced from that of a 6.2-second start for starts of 10 to 15 seconds duration. However, starts of 10 to 15 seconds duration have a larger number of high stress cycles than those of a 6.2-second start.

Figure 2-8 shows the range of values for maximum stress amplitude that can occur for the various start conditions analyses. A coastdown result is also shown for comparison. The worst case results are for the starting position that produces the highest maximum stress amplitudes, whereas, the best case results are for the starting position that produces the lowest maximum stress amplitude.

Table 2.1

Stiffness and Inertias for Torsional Dynamic Analysis of DSRV-20-4 13-inch by 13-inch Crankshaft at San Onofre

Inertia Location	Inertia (lb. ft. sec^2)	Stiffness (ft. lb./rad)
Front Gear	11.8	
		53.2×10^6
Cylinder No. 1	143.1	
		101.9×10^6
Cylinder No. 2	141.6	
		101.9×10^6
Cylinder No. 3	141.6	
		101.9×10^6
Cylinder No. 4	141.6	
		101.9×10^6
Cylinder No. 5	141.6	
		101.9×10^6
Cylinder No. 6	141.6	
		101.9×10^6
Cylinder No. 7	141.6	
		101.9×10^6
Cylinder No. 8	141.6	
		101.9×10^6
Cylinder No. 9	141.6	
		101.9×10^6
Cylinder No. 10	144.5	
		72.7×10^6
Flywheel	1,503.9	
		485.6×10^6
Generator	11,114.3	

Table 2.2

Energy per Cycle for Slow and Fast Starts

Event	Energy/Cycle (ft-lbs/cycle)			Efficiency %
	ΔKE (Theoretical)	∫Tdθ (Actual)	Friction	
Slow start (22-second)	18403	21351	2984	84.0
Fast start (6.2-second)	72966	78327	5361	92.7

Table 2.3

IND Input Parameters for Slow Starts

Startup Duration (sec)	Power/Cylinder (HP)	Efficiency %	Average Peak Pressure (psi)
6.2	498	92.7	1167
10	408	90.6	1034
11	384	90.0	999
12	361	89.5	964
13	337	88.9	929
14	314	88.4	899
15	290	87.8	859
22	125.5	84.0	612

Table 2.4

Maximum Amplitude of Nominal Shear Stress for Different Startup Times
(psi)

Initial Start Angle (degrees)	Duration of Startup (sec)							
	6.2	10	11	12	13	14	15	22
9	20474	18415	17400	14465	21072	12824	20571	12275
81	23993	17984	21545	15022	21457	13344	20057	11676
153	24410	19389	21809	16148	19139	14048	19055	11476
225	21600	20363	20098	17011	16607	15383	16287	12008
297	17873	18833	18082	16704	19055	19458	13205	13245
369	13521	16009	16454	20613	13519	21795	11767	14257
441	10764	18916	16287	22838	13661	13752	12161	14326
513	10882	21628	17956	21281	14729	19389	14368	14952
585	12245	21378	18680	18582	15536	16635	17525	15049
657	15286	19235	17776	15800	17358	13829	20126	13992
Highest Maximum Amplitude / Lowest Maximum Amplitude	2.27	1.35	1.34	1.58	1.59	1.70	1.75	1.31

Table 2.5

Maximum Amplitude of Free-End Vibration for Different Startup Times
(degrees)

Initial Start Angle (degrees)	Duration of Startup (sec)							
	6.2	10	11	12	13	14	15	22
9	2.7	2.5	2.4	2.0	2.9	1.8	2.8	1.7
81	3.3	2.4	2.9	2.1	2.9	1.9	2.8	1.6
153	3.3	2.6	3.0	2.2	2.7	2.0	2.7	1.6
225	3.0	2.8	2.7	2.4	2.3	2.1	2.3	1.7
297	2.5	2.6	2.4	2.3	2.0	2.7	1.9	1.9
369	1.9	2.2	2.2	2.8	1.9	3.0	1.7	2.0
441	1.5	2.6	2.2	3.1	1.9	2.9	1.7	2.0
513	1.4	2.9	2.5	2.9	2.0	2.7	1.9	2.0
585	1.6	2.9	2.6	2.5	2.2	2.3	2.4	2.1
657	2.0	2.7	2.5	2.2	2.3	2.0	2.7	1.9

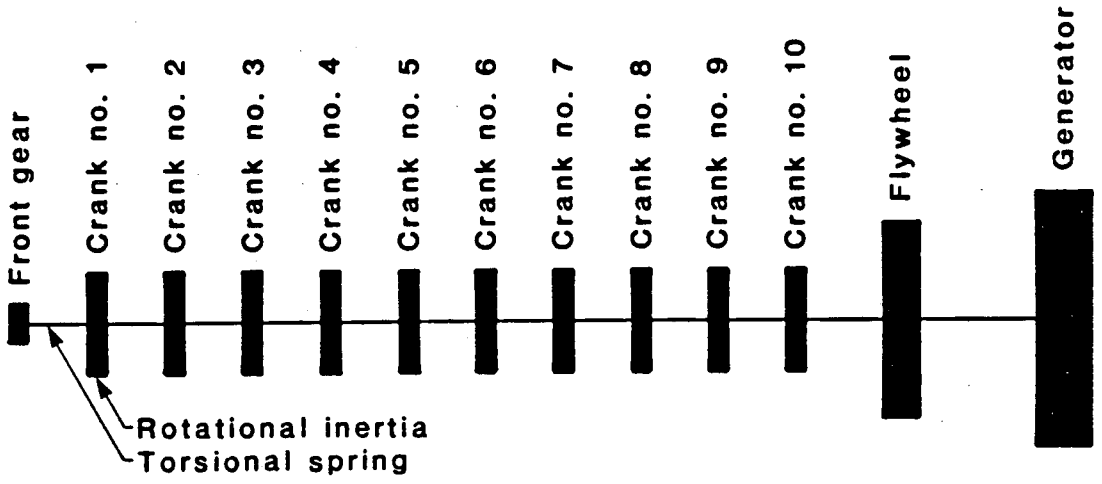

Figure 2-1. Dynamic model of DSRV-20-4 13-inch by 13-inch crankshaft at San Onofre

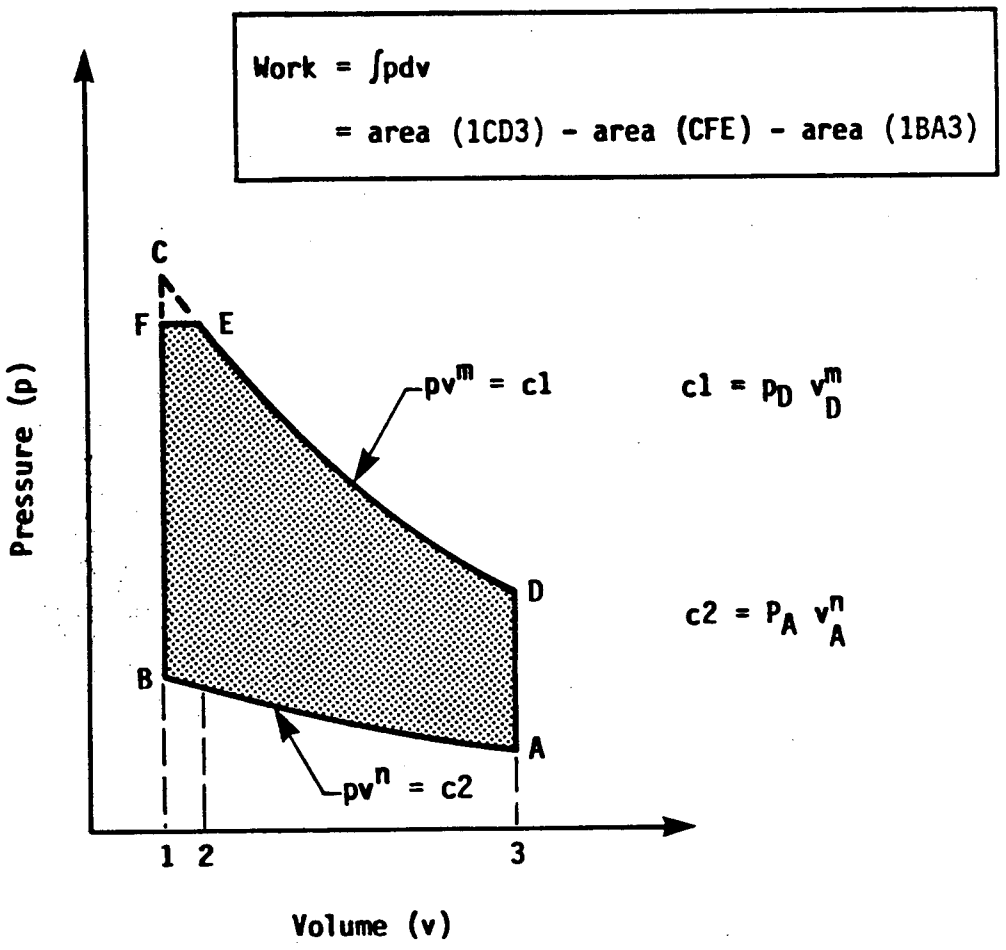

Figure 2-2. Schematic indicating work done in a single compression-expansion cycle

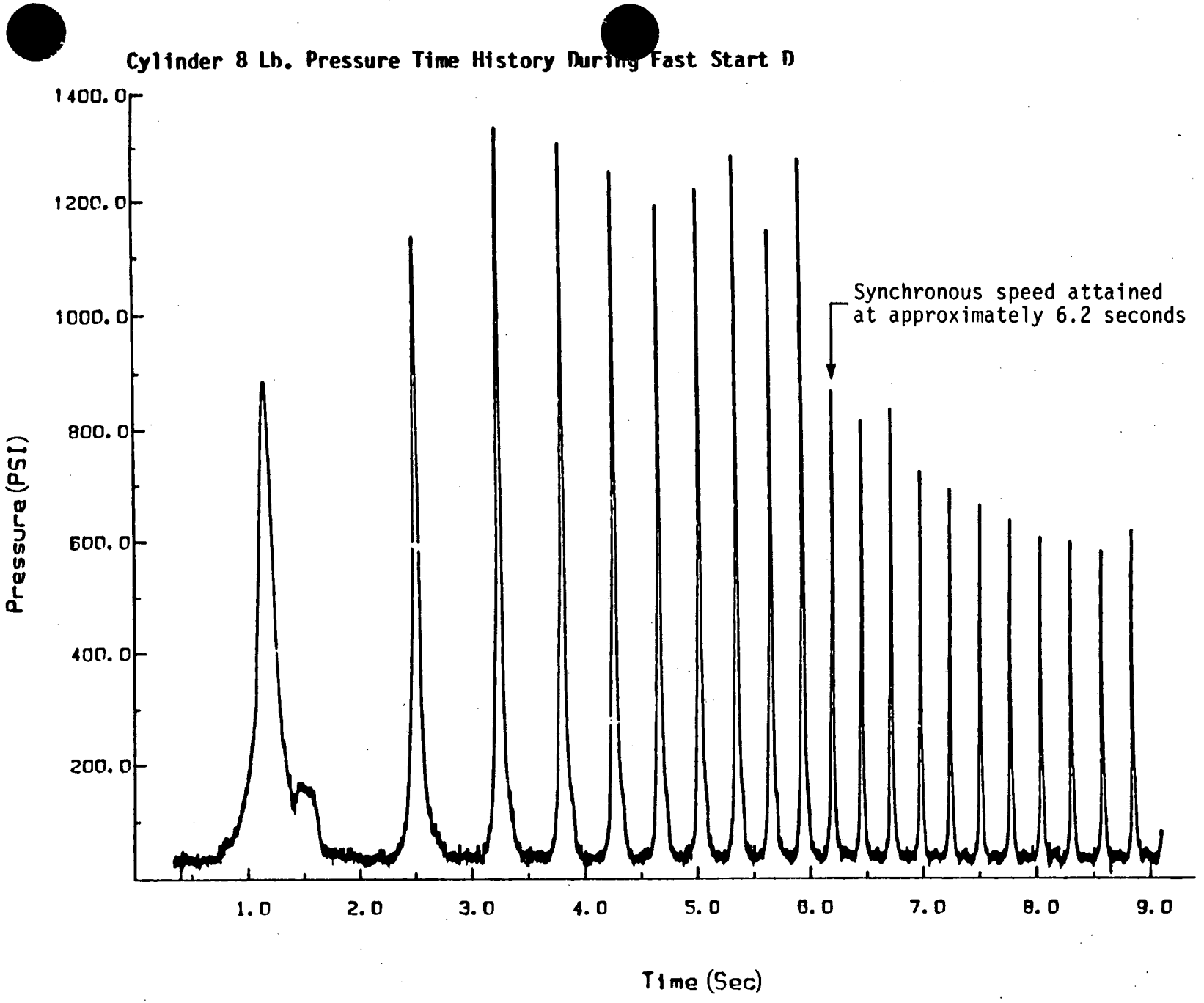

Figure 2-3. Pressure loading during fast start D

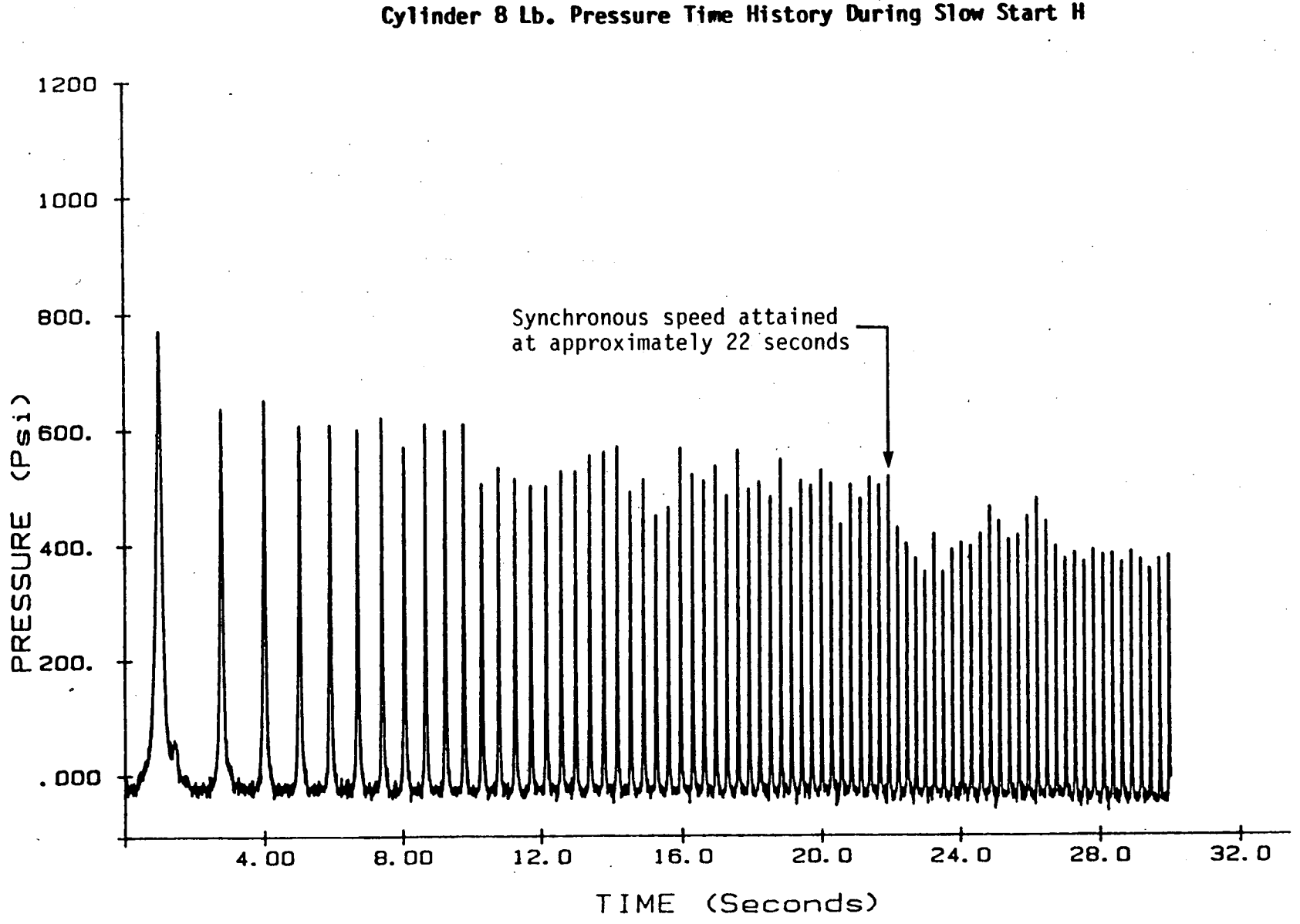

Figure 2-4. Pressure loading during slow start H

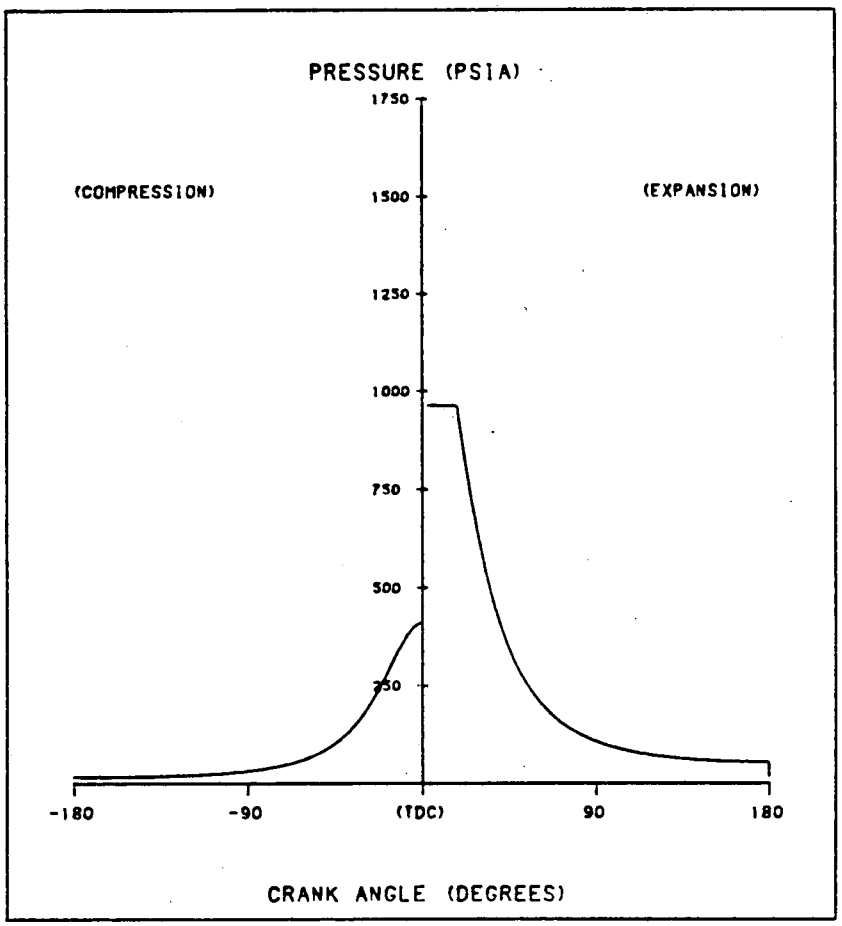

BHP	7220.0
# CYLINDERS	20
BORE (IN)	17.0
STROKE (IN)	21.0
CL-CL LEN. (IN)	46.125
COMP. RATIO	11.57
POLY. EXP.	1.33
EFFICIENCY	0.89
PEAK PRESS. (PSIA)	964.0
INT/EXH PRESS. (PSIA)	15.8
IMEP (PSIA)	148.9

Figure 2-5. Theoretical pressure curve for a 12-second slow start event

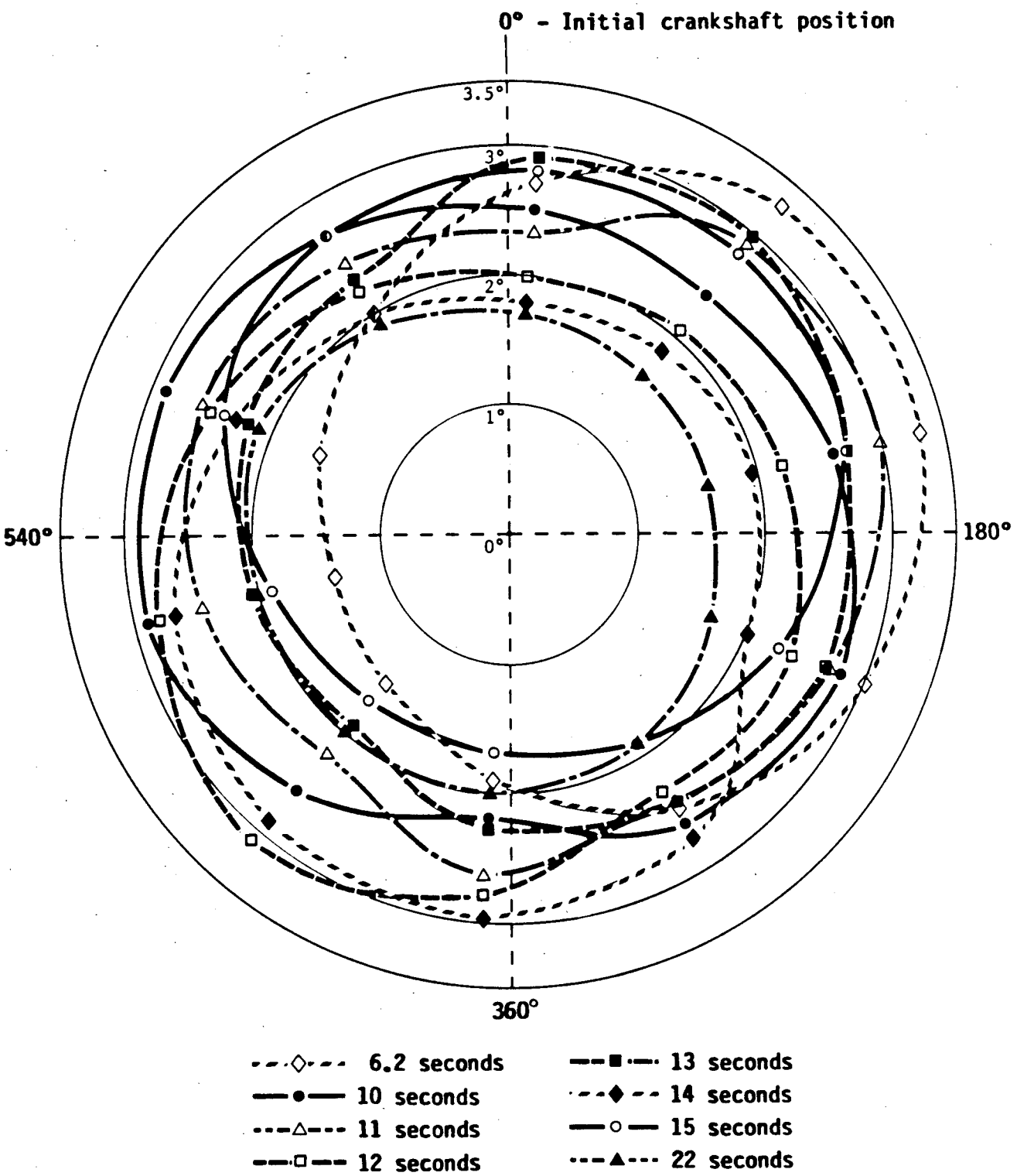

Figure 2-6. Effect of initial crankshaft position and duration of startup on free-end vibration

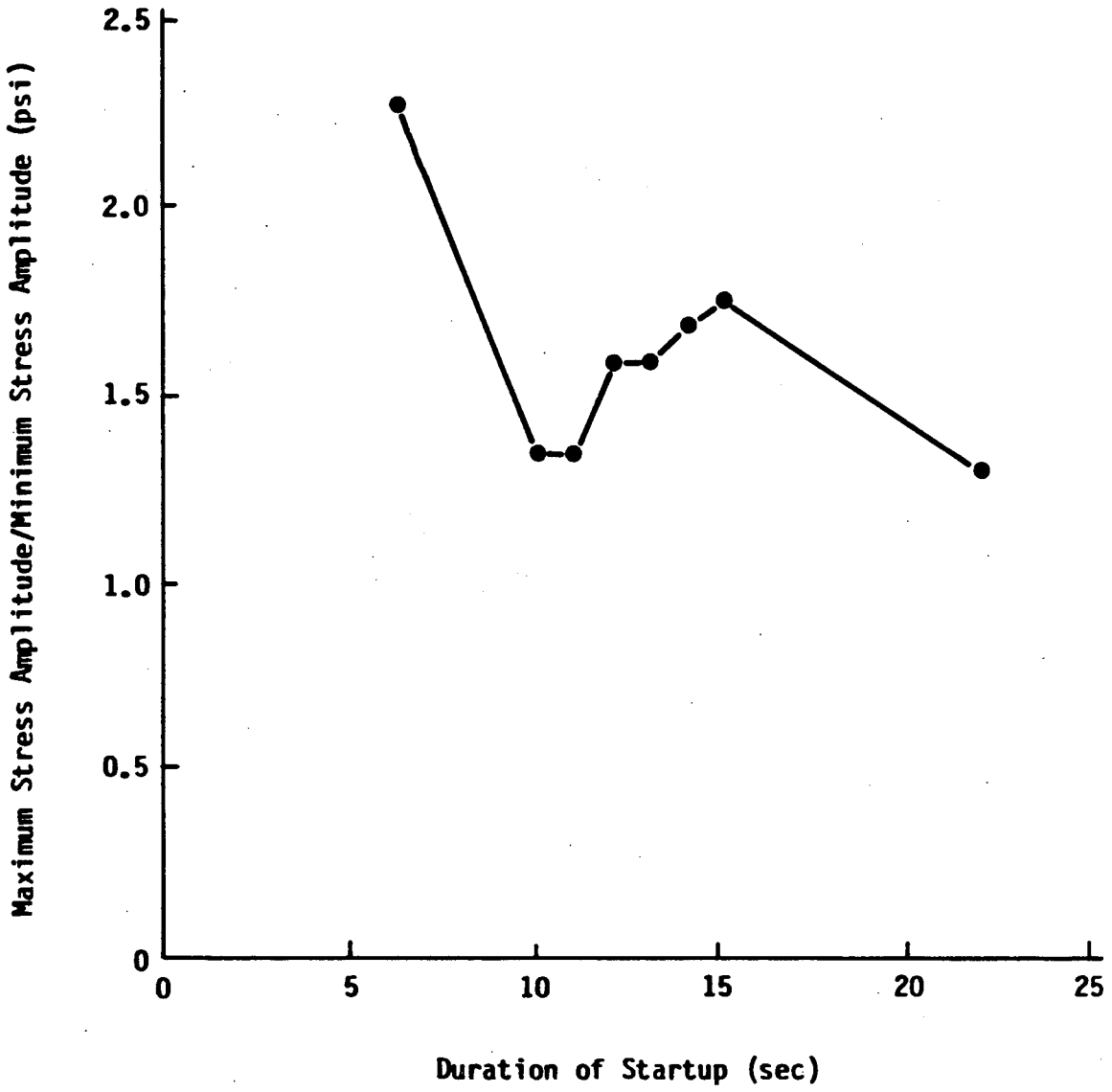

Figure 2-7. Effect of duration of startup on ratio of maximum stress to minimum stress

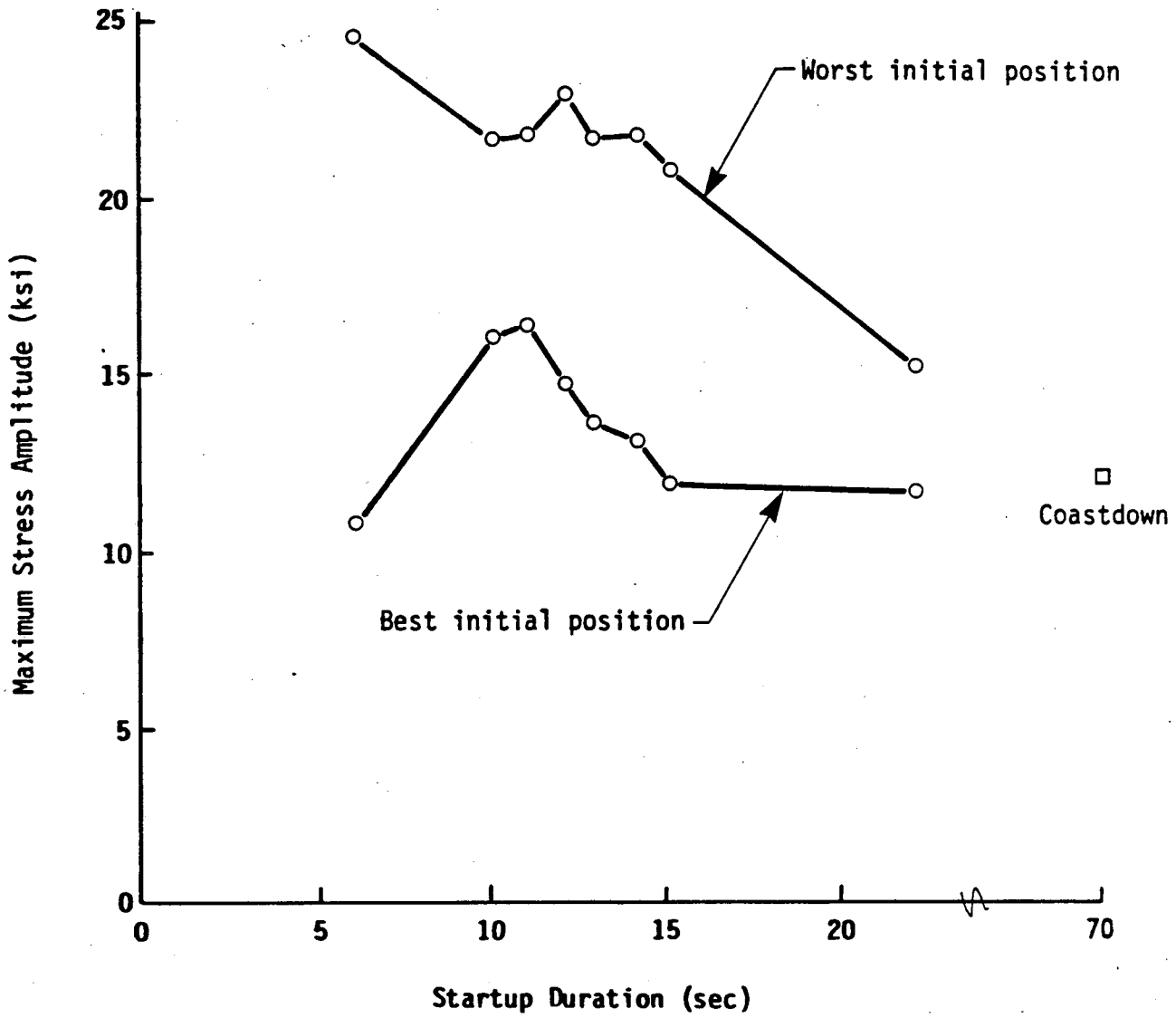

Figure 2-8. Maximum stress amplitude for best and worst initial crankshaft positions

3.0 RELATIVE FATIGUE CRACK GROWTH RATES FOR SLOW START EVENTS

In this section the nominal torsional stresses calculated in Section 2 will be used to estimate crack growth rates. The BIGIF fracture mechanics code [4] is used to calculate crack propagation rates. The crack propagation rates are determined as a function of the number of start-stops rather than calendar time.

3.1 Crack Initiation

Previous analyses of fast start and coastdown conditions at SONGS [1] indicated that crack initiation could be expected to occur due to both fast starts and coastdowns. Some stress levels during the 10- to 15-second starts, while somewhat lower than those for the fast start are still higher than the endurance limit, indicating that crack initiation could be expected to occur. The number of start-stops to initiate a crack would be greater for 10- to 15-second starts compared with fast starts. Further work to quantify the amount of improvement for the 10- to 15-second startups has not been undertaken, because, for a conservative design, an initial crack is assumed, and thus, crack propagation life governs the design. The size of the initial assumed crack is the size that can be reliably detected during inspections and has been taken to be 20 mils in length by 10 mils in depth [5].

3.2 Crack Growth Model

The geometric model used in the prediction of crack growth rates is the one degree of freedom (1 DOF) edge crack used in previous analyses performed during fast start and coastdown conditions at SONGS [1]. This model is shown in Figure 3-1. The oil hole surface is modeled and a crack of size a has freedom to grow under a univariate stress field. The stress field chosen consists of k_t of 4 on the oil hole surface, which decays to unity with increasing distance from the oil hole surface. A 5-mil deep crack was introduced at the oil hole surface. This is the more conservative of the two models used in the previous crack growth studies [1]. The material and stress field data used for the present analyses are the same as those used in the previous analyses of the coastdown and fast start events [1].

3.3 Crack Growth Results

Crack propagation analyses were performed for all startup durations analyzed. Two types of loading histories were considered for the analyses of the slow start events; the worst case, the initial crankshaft position which produced the most vibration, and the average case, the average of all 10 initial crankshaft positions analyzed in Section 2. The load history contains the data from the startup event and coastdown.

The number of start-stops required to propagate a 10-mil deep crack to a depth of 18 mils is used to estimate life. Oil hole inspections are designed to detect 10-mil deep cracks. An 18-mil deep crack will propagate under steady-state loads [1]. Thus, the window between 10 and 18 mils represents the safe operating range based on the conservative 1 DOF crack growth model.

Table 3.1 shows the relative number of start-stops required to grow a crack from 10 to 18 mils for each of the start durations considered. When all initial positions are averaged, there is some improvement in the crack growth rates between the 10- to 15-second starts and the fast starts although this improvement is not significant. Twenty-two-second slow starts produce crack growth rates significantly slower than the 10- to 15-second and fast startups.

Table 3.1

Relative Comparison of Number of Start-Stop Events Required to Grow a Crack from 10 Mils to 18 Mils

Start Duration (seconds)	Number of Start-Stop Events / Number of 6.2 Second Fast Start-Stop Events	
	Worst Case	Average Case
6.2	1.00	1.00
10	1.35	0.97
11	1.31	1.03
12	1.12	1.00
13	1.17	1.10
14	1.18	1.07
15	1.43	1.11
22	2.42	1.69

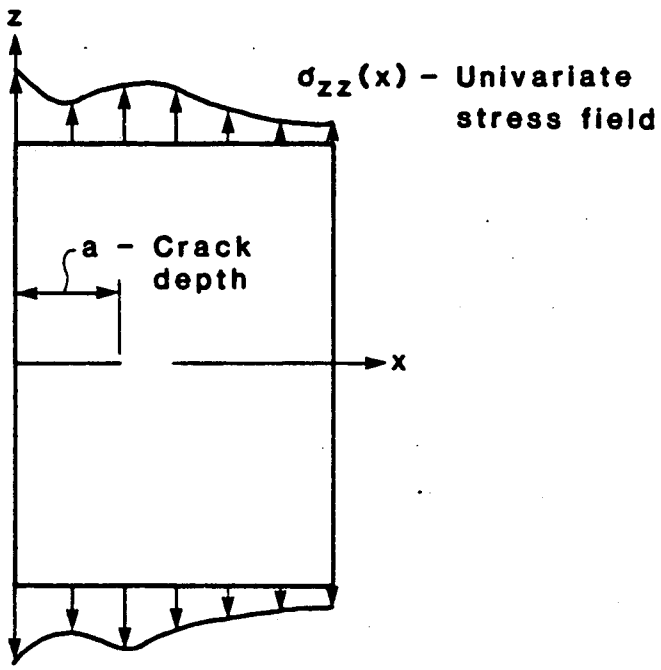

Figure 3-1. Single degree of freedom crack model

4.0 CONCLUSIONS

The following conclusions are made:

1. Initial crankshaft position has a significant effect on crankshaft response for 10- to 15-second duration starts. However, this effect is smaller than that for fast starts.

2. The maximum stress amplitude for 10- to 15-second starts is somewhat less than that due to fast starts. However, the longer starts have more high stress cycles.

3. Twenty-two-second slow starts produce maximum stress levels that are lower than those due to fast starts and the 10- to 15-second starts.

4. Crack initiation could be expected to occur for all startup and coastdown events. The number of start-stops to initiate a crack is expected to be greater for a 10- to 15-second start than for a fast start. However, for reasons explained in Section 3, crack propagation life governs the design.

5. Although there is some improvement in crack growth rates between the 10- to 15-second starts and the fast starts, the improvement is not significant.

6. Crack growth will be slower for the 22-second start than for either the fast start or the 10- to 15-second starts.

References

1. "Evaluation of Transient Conditions on Emergency Diesel Generator Crankshafts at San Onofre Nuclear Generating Station Unit 1," by Failure Analysis Associates, Report No. 84-12-14, Revision 1.0, April 1985.

2. FaAA-PA-R-86-04-16, Letter Report to Dave Rickett of Southern California Edison, Re: Duration of Slow Start Event "H", April 1986.

3. Yang, Roland, "Torsional and Lateral Critical Speed Analysis, Engine Numbers 75041/41 Delaval Enterprise Engine Model DSRV-20-4, 6000 KW/8303 BHP at 450 RPM," for Southern California Edison Company, Delaval Engine and Compressor Division, Oakland, California, October 22, 1975.

4. "BIGIF - Fracture Mechanics Code for Structures," Manuals 1-3, Failure Analysis Associates (April 1981).

5. "Eddy-Current Examination DG1A Crankshaft San Onofre Nuclear Electric Generating Station August 1984," by Failure Analysis Associates, Report No. 84-10-2, October 1984.

FaAA-84-6-54

PA07396-PRJ-R3310A

EVALUATION OF EMERGENCY DIESEL GENERATOR CRANKSHAFTS AT MIDLAND AND SAN ONOFRE NUCLEAR GENERATING STATIONS

Prepared by

Failure Analysis Associates
Palo Alto, California

June 1984

STATEMENT OF APPLICABILITY

This report addresses the structural integrity of crankshafts in Transamerica Delaval Inc. (TDI) DSRV-12-4 AND DSRV-20-4 engines installed at the Midland and San Onofre nuclear generating stations. These findings together with the results of the previous report on DSR-48 and DSRV-16-4 diesel generators at the Shoreham and Grand Gulf nuclear power stations complete the generic investigation of TDI diesel generator crankshafts.

Plant specific confirmation of individual diesel generator response consistent with the generic conclusions and inspection recommendations presented thus far will be addressed in individual plant Phase II Design Review/Quality Revalidation Reports.

EXECUTIVE SUMMARY

REVIEW OF CONSUMER POWER COMPANY'S DSRV-12-4 13-INCH BY 13-INCH CRANKSHAFT AT MIDLAND

DSRV-12-4 13-INCH CRANKSHAFTS AT MIDLAND NUCLEAR POWER STATION

The structural integrity of the 13-inch by 13-inch diameter crankshafts installed in the emergency diesel generators at the Midland Nuclear Power Station has been evaluated by testing and analysis. Conventional analytical techniques typically utilized by the diesel engine industry show that the crankshafts comply with DEMA requirements. Angular displacements of the free end of the crankshaft were measured at and above full-rated load at TDI. The torsiograph measurements of twist taken during factory tests showed that the crankshafts meet the DEMA requirements. The measured shaft response was greater than that predicted by the modal superposition analysis.

A torsiograph test should be conducted to determine the total response.

The oil holes in main journal number 5 are more critical in torsion than are the crankpin fillets and should be inspected.

REVIEW OF SOUTHERN CALIFORNIA EDISON COMPANY'S DSRV-20-4 13-INCH BY 13-INCH CRANKSHAFT AT SAN ONOFRE

DSRV-20-4 13-INCH BY 13-INCH CRANKSHAFTS AT SAN ONOFRE NUCLEAR POWER STATION

The structural integrity of the 13-inch by 13-inch diameter crankshafts installed in the emergency diesel generators at the San Onofre Nuclear Power Station has been evaluated by analysis. Conventional analytical techniques typically utilized by the diesel engine industry show that the crankshafts comply with DEMA requirements.

A modal superposition analysis was conducted and shows that the crankshaft meets the combined response requirement of DEMA.

TABLE OF CONTENTS

TABLE OF CONTENTS

PART 1:

REVIEW OF DSRV-12-4
13-INCH BY 13-INCH CRANKSHAFTS
AT MIDLAND

1.0 INTRODUCTION TO REVIEW OF DSRV-12-4 13-INCH BY 13-INCH CRANKSHAFT AT MIDLAND

This report presents Failure Analysis Associates' findings on the adequacy of the crankshafts in the emergency diesel engines at Midland Nuclear Station. The crankshaft is required to meet the recommendations of the Diesel Engine Manufacturers Association (DEMA). In Section 2.0, the design calculations and torsiograph test results of Transamerica Delaval Inc. (TDI) [1-1, 1-2] are reviewed for compliance with the DEMA stress allowables. In Section 3.0, a torsional dynamic analysis is used to compute nominal torsional stresses at each crank throw.

1.1 Industry Experience

The following information has not been verified by FaAA and consequently is not subject to FaAA's usual quality assurance procedures. Based upon information supplied by TDI [1-3, 1-4] three DSRV-16-4 13-inch by 13-inch crankshafts have failed since 1976. These crankshafts are similar in geometry to the DSRV-12-4 13-inch by 13-inch crankshafts. These failures were all attributed to torsional fatigue cracks initiating in the oil holes of Main Journal Nos. 6 or 8 (i.e., between Cylinder Nos. 5 and 6 and between Cylinder Nos. 7 and 8).

TDI subsequently modified the location of the oil hole and increased the radius at the intersection of the hole and the main journal. While increasing the radius should make the journal less subject to machining irregularities, it does not reduce the concentrated stress. Furthermore, the torsional stress is independent of angular location around the journal. Thus this area is still considered to be critical.

The failures are as follows: [1-4]

Date	Serial No.	Site	Location of Failure
Feb. 1976	73048	Mora, Minnesota	Main Journal No. 8
June 1976	73038	Anamax	Main Journal No. 8
March 1979	73034	Anamax	Main Journal No. 6

It was found that these engines had a 4th order critical speed at 446 rpm, which is close to the operating speed of 450 rpm. The engines were then fitted with four small counter-weights which moved this critical speed down to about 430 rpm. The nearest critical speed of DSRV-12-4 is 425 rpm. The failures indicate that the oil hole on the main journal has a lower margin of safety than the crankpin fillet for torsional fatigue cracking.

Section 1 References

1-1 "Torsional Critical Speed Calculations, Engine Numbers 77001/04 Delaval-Enterprise Engine model DSRV-12-4, 5250 KW, 7313 BHP @ 450 RPM, 225 BMEP," Transamerica Delaval Inc., Engine and Compressor Division, Oakland, California, undated.

1-2 Pellum, Lee, "Torsiograph of Consumers Power Company, Engine No. 77001, Generator Set DSRV-12-4, 7313 BHP 5250 KW @ 450 RPM, 225 BMEP in Oakland Plant," Transamerica Delaval Inc., Engine and Compressor Division, Oakland, California, July 19, 1978.

1-3 Transamerica Delaval Memo on cracked Anamax crankshaft, from Harold V. Schilling to E. G. Deane, Dec. 11, 1979.

1-4 Telephone conversation with Roland Yang, Transamerica Delaval, April 1984.

2.0 COMPLIANCE OF CRANKSHAFT WITH DIESEL ENGINE MANUFACTURERS ASSOCIATION RECOMMENDATIONS

The purchase specifications for the diesel generator sets require that the recommendations of the Diesel Engine Manufacturers Association, DEMA [2-1], be followed. These recommendations state:

> In the case of constant speed units, such as generator sets, the objective is to insure that no harmful torsional vibratory stresses occur within five percent above and below rated speed.
>
> For crankshafts, connecting shafts, flange or coupling components, etc., made of conventional materials, torsional vibratory conditions shall generally be considered safe when they induce a superimposed stress of less than 5000 psi, created by a single order of vibration, or a superimposed stress of less than 7000 psi, created by the summation of the major orders of vibration which might come into phase periodically.

Transamerica Delaval Inc. (TDI) performed a torsional critical speed analysis of the crankshafts [2-2]. In Section 2.1, this analysis is reviewed for compliance with the above allowable stresses. Also, TDI conducted a torsiograph test on a 13-inch by 13-inch crankshaft for one of the Midland engines in TDI's Oakland plant [2-3]. In Section 2.2, the test results are compared with the above allowable stresses.

2.1 Review of TDI Torsional Critical Speed Analysis

Diesel generator torques due to dynamic response are usually calculated in two steps. First, the torsional mode shapes and natural frequencies of vibration are calculated. Second, the dynamic forced vibration response due to gas pressure and reciprocating inertia loading is calculated. TDI calculated the response at 100% of the rated load, 5250 kW.

2.1.1 Natural Frequencies

The first step in a torsional critical speed analysis is to determine the natural frequencies of the crankshaft. The engine speed at which a given order resonates may then be calculated. The diesel generator is modeled as a

system of lumped mass moments of inertia interconnected by torsional springs, as shown in Figure 2-1. The inertia and stiffness values are shown in Table 2.1.

It has long been standard practice in the diesel engine industry to solve this eigenvalue problem by the Holzer method [2-4]. This method has been used for at least 40 years [2-5], and thus is well established.

TDI used the Holzer method to calculate the system's first three natural frequencies, which are shown in Table 2.2. The first natural frequency was found to be 35.7 Hz.

2.1.2 Nominal Stresses

The second step in a torsional critical speed analysis is to determine the dynamic torsional response of the crankshaft due to gas pressure and reciprocating inertia loading. The 1st order is a harmonic which repeats once per revolution of the crankshaft. For a four-stroke engine, harmonics of order 0.5, 1.0, 1.5, 2.0, 2.5... exist. TDI performs this calculation for each order of vibration up to 12.0 separately. For each order, the applied torque at a cylinder due to gas pressure and reciprocating inertia is calculated. The values of this torque for each order are usually normalized by dividing by the piston area and throw radius. The normalized value for the nth order is referred to as T_n. The values of T_n for signifcant orders used by TDI are shown in Table 2.3. These values may be compared to those recommended by Lloyd's Register of Shipping, LRS [2-6]. TDI's values are higher than LRS's values for the most significant orders, and are thus more conservative than Lloyd's. The response is then calculated by one procedure if the harmonic is at resonance and by another if the harmonic is away from resonance.

At resonance, the torsional vibration amplitudes would increase indefinitely in the absence of damping. The solution is obtained by balancing the energy input with the energy loss due to damping. TDI used an empirical form of hysteresis damping due to friction. The purpose of this calculation is to ensure that the diesel generator can be brought up to operating speed without

undergoing excessive stresses as critical speeds are passed. Since the engine runs at 450 rpm and the nearest critical speed is 428 rpm, which corresponds to the 5th order, the resonant response is not important.

Away from resonance, the torsional vibrations reach a steady-state level even without the aid of any damping. The magnitude of this response for each structural mode and loading order is calculated as the product of a dynamic amplification factor and an equivalent static equilibrium amplitude. The equivalent static equilibrium amplitude is computed using a modal load and modal stiffness [2-7] for the nth order harmonic and given mode shape. The nominal shear stress, τ, in the 13-inch pin of Crankpin No. 6 for each order is then calculated from the dynamic torque, T, using $\tau = Tr/J$, where r is the pin radius and J is the polar moment of inertia.

TDI calculated the response for the first three modes and plotted the results for only the first mode since higher modes produce much smaller stresses. The nominal shear stresses for the significant orders are shown in Table 2.4. It is seen that the largest single order stress of 1210 psi for the $3\ ^1/_2$ order is well below the 5000 psi DEMA allowable.

TDI does not calculate the associated phase angle with the response of each order, so that it is not possible to calculate the combined response. The computation of the combined response is reported in Section 3.0.

2.2 Review of Transamerica Delaval Inc. Torsiograph Test

Torsiograph tests are commonly used to confirm torsional vibration calculations. The test is usually performed in two stages. The first stage is performed without load at variable speed and is used to determine the location of critical speeds. The second stage is performed at rated speed of 450 rpm with variable load, and is used to confirm the forced vibration calculations.

2.2.1 Natural Frequencies

The variable speed torsiograph test found the first natural frequency to be 35.7 Hz by locating the $5\frac{1}{2}$ order and 6th order resonance. This value is the same as TDI's computed value of 35.7 Hz.

2.2.2 Nominal Stresses

The torsiograph provides the angular displacement response of the free end of the crankshaft. This displacement is usually decomposed into components corresponding to each order. The peak-to-peak response is also obtained.

The nominal shear stress, τ, in Crankpin No. 6 may be established from the amplitude of free-end vibration by assuming the shaft is vibrating in the first mode. The nominal shear stress is then found to be 10927 psi per degree of free-end vibration from the TDI analysis [2-2].

TDI tabulated the single order and total response for both 5250 kW (100% of rated load) and for 110% load. These values have been factored to obtain nominal shear stresses and are shown in Table 2.5. The results at 5250 kW show that the largest single order has a stress of 1814 psi which is well below the DEMA allowable of 5000 psi.

The measured response (Table 2.5) was larger than that calculated by TDI and shown in Table 2.4. TDI determined the stress to be 1945 psi at 110% load, also well below the DEMA allowable. In determining the combined total response, TDI utilized the Bell & Howell C.E.C. instrumentation. Subsequent examination of the data analysis characteristics of this instrumentation revealed that the B & H unit measured twice the square root of the sum of the squares, SRSS, of the amplitudes of individual orders rather than the true peak-to-peak. The peak-to-peak range divided by two is larger than the SRSS. The true peak-to-peak range should be measured by conducting a torsiograph test.

Section 2 References

2-1 Standard Practices for Low and Medium Speed Stationary Diesel and Gas Engines. Diesel Engine Manufacturers Association, 6th ed., 1972.

2-2 "Torsional Critical Speed Calculations, Engine Numbers 77001/04 Delaval-Enterprise Engine Model DSRV-12-4, 5250 kW, 7313 BHP @ 450 RPM, 225 BMEP," Transamerica Delaval Inc., Engine and Compressor Division, Oakland, California, undated.

2-3 Pellum, Lee, "Torsiograph of Consumers Power Company, Engine No. 77001, Generator Set DSRV-12-4, 7313 BHP 5250 kW @ 450 RPM, 225 BMEP in Oakland Plant," Transamerica Delaval Inc., Engine and Compressor Division, Oakland, California, July 19, 1978.

2-4 Thomson, William T., Theory of Vibration with Applications. Second edition, Prentice-Hall, 1981.

2-5 Den Hartog, J., Mechanical Vibrations. Third edition, McGraw-Hill, 1947.

2-6 Lloyd's Register of Shipping, Guidance Notes on Torsional Vibration Characteristics of Main and Auxillary Oil Engines.

2-7 Craig, Roy R., Jr., Structural Dynamics: An Introduction to Computer Methods. Wiley, 1981.

TABLE 2.1

STIFFNESS AND INERTIAS FOR TORSIONAL DYNAMIC ANALYSIS
OF DSRV-12-4 13-INCH BY 13-INCH CRANKSHAFT AT MIDLAND

Inertia Location	Inertia (lb. ft. sec^2)	Stiffness (ft. lb./rad)
Front Gear	14.7	53.2×10^6
Cylinder No. 1	104.0	101.9×10^6
Cylinder No. 2	102.6	101.9×10^6
Cylinder No. 3	102.6	101.9×10^6
Cylinder No. 4	102.6	101.9×10^6
Cylinder No. 5	102.6	101.9×10^6
Cylinder No. 6	105.5	72.7×10^6
Flywheel	1489.7	475.4×10^6
Generator	6691.7	

TABLE 2.2

TORSIONAL NATURAL FREQUENCIES FROM TDI ANALYSIS OF DSRV-12-4
13-INCH BY 13-INCH CRANKSHAFT AT MIDLAND

Mode	Natural Frequency (Hz)
1	35.7
2	94.5
3	112.1

TABLE 2.3

TORSIONAL LOADINGS FOR TDI ANALYSIS OF DSRV-12-4
13-INCH BY 13-INCH CRANKSHAFT AT MIDLAND

Order	Torsional Loading, T_n (psi)
1.5	129.2
2.5	71.6
3.0	16.5
3.5	42.7
4.5	23.7
5.5	7.1
6.0	5.7

TABLE 2.4

SINGLE-ORDER NOMINAL SHEAR STRESSES FROM TDI ANALYSIS
OF DSRV-12-4 13-INCH BY 13-INCH CRANKSHAFT AT MIDLAND

Order	Amplitude of Nominal Shear Stress (psi)
1.5	123
2.5	1096
3.0	536
3.5	1210
4.5	341
5.5	223
6.0	384
DEMA Allowable for Single Order	5000

TABLE 2.5

NOMINAL SHEAR STRESSES CALCULATED FROM TDI TORSIOGRAPH TEST OF DSRV-12-4 13-INCH BY 13-INCH CRANKSHAFT AT MIDLAND

Order	Amplitude of Free-End Vibration (degrees)		Amplitude of Nominal Shear Stress (psi)*	
	100% load	110% load	100% load	110% load
1.5	0.020	0.024	219	262
2.5	0.166	0.178	1814	1945
3.0	0.095	0.110	1038	1202
3.5	0.166	0.174	1814	1901
4.5	0.035	0.035	382	382
5.5	0.055	0.055	601	601
6.0	0.095	0.099	1038	1082
DEMA Allowable for a Single Order			5000	5000
SRSS**	0.205	0.225	2240	2459
DEMA Allowable $^1/_2$ peak to peak			7000	7000

* Amplitude of nominal shear stress is calculated to be 10,927 psi per degree of free-end rotational amplitude.

** Measurement corresponds to the square root of the sum of the squares, SRSS, of individual orders rather than the peak-to-peak divided by two.

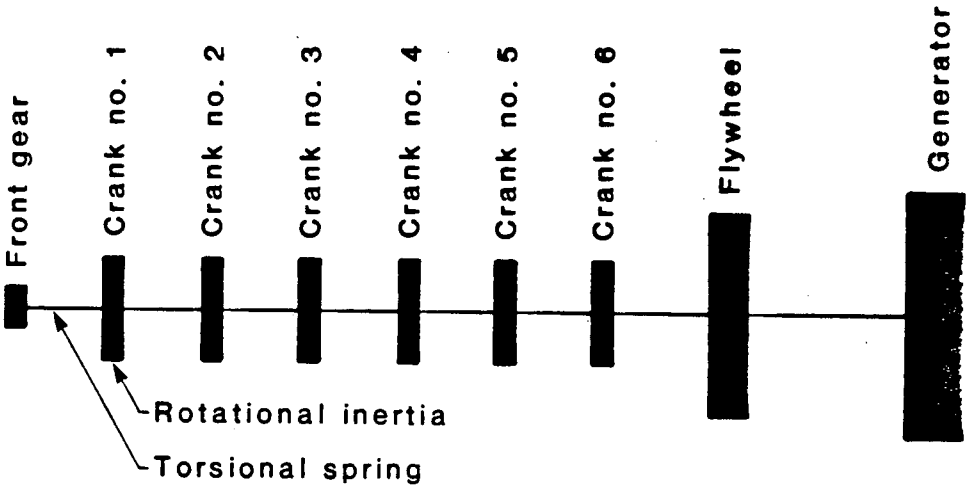

Figure 2-1. TDI dynamic model of DSRV-12-4 13-inch by 13-inch crankshaft at Midland.

3.0 CRANKSHAFT DYNAMIC TORSIONAL ANALYSIS

In Section 2.0 it was found that the crankshafts satisfy the DEMA single order nominal stress recommendation of 5000 psi for both 5250 kW (100% of rated load) and 110% load. However, the stresses for combined orders were neither calculated nor measured by TDI, and thus could not be compared to the DEMA recommended limit of 7000 psi. A dynamic torsional analysis of the crankshaft is performed to determine the true range of torque at each crank throw. The FaAA dynamic model allows all orders and modes to be summed using appropriate phase angles. In this section this model is compared with TDI torsiograph test data for the amplitudes of free-end vibration.

3.1 Torsional Model

FaAA developed a dynamic torsional model of the crankshaft to supplement TDI's conventional forced vibration calculations. The original TDI procedure did not compute the phase relationship between the various orders or modes, so it was not possible to compute the true summation. The actual maximum stress is a direct result of this summation. Furthermore, the original TDI method always predicted maximum stress in Crankpin No. 6, which is generally true for the first mode but not true for the combined response. The dynamic model developed used the same idealized lumped inertia and torsional spring model as the TDI analysis (Figure 2-1 and Table 2.1).

The first three torsional natural frequencies for the replacement crankshaft are shown in Table 3.1. The natural frequencies are in agreement with those computed and measured by TDI.

When the diesel generator is running at a given speed and power level, the forced vibration problem is steady-state where both load and response repeat themselves every two revolutions of the crankshaft. To model the dynamic response, a modal superposition analysis [3-1] was used with harmonic load input. The calculation of the harmonic loads will be discussed in the next section.

3.2 Harmonic Loading

To calculate the harmonic loading on a crankshaft it is necessary to consider gas pressure, reciprocating inertia, and frictional loads. The gas pressure loading may be obtained from pressure versus crank angle data. This pressure was measured in a Stone & Webster Engineering Corporation (SWEC) test on a similar TDI series R-4 cylinder at Shoreham Nuclear Power Station [3-2]. The pressure was measured in Cylinder No. 7 by inserting a probe through the air start valve. A top dead center, TDC, mark for Cylinder No. 7 was simultaneously recorded by a probe on the flywheel. The pressure data at 100% load was analyzed by FaAA to obtain the pressure curve shown in Figure 3-1. The pressure variation with crank angle is assumed to be the same on the articulated side as on the master side.

The reciprocating mass of the connecting rod and piston was found to be 820 lbs for each connecting rod. This mass causes reciprocating inertia torque on the crankshaft. The effect of this torque was combined with the gas pressure torque.

The total torque was then resolved into its sine and cosine harmonics corresponding to each order. These torque harmonics were used in the steady-state analysis. The magnitude of the torque harmonics are normalized by dividing by the piston area and throw radius. The resulting normalized torques for the most significant orders are shown in Table 3.2.

3.3 Comparison of Calculated Response With Test Data

The response due to the first 24 orders and all 9 modes is calculated using modal superposition with 2.5% of critical damping for each mode. The actual value of damping used has little effect on the response since the orders are not at resonance at 450 rpm.

The calculated amplitude of free-end displacement is compared to the amplitude measured by TDI, in Table 3.3. It is seen that the analysis underpredicts the response. This may be due to engine imbalance and should be

checked when the crankshaft is torsiographed. The vector summation from the FaAA analysis is half the peak-to-peak displacement. The largest response occurs for the $3^1/2$ order.

The stresses in Table 3.4 show that the stress level is highest between cylinders 4 and 5. The highest nominal shear stress amplitude is found to be 4886 psi. This value is lower than the 7000 psi DEMA allowable for combined orders, even though the calculated value was computed using all modes. The computed torque as a function of crank angle for each crank throw is shown in Figure 3-2. The nominal shear stress amplitudes for 110% load may be calculated by extrapolation and are found to be below the DEMA recommended allowables.

3.4 Nominal Stresses for Underspeed and Overspeed Conditions

DEMA requires crankshaft stresses to remain within the allowables over a speed range of 450 RPM ± 5%. Modal superposition calculations were performed at 427.5 RPM and 472.5 RPM. The torsional loading at this speed is not known, but was assumed to be the same as that at 450 RPM.

At 95% speed the free-end response is shown in Table 3.5. The nominal shear stresses are shown in Table 3.6, and are below the 7000 psi DEMA allowable for combined orders, even though the calculated value was computed using all modes.

At 105% speed the free-end response is shown in Table 3.7. The nominal shear stresses are shown in Table 3.8, and are below the 7000 psi DEMA allowable for combined orders, even though the calculated value was computed using all modes.

Section 3 References

3-1 Timoshenko, S., D.H. Young, and W. Weaver, Jr., Vibration Problems in Engineering. Fourth edition, Wiley, 1974.

3-2 Bercel, E., and Hall, J.R., "Field Test of Emergency Diesel Generator 103," Stone & Webster Engineering Corporation, April 1984.

TABLE 3.1

TORSIONAL NATURAL FREQUENCIES FOR DSRV-12-4
13-INCH BY 13-INCH CRANKSHAFT AT MIDLAND
FROM FaAA ANALYSIS

Mode	Natural Frequency (Hz)
1	35.67
2	94.46
3	112.09

TABLE 3.2

TORSIONAL LOADING FOR FaAA ANALYSIS OF DSRV-12-4
13-INCH BY 13-INCH CRANKSHAFT AT MIDLAND AT 100% LOAD

Order	Torsional Loading, T_n (psi)
1.5	112.0
2.5	77.0
3.5	48.0
4.0	33.0
4.5	26.2
5.5	15.5

TABLE 3.3

FREE-END VIBRATION AT 100% LOAD AND 450 RPM FOR DSRV-12-4
13-INCH BY 13-INCH CRANKSHAFT AT MIDLAND

Order	Amplitude of Vibration (degrees)	
	FaAA Analysis	TDI Test
0.5	0.028	0.059
1.0	0.001	0.020
1.5	0.014	0.020
2.0	0.000	-
2.5	0.130	0.166
3.0	0.070	0.095
3.5	0.141	0.166
4.0	0.000	-
4.5	0.033	0.035
5.0	0.018	0.031
5.5	0.040	0.055
6.0	0.069	0.095
6.5	0.004	-
7.0	0.003	-
7.5	0.000	-
8.0	0.002	-
Vector Summation	0.346	-

TABLE 3.4

NOMINAL SHEAR STRESSES AT 100% LOAD AND 450 RPM FOR DSRV-12-4 13-INCH BY 13-INCH CRANKSHAFT AT MIDLAND FROM FaAA ANALYSIS

Location	Amplitude of Nominal Shear Stress (psi)	
	$3^1/_2$ Order	Total
Between Cylinder No. 1 and Cylinder No. 2	729	2825
Between Cylinder No. 2 and Cylinder No. 3	1290	4162
Between Cylinder No. 3 and Cylinder No. 4	1542	3345
Between Cylinder No. 4 and Cylinder No. 5	1519	4886
Between Cylinder No. 5 and Cylinder No. 6	1172	3701
Between Cylinder No. 6 and Flywheel	694	2587

TABLE 3.5

FREE-END VIBRATION AT 100% LOAD AND 95% SPEED
FOR DSRV-12-4 13-INCH BY 13-INCH CRANKSHAFT
AT MIDLAND FROM FaAA ANALYSIS

Order ~~Location~~	Amplitude of Vibration (degrees)
0.5	0.028
1.0	0.001
1.5	0.014
2.0	0.000
2.5	0.126
3.0	0.065
3.5	0.128
4.0	0.000
4.5	0.020
5.0	0.038
5.5	0.067
6.0	0.092
6.5	0.006
7.0	0.003
7.5	0.000
8.0	0.002
Vector Summation	0.359

TABLE 3.6

NOMINAL SHEAR STRESSES AT 100% LOAD AND 95% SPEED
FOR DSRV-12-4 13-INCH BY 13-INCH CRANKSHAFT
AT MIDLAND FROM FaAA ANALYSIS

Location	Amplitude of Nominal Shear Stress (psi)	
	$3^1/_2$ Order	Total
Between Cylinder No. 1 and Cylinder No. 2	692	2797
Between Cylinder No. 2 and Cylinder No. 3	1220	4082
Between Cylinder No. 3 and Cylinder No. 4	1450	3520
Between Cylinder No. 4 and Cylinder No. 5	1403	4799
Between Cylinder No. 5 and Cylinder No. 6	1046	4138
Between Cylinder No. 6 and Flywheel	559	2932

TABLE 3.7

FREE-END VIBRATION AT 100% LOAD AND 105% SPEED FOR
DSRV-12-4 13-INCH BY 13-INCH CRANKSHAFT AT
MIDLAND FROM FaAA ANALYSIS

Order Location	Amplitude of Vibration (degrees)
0.5	0.028
1.0	0.001
1.5	0.014
2.0	0.000
2.5	0.134
3.0	0.077
3.5	0.158
4.0	0.000
4.5	0.070
5.0	0.011
5.5	0.027
6.0	0.055
6.5	0.003
7.0	0.003
7.5	0.000
8.0	0.002
Vector Summation	0.380

TABLE 3.8

NOMINAL SHEAR STRESSES AT 100% LOAD AND 105% SPEED
FOR DSRV-12-4 13-INCH BY 13-INCH CRANKSHAFT
AT MIDLAND FROM FaAA ANALYSIS

Location	Amplitude of Nominal Shear Stress (psi)	
	$3^1/_2$ Order	Total
Between Cylinder No. 1 and Cylinder No. 2	778	2928
Between Cylinder No. 2 and Cylinder No. 3	1383	4191
Between Cylinder No. 3 and Cylinder No. 4	1663	3715
Between Cylinder No. 4 and Cylinder No. 5	1672	5416
Between Cylinder No. 5 and Cylinder No. 6	1339	4164
Between Cylinder No. 6 and Flywheel	875	3191

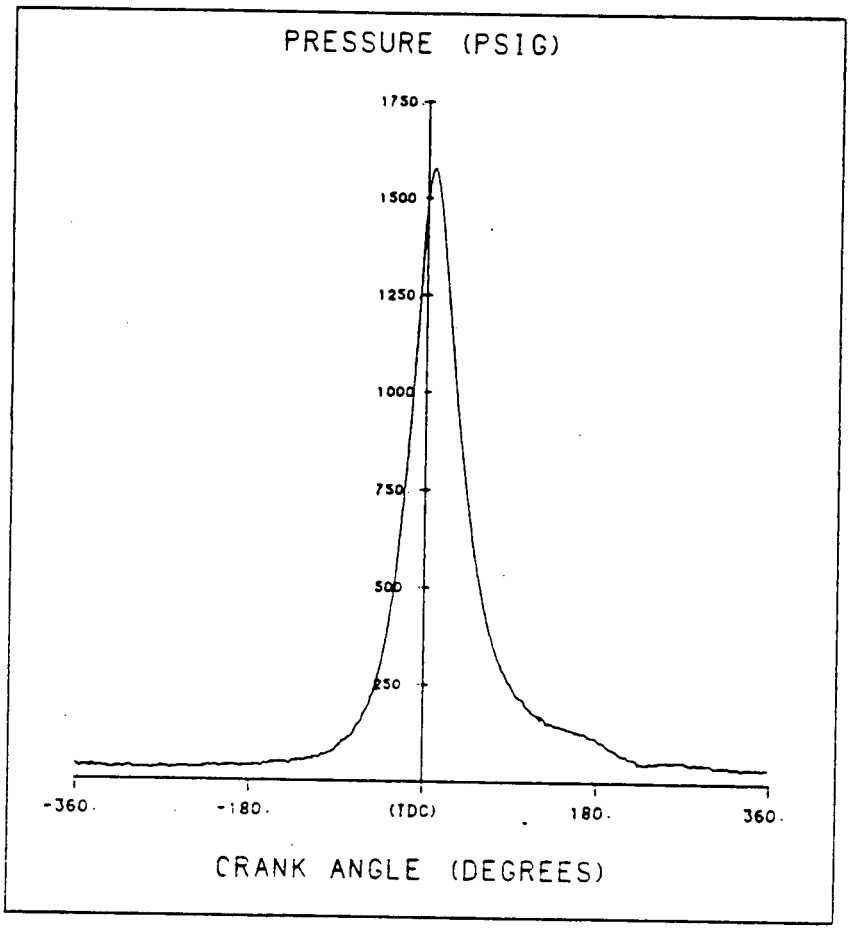

Figure 3-1. Measured pressure in Cylinder no. 7 versus crank angle at 100% load on a DSR-48 engine at Shoreham.

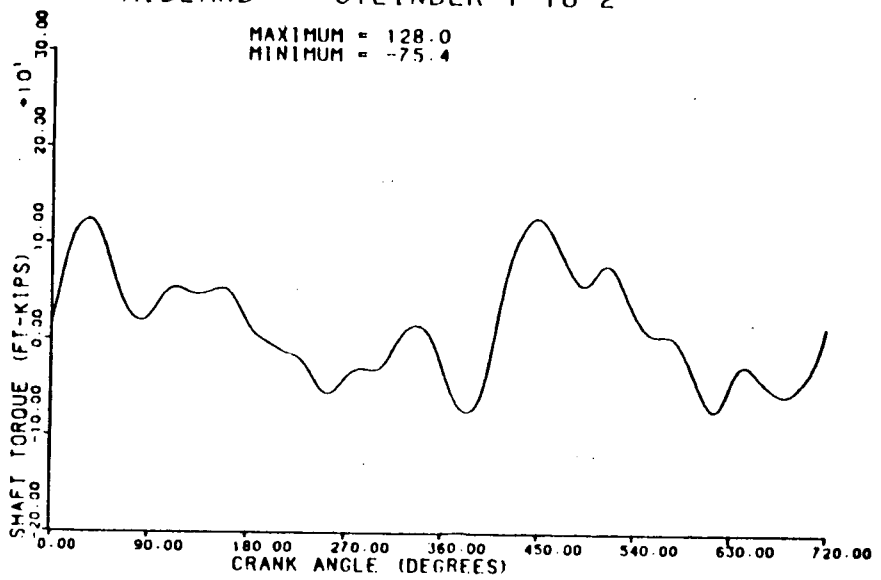

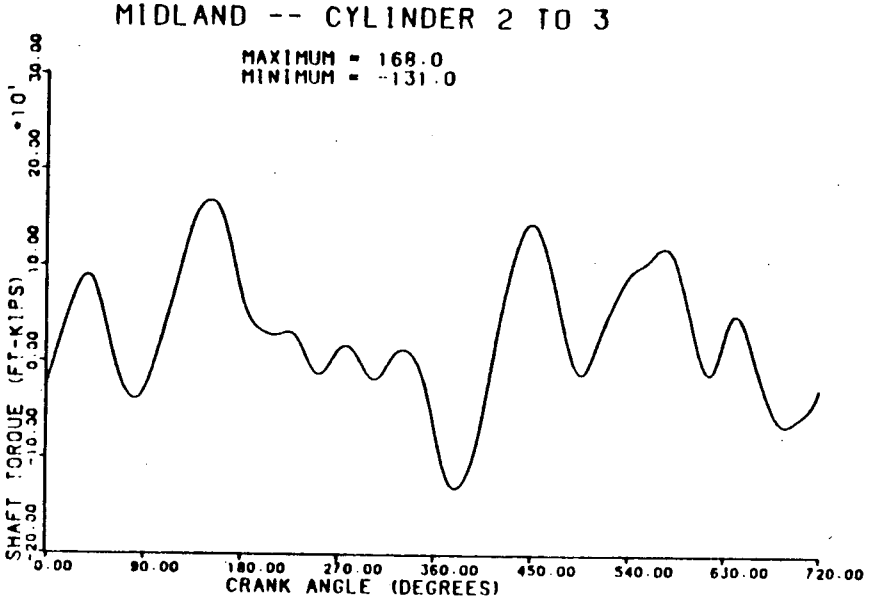

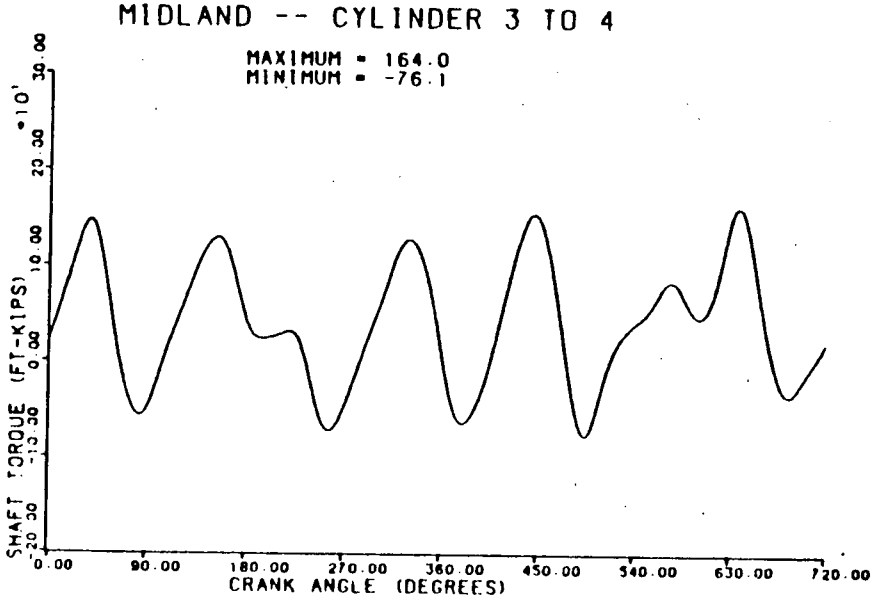

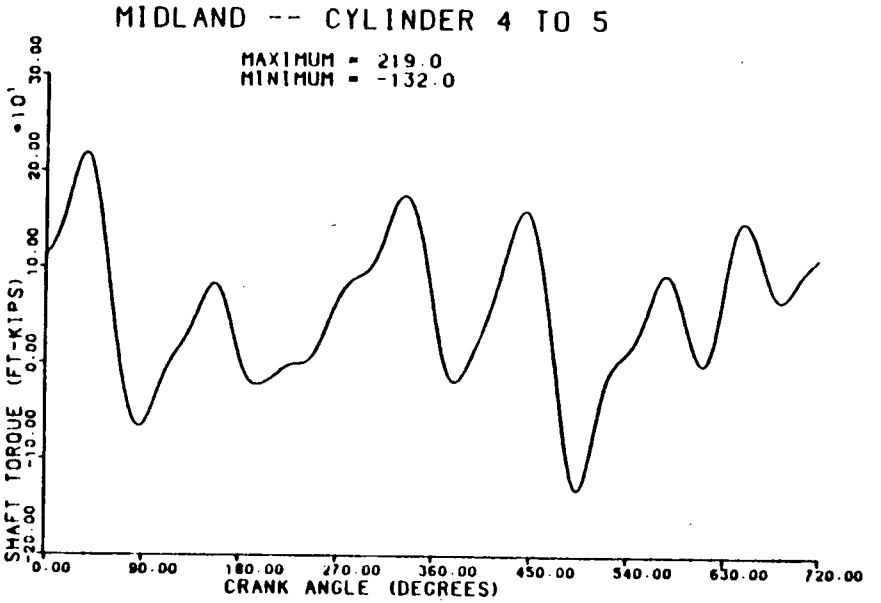

Figure 3-2. Dynamic model torsional response of DSRV-12-4 13-inch by 13-inch crankshaft for 5250 kw load at Midland.

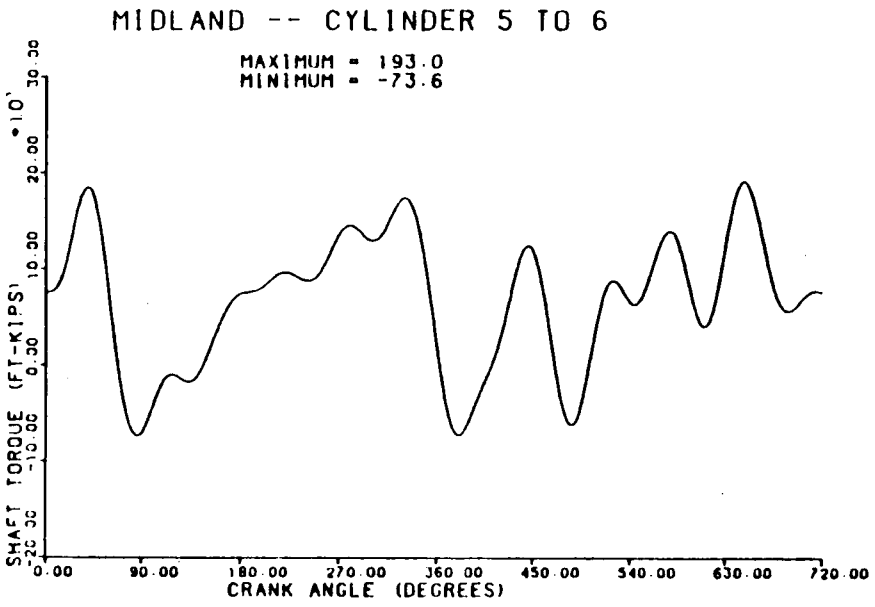

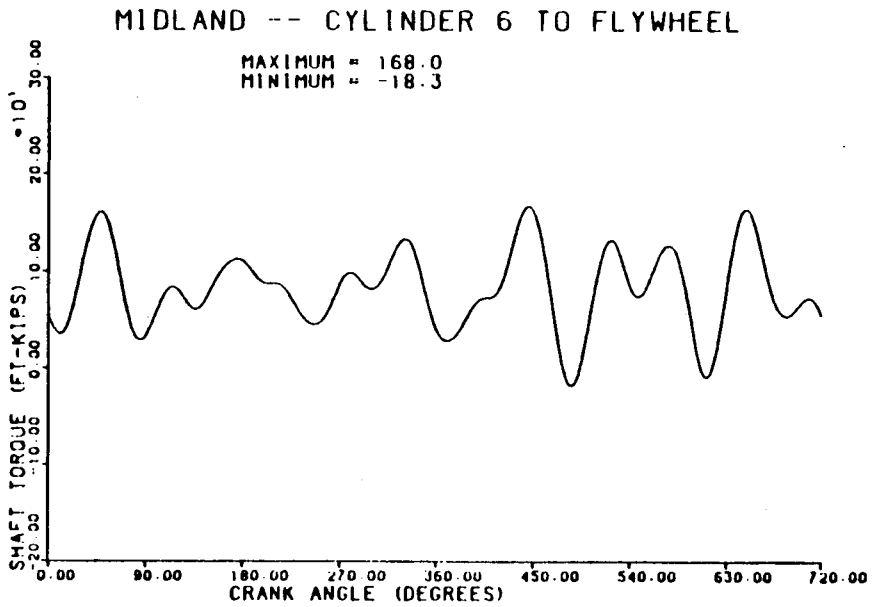

Figure 3-2 (continued).

4.0 RECOMMENDATIONS AND CONCLUSIONS FOR DSRV-12-4 CRANKSHAFTS

The crankshafts are adequate for their intended service provided the recommendations below are followed.

The following recommendations are made:

1. The oil holes in the main journal number 5 represent a more critical stress concentration in torsion than the crankpin fillets and should be inspected for fatigue cracks and machining discontinuities.

2. The combined response should be measured by torsiograph testing.

The following conclusions are made:

1. The design calculations performed by TDI are appropriate, although they underpredict the crankshaft response, and show that the crankshaft stresses are below DEMA recommendations for a single order. The stress resulting from combined orders is not calculated by this method.

2. The TDI torsiograph test results on the Midland engine show that the crankshaft stresses are below the DEMA recommended levels for a single order for both 5250 kW (100% rated load) and 110% load. The peak-to-peak response was not measured.

PART 2:

REVIEW OF DSRV-20-4
13-INCH BY 13-INCH CRANKSHAFTS
AT SAN ONOFRE

5.0 INTRODUCTION TO REVIEW OF DSRV-20-4 13-INCH BY 13-INCH CRANKSHAFT AT SAN ONOFRE

This report presents Failure Analysis Associates' findings on the adequacy of the crankshafts in the emergency diesel engines at San Onofre Nuclear Power Station. The crankshaft is required to meet the recommendations of the Diesel Engine Manufacturers Association (DEMA). In Section 6.0, the design calculations of Transamerica Delaval Inc. (TDI) [5-1] are reviewed for compliance with the DEMA stress allowables. In Section 7.0, a torsional dynamic analysis is used to compute nominal torsional stresses at each crank throw.

Section 5 References

5-1 Yang, Roland, "Torsional and Lateral Critical Speed, Engine Numbers 75041/42 Delaval-Enterprise Engine Model DSRV-20-4 6000 KW/8303 BHP at 450 RPM for Southern California Edison Company." Transamerica Delaval Inc., Engine and Compressor Division, Oakland, California, October 22, 1975. Updated.

6.0 COMPLIANCE OF CRANKSHAFT WITH DIESEL ENGINE MANUFACTURERS ASSOCIATION RECOMMENDATIONS

The purchase specifications for the diesel generator sets require that the recommendations of the Diesel Engine Manufacturers Association, DEMA [6-1], be followed. These recommendations state:

> In the case of constant speed units, such as generator sets, the objective is to insure that no harmful torsional vibratory stresses occur within five percent above and below rated speed.
>
> For crankshafts, connecting shafts, flange or coupling components, etc., made of conventional materials, torsional vibratory conditions shall generally be considered safe when they induce a superimposed stress of less than 5000 psi, created by a single order of vibration, or a superimposed stress of less than 7000 psi, created by the summation of the major orders of vibration which might come into phase periodically.

In October, 1975, Transamerica Delaval Inc. (TDI) performed a torsional critical speed analysis of the crankshafts [6-2]. In Section 6.1, this analysis is reviewed for compliance with the above allowable stresses.

6.1 Review of TDI Torsional Critical Speed Analysis

Diesel generator torques due to dynamic response are usually calculated in two steps. First, the torsional mode shapes and natural frequencies of vibration are calculated. Second, the dynamic forced vibration response due to gas pressure and reciprocating inertia loading is calculated. TDI calculated the response at 100% of the rated load, 6000 kW.

6.1.1 Natural Frequencies

The first step in a torsional critical speed analysis is to determine the natural frequencies of the crankshaft. The engine speed at which a given order resonates may then be calculated. The diesel generator is modeled as a system of lumped mass moments of inertia interconnected by torsional springs,

as shown in Figure 6-1. The inertia and stiffness values are shown in Table 6.1.

It has long been standard practice in the diesel engine industry to solve this eigenvalue problem by the Holzer method [6-3]. This method has been used for at least 40 years [6-4], and thus is well established.

TDI used the Holzer method to calculate the system's first three natural frequencies, which are shown in Table 6.2. The first natural frequency was found to be 19.9 Hz.

6.1.2 Nominal Stresses

The second step in a torsional critical speed analysis is to determine the dynamic torsional response of the crankshaft due to gas pressure and reciprocating inertia loading. The 1st order is a harmonic which repeats once per revolution of the crankshaft. For a four-stroke engine, harmonics of order 0.5, 1.0, 1.5, 2.0, 2.5... exist. TDI performs this calculation for each order of vibration up to 12.0 separately. For each order, the applied torque at a cylinder due to gas pressure and reciprocating inertia is calculated. The values of this torque for each order are usually normalized by dividing by the piston area and throw radius. The normalized value for the nth order is referred to as T_n. The values of T_n for signifcant orders used by TDI are shown in Table 6.3. These values may be compared to those recommended by Lloyd's Register of Shipping, LRS [6-5]. TDI's values are higher than LRS's values for low orders and lower for high orders and should be confirmed by torsiograph testing. The response is then calculated by one procedure if the harmonic is at resonance and by another if the harmonic is away from resonance.

At resonance, the torsional vibration amplitudes would increase indefinitely in the absence of damping. The solution is obtained by balancing the energy input with the energy loss due to damping. TDI used an empirical form of hysteresis damping due to friction. The purpose of this calculation is to ensure that the diesel generator can be brought up to operating speed without undergoing excessive stresses as critical speeds are passed. Since the engine

runs at 450 rpm and no significant critical speed is nearby, the resonant response is not important.

Away from resonance, the torsional vibrations reach a steady-state level even without the aid of any damping. The magnitude of this response for each structural mode and loading order is calculated as the product of a dynamic amplification factor and an equivalent static equilibrium amplitude. The equivalent static equilibrium amplitude is computed using a modal load and modal stiffness [6-6] for the nth order harmonic and given mode shape. The nominal shear stress, τ, in the 13-inch pin of Crankpin No. 10 for each order is then calculated from the dynamic torque, T, using $\tau = Tr/J$, where r is the pin radius and J is the polar moment of inertia.

TDI calculated the response for the first three modes and plotted the results for the first two modes since higher modes produce much smaller stresses. The nominal shear stresses for the significant orders are shown in Table 6.4. It is seen that the largest single order stress of 408 psi for the $2\frac{1}{2}$ order is well below the 5000 psi DEMA allowable.

TDI does not calculate the associated phase angle with the response of each order, so that it is not possible to calculate the combined response. The computation of the combined response is reported in Section 7.0.

Section 6 References

6-1 Standard Practices for Low and Medium Speed Stationary Diesel and Gas Engines. Diesel Engine Manufacturers Association, 6th ed., 1972.

6-2 Yang, Roland, "Torsional and Lateral Critical Speed, Engine Numbers 75041/42 Delaval-Enterprise Engine Model DSRV-20-4 6000 KW/8303 BHP at 450 RPM for Southern California Edison Company." Transamerica Delaval Inc., Engine and Compressor Division, Oakland, California, October 22, 1975. Updated

6-3 Thomson, William T., Theory of Vibration with Applications. Second edition, Prentice-Hall, 1981.

6-4 Den Hartog, J., Mechanical Vibrations. Third edition, McGraw-Hill, 1947.

6-5 Lloyd's Register of Shipping, Guidance Notes on Torsional Vibration Characteristics of Main and Auxillary Oil Engines.

6-6 Craig, Roy R., Jr., Structural Dynamics: An Introduction to Computer Methods. Wiley, 1981.

TABLE 6.1

STIFFNESS AND INERTIAS FOR TORSIONAL DYNAMIC ANALYSIS
OF DSRV-20-4 13-INCH BY 13-INCH CRANKSHAFT AT SAN ONOFRE

Inertia Location	Inertia (lb. ft. sec^2)	Stiffness (ft. lb./rad)
Front Gear	11.8	53.2×10^6
Cylinder No. 1	143.1	101.9×10^6
Cylinder No. 2	141.6	101.9×10^6
Cylinder No. 3	141.6	101.9×10^6
Cylinder No. 4	141.6	101.9×10^6
Cylinder No. 5	141.6	101.9×10^6
Cylinder No. 6	141.6	101.9×10^6
Cylinder No. 7	141.6	101.9×10^6
Cylinder No. 8	141.6	101.9×10^6
Cylinder No. 9	141.6	101.9×10^6
Cylinder No. 10	144.5	72.7×10^6
Flywheel	1503.9	485.6×10^6
Generator	11114.3	

TABLE 6.2

TORSIONAL NATURAL FREQUENCIES FROM TDI ANALYSIS OF DSRV-20-4
13-INCH BY 13-INCH CRANKSHAFT AT SAN ONOFRE

Mode	Natural Frequency (Hz)
1	19.9
2	56.0
3	90.0

TABLE 6.3

TORSIONAL LOADINGS FOR TDI ANALYSIS OF DSRV-20-4
13-INCH BY 13-INCH CRANKSHAFT AT SAN ONOFRE
AT 6000 KW

Order	Torsional Loading, T_n (psi)
1.5	94.6
2.5	55.3
3.5	20.1
4.5	11.6
5.0	8.6
5.5	6.6

TABLE 6.4

SINGLE-ORDER NOMINAL SHEAR STRESSES FROM TDI ANALYSIS OF DSRV-20-4
13-INCH BY 13-INCH CRANKSHAFT AT SAN ONOFRE AT 6000 KW

Order	Amplitude of Nominal Shear Stress (psi)
1.5	168
2.5	408
3.5	57
4.5	148
5.0	120
5.5	40
DEMA Allowable for Single Order	5000

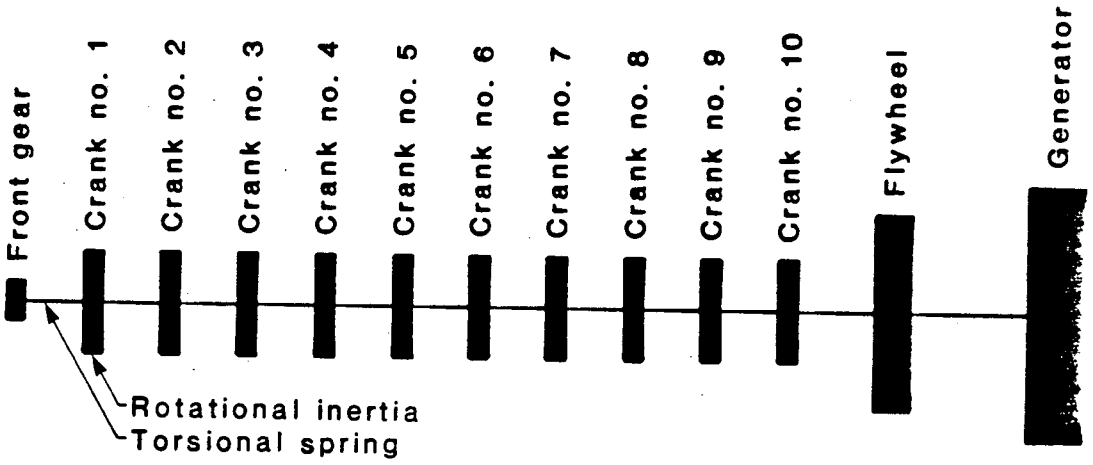

Figure 6-1. TDI dynamic model of DSRV-20-4 13-inch by 13-inch crankshaft at San Onofre.

7.0 CRANKSHAFT DYNAMIC TORSIONAL ANALYSIS

In Section 6.0 it was found that the crankshafts satisfy the DEMA single order nominal stress recommendation of 5000 psi for 6000 kW (100% of rated load). However, the stresses for combined orders were not calculated by TDI, and thus could not be compared to the DEMA recommended limit of 7000 psi. A dynamic torsional analysis of the crankshaft is performed to determine the true range of torque at each crank throw. The FaAA dynamic model allows all orders and modes to be summed using appropriate phase angles.

7.1 Torsional Model

FaAA developed a dynamic torsional model of the crankshaft to supplement TDI's conventional forced vibration calculations. The original TDI procedure did not compute the phase relationship between the various orders or modes, so it was not possible to compute the true summation. The actual maximum stress is a direct result of this summation. Furthermore, the original TDI method always predicted maximum stress in Crankpin No. 10, which is generally true for the first mode but not true for the combined response. The dynamic model developed used the same idealized lumped inertia and torsional spring model as the TDI analysis (Figure 6-1 and Table 6.1).

The first three torsional natural frequencies for the replacement crankshaft are shown in Table 7.1. The natural frequencies are in agreement with those computed and measured by TDI.

When the diesel generator is running at a given speed and power level, the forced vibration problem is steady-state where both load and response repeat themselves every two revolutions of the crankshaft. To model the dynamic response, a modal superposition analysis [7-1] was used with harmonic load input. The calculation of the harmonic loads will be discussed in the next section.

7.2 Harmonic Loading

To calculate the harmonic loading on a crankshaft it is necessary to consider gas pressure, reciprocating inertia, and frictional loads. The gas pressure loading may be obtained from pressure versus crank angle data. This pressure was measured in a Stone & Webster Engineering Corporation (SWEC) test on a similar TDI series R-4 cylinder at Shoreham Nuclear Power Station [7-2]. The pressure was measured in Cylinder No. 7 by inserting a probe through the air start valve. A top dead center, TDC, mark for Cylinder No. 7 was simultaneously recorded by a probe on the flywheel. The pressure data at 100% load was reduced by FaAA to obtain the pressure curve shown in Figure 7-1. This pressure data corresponds to 8750 kW so that the calculations are carried out for this load rather than the 6000 kW rated load. This results in a conservative analysis.

The reciprocating mass of the connecting rod and piston was found to be 820 lbs for each connecting rod. This mass causes reciprocating inertia torque on the crankshaft. The effect of this torque was combined with the gas pressure torque.

The total torque was then resolved into its sine and cosine harmonics corresponding to each order. These torque harmonics were used in the steady-state analysis. The magnitude of the torque harmonics are normalized by dividing by the piston area and throw radius. The resulting normalized torques for the most significant orders are shown in Table 7.2.

7.3 Calculated Response

The response due to the first 24 orders and all 13 modes is calculated using modal superposition with 2.5% of critical damping for each mode. The actual value of damping used has little effect on the response since the orders are not at resonance at 450 rpm.

The calculated amplitude of free-end displacement is shown in

Table 7.3. The vector summation from the FaAA analysis is half the peak-to-peak displacement. The largest response occurs for the $2^1/2$ order.

The stresses in Table 7.4 show that the stress level is highest between cylinders 3 and 4, and 8 and 9. The highest nominal shear stress amplitude is found to be 4018 psi. This value is lower than the 7000 psi DEMA allowable for combined orders, even though the calculated value was computed using all modes. The computed torque as a function of crank angle for each crank throw is shown in Figure 3-2.

7.4 Nominal Stresses for Underspeed and Overspeed Conditions

DEMA requires crankshaft stresses to remain within the allowables over a speed range of 450 RPM ± 5%. Modal superposition calculations were performed at 427.5 RPM and 472.5 RPM. The torsional loading at this speed is not known, but was assumed to be the same as that at 450 RPM.

At 95% speed the free-end response is shown in Table 7.5. The nominal shear stresses are shown in Table 7.6, and are below the 7000 psi DEMA allowable for combined orders, even though the calculated value was computed using all modes.

At 105% speed the free-end response is shown in Table 7.7. The nominal shear stresses are shown in Table 7.8, and are below the 7000 psi DEMA allowable for combined orders, even though the calculated value was computed using all modes.

Section 7 References

7-1 Timoshenko, S., D.H. Young, and W. Weaver, Jr., Vibration Problems in Engineering. Fourth edition, Wiley, 1974.

7-2 Bercel, E., and Hall, J.R., "Field Test of Emergency Diesel Generator 103," Stone & Webster Engineering Corporation, April 1984.

TABLE 7.1

TORSIONAL NATURAL FREQUENCIES OF DSRV-20-4
13-INCH BY 13-INCH CRANKSHAFT AT SAN ONOFRE
FROM FaAA ANALYSIS

Mode	Natural Frequency (Hz)
1	19.90
2	56.72
3	89.95

TABLE 7.2
TORSIONAL LOADING FOR FaAA ANALYSIS OF DSRV-20-4
13-INCH BY 13-INCH CRANKSHAFT AT SAN ONOFRE

Order	Torsional Loading, T_n (psi)
1.5	112.0
2.5	77.0
3.5	48.0
4.0	33.0
4.5	26.2
5.5	15.5

TABLE 7.3

FREE-END VIBRATION AT 8750 KW AND 450 RPM FOR
DSRV-20-4 13-INCH BY 13-INCH CRANKSHAFT
AT SAN ONOFRE

Order	Amplitude of Vibration (degrees)
0.5	0.078
1.0	0.007
1.5	0.037
2.0	0.002
2.5	0.074
3.0	0.007
3.5	0.011
4.0	0.000
4.5	0.011
5.0	0.047
5.5	0.012
6.0	0.013
6.5	0.001
7.0	0.003
7.5	0.001
8.0	0.001
Vector Summation	0.173

TABLE 7.4

NOMINAL SHEAR STRESSES AT 8750 KW AND 450 RPM FOR DSRV-20-4
13-INCH BY 13-INCH CRANKSHAFT AT SAN ONOFRE

Location	Amplitude of Nominal Shear Stress (psi)		
	2 1/2 Order	1/2 Order	Total
Between Cylinder No. 1 and Cylinder No. 2	779	202	2619
Between Cylinder No. 2 and Cylinder No. 3	133	383	3646
Between Cylinder No. 3 and Cylinder No. 4	547	528	3861
Between Cylinder No. 4 and Cylinder No. 5	250	620	3263
Between Cylinder No. 5 and Cylinder No. 6	250	559	3380
Between Cylinder No. 6 and Cylinder No. 7	347	623	3373
Between Cylinder No. 7 and Cylinder No. 8	403	533	3648
Between Cylinder No. 8 and Cylinder No. 9	417	524	4018
Between Cylinder No. 9 and Cylinder No. 10	1129	213	3829
Between Cylinder No. 10 and Flywheel	457	15	2150

TABLE 7.5

FREE-END VIBRATION AT 8750 KW AND 95% SPEED FOR
DSRV-20-4 13-INCH BY 13-INCH CRANKSHAFT AT SAN ONOFRE

Order	Amplitude of Vibration (degrees)
0.5	0.078
1.0	0.005
1.5	0.036
2.0	0.002
2.5	0.046
3.0	0.011
3.5	0.017
4.0	0.000
4.5	0.021
5.0	0.052
5.5	0.008
6.0	0.012
6.5	0.000
7.0	0.002
7.5	0.000
8.0	0.005
Vector Summation	0.161

TABLE 7.6

NOMINAL SHEAR STRESSES AT 8750 KW AND 95% SPEED FOR DSRV-20-4
13-INCH BY 13-INCH CRANKSHAFT AT SAN ONOFRE

Location	Amplitude of Nominal Shear Stress (psi)		
	$2^1/_2$ Order	$^1/_2$ Order	Total
Between Cylinder No. 1 and Cylinder No. 2	750	172	2544
Between Cylinder No. 2 and Cylinder No. 3	71	382	3685
Between Cylinder No. 3 and Cylinder No. 4	616	527	3861
Between Cylinder No. 4 and Cylinder No. 5	132	619	3139
Between Cylinder No. 5 and Cylinder No. 6	869	653	3280
Between Cylinder No. 6 and Cylinder No. 7	185	621	3356
Between Cylinder No. 7 and Cylinder No. 8	518	532	3661
Between Cylinder No. 8 and Cylinder No. 9	225	389	3991
Between Cylinder No. 9 and Cylinder No. 10	947	212	3682
Between Cylinder No. 10 and Flywheel	250	13	2150

TABLE 7.7

FREE-END VIBRATION AT 8750 KW AND 105% SPEED FOR DSRV-20-4
13-INCH BY 13-INCH CRANKSHAFT AT SAN ONOFRE

Order	Amplitude of Vibration (degrees)
0.5	0.078
1.0	0.008
1.5	0.039
2.0	0.003
2.5	0.159
3.0	0.006
3.5	0.008
4.0	0.000
4.5	0.004
5.0	0.042
5.5	0.018
6.0	0.015
6.5	0.001
7.0	0.006
7.5	0.001
8.0	0.001
Vector Summation	0.248

TABLE 7.8

NOMINAL SHEAR STRESSES AT 8750 KW AND 105% SPEED FOR DSRV-20-4
13-INCH BY 13-INCH CRANKSHAFT AT SAN ONOFRE

Location	Amplitude of Nominal Shear Stress (psi)		
	$2^1/_2$ Order	$^1/_2$ Order	Total
Between Cylinder No. 1 and Cylinder No. 2	796	202	2700
Between Cylinder No. 2 and Cylinder No. 3	389	383	3682
Between Cylinder No. 3 and Cylinder No. 4	713	529	4118
Between Cylinder No. 4 and Cylinder No. 5	633	621	3397
Between Cylinder No. 5 and Cylinder No. 6	1215	655	3455
Between Cylinder No. 6 and Cylinder No. 7	874	624	3647
Between Cylinder No. 7 and Cylinder No. 8	978	546	4194
Between Cylinder No. 8 and Cylinder No. 9	1042	392	4436
Between Cylinder No. 9 and Cylinder No. 10	1508	215	4039
Between Cylinder No. 10 and Flywheel	1123	16	2925

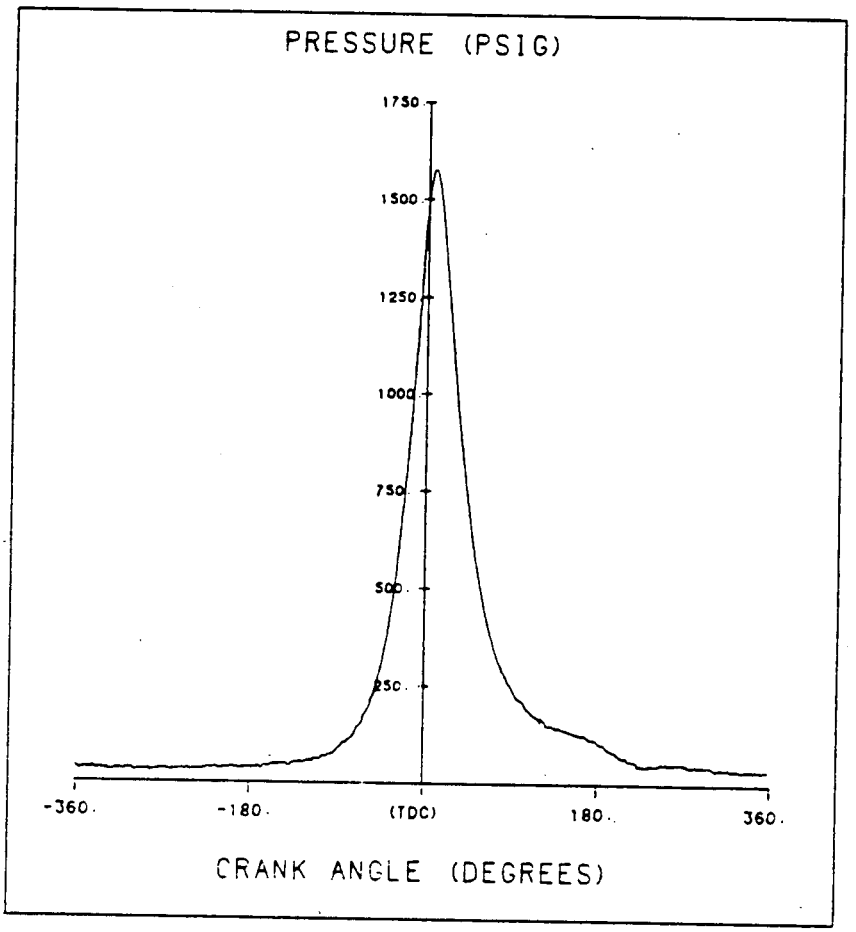

Figure 7-1. Measured pressure in Cylinder no. 7 versus crank angle at 100% load on a DSR-48 engine at Shoreham.

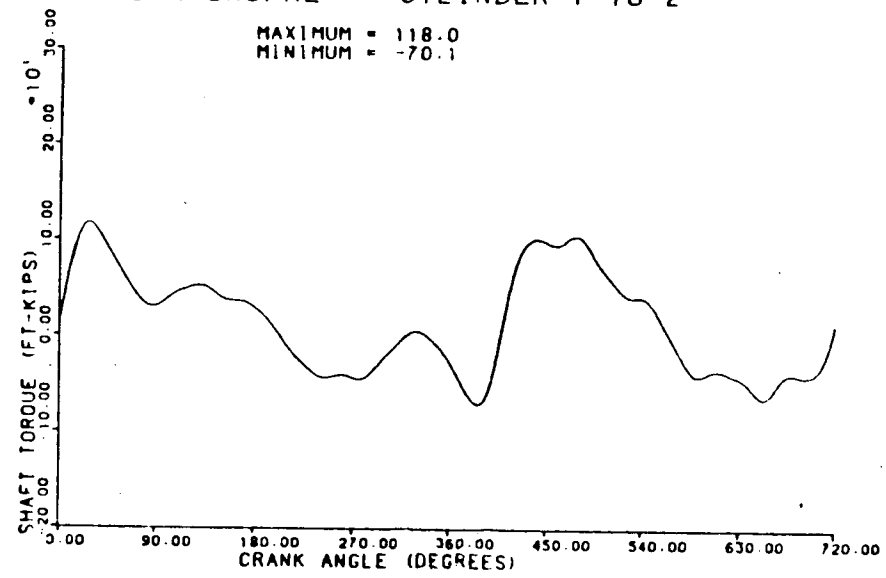

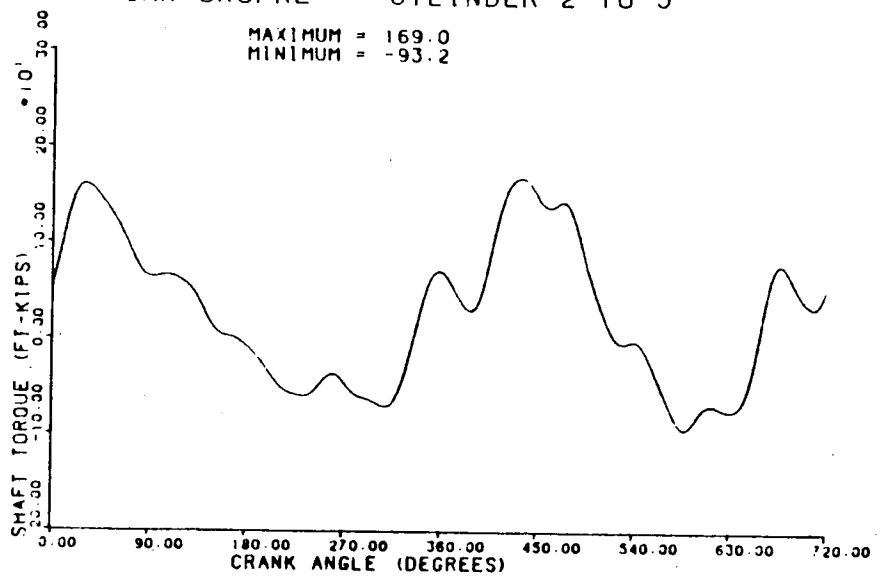

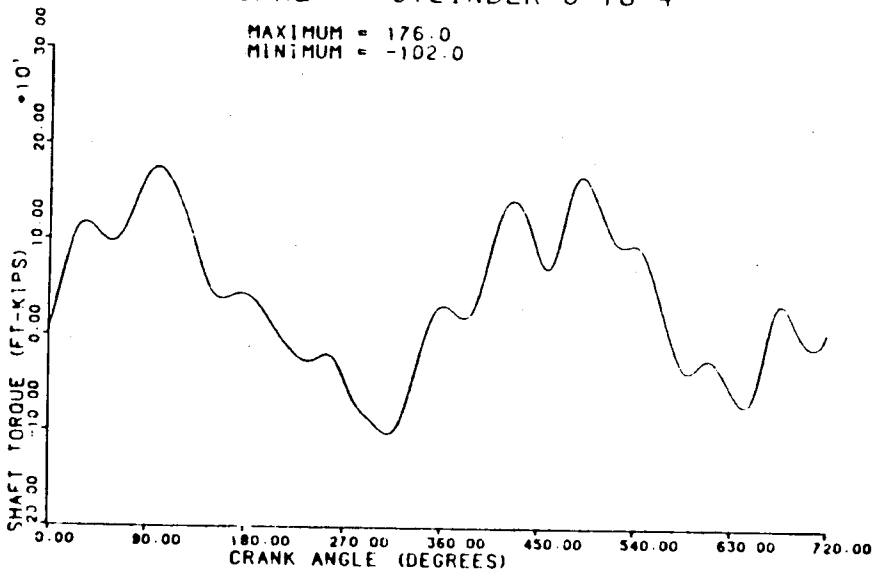

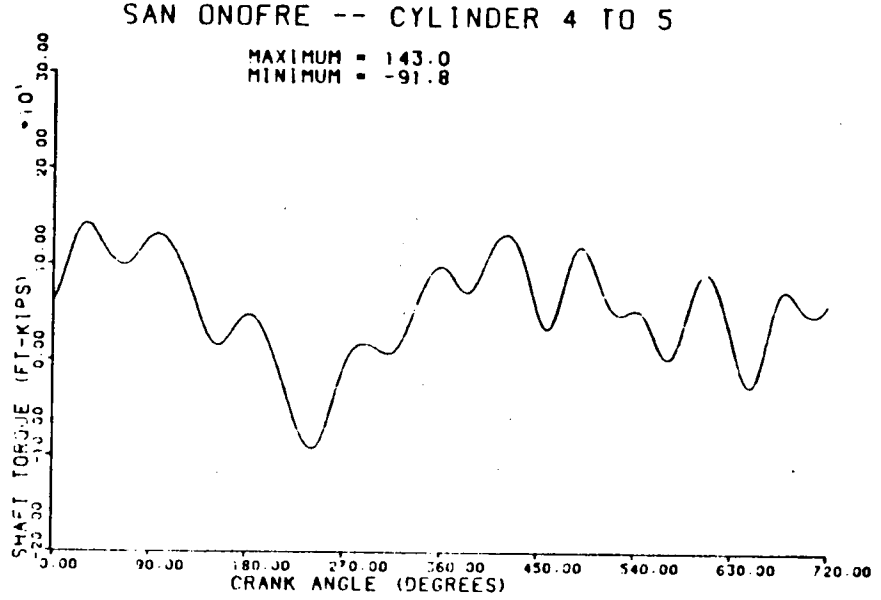

Figure 7-2. Dynamic model torsional response of DSRV-20-4 13-inch by 13-inch crankshaft for 8750 kw load at San Onofre.

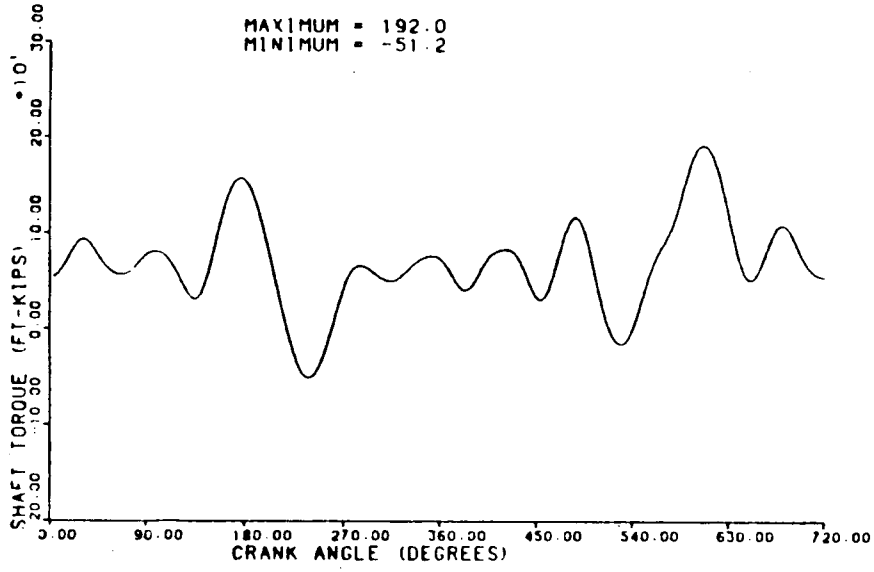

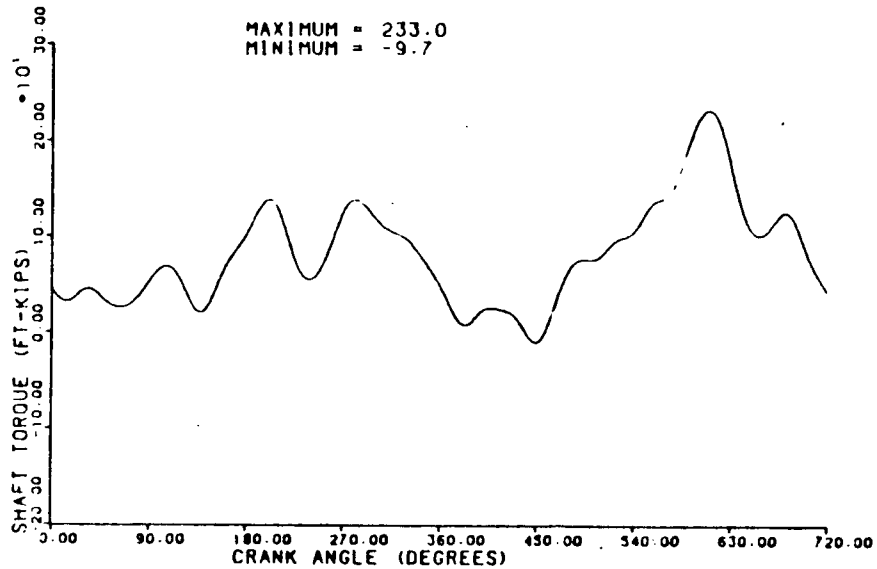

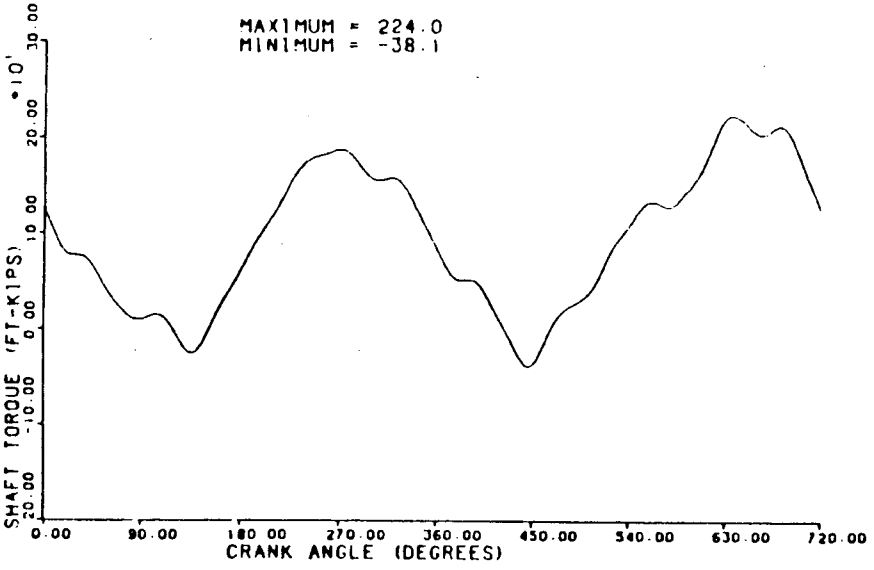

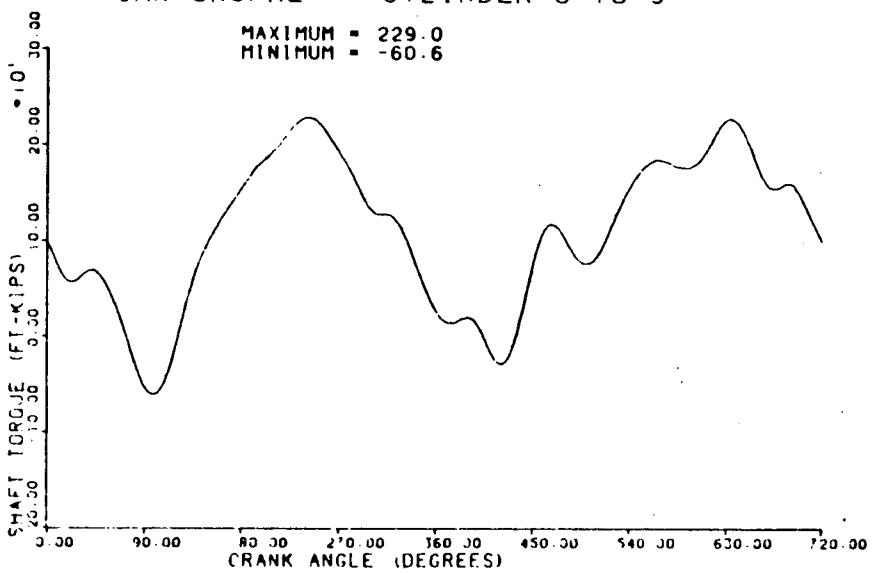

Figure 7-2 (continued).

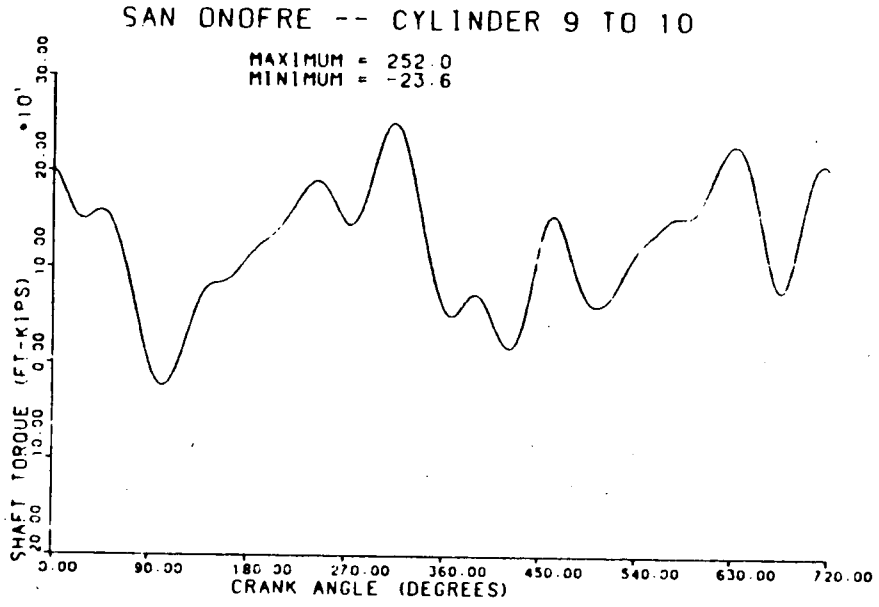

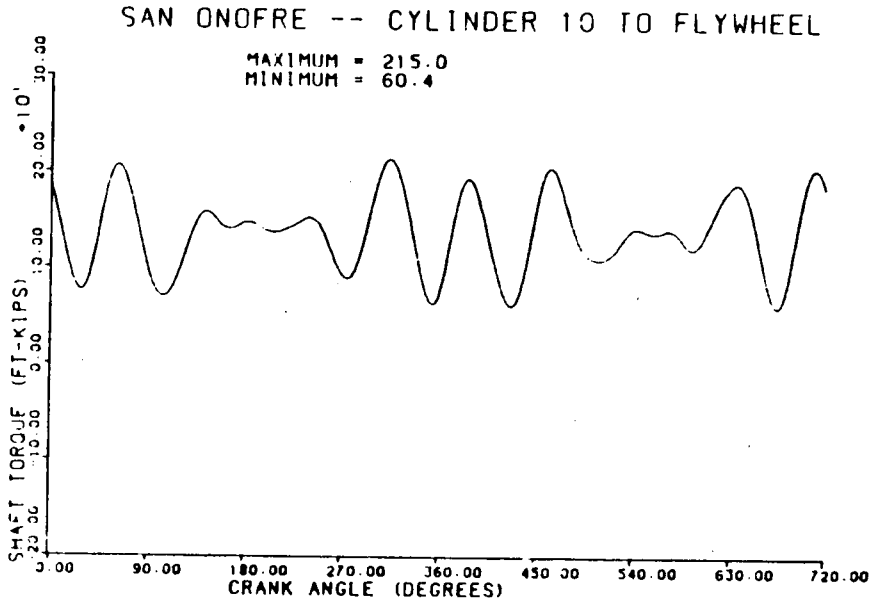

Figure 7-2 (continued).

8.0 RECOMMENDATIONS AND CONCLUSIONS FOR DSRV-20-4 CRANKSHAFT

The crankshafts are adequate for their intended service provided a torsiograph test is conducted to confirm the torsional system natural frequencies and measure the combined response.

It is concluded that the design calculations originally performed by TDI are appropriate and show that the crankshaft stresses are below DEMA recommendations for a single order. The stress resulting from combined orders is not calculated by this method.

FaAA-84-12-14
Revision 1.0

EVALUATION OF TRANSIENT CONDITIONS ON EMERGENCY DIESEL GENERATOR CRANKSHAFTS AT SAN ONOFRE NUCLEAR GENERATING STATION UNIT 1

Prepared by

Failure Analysis Associates
Palo Alto, California

Prepared for

TDI Diesel Generator Owners' Group
Charlotte, North Carolina

April 1985

TABLE OF CONTENTS

1.0 INTRODUCTION

This report summarizes the results of inspections, testing, and analyses performed on the emergency diesel generator crankshafts at San Onofre Nuclear Generating Station Unit 1. The inspections discovered the presence of fatigue cracks in main journal oil holes. The results of these inspections along with a report of operating history and the effect of drilling out the oil holes are discussed in Section 2.

A test program to measure the dynamic response of the crankshaft and cylinder pressures under transient start-up and coastdown conditions was undertaken. The results of this test program are reported in Section 3. A transient torsional analytical model of the crankshaft under start-up and coastdown conditions is used to predict response in Section 4. This model is used to determine the time-dependent nominal torsional stress at each main journal. Tests and analyses of the crankshaft under steady state conditions have been reported separately.

In Section 5, life predictions are made by considering the stress concentration around the oil holes and the nominal torsional stress history calculated in the previous section. The effect on life prediction of alternative strategies to control start-up stresses are determined.

2.0 BACKGROUND

Eddy-current inspections in the crankshaft main journal oil hole regions of Diesel Generator 1, DG1, in July and August, 1984, and of Diesel Generator 2, DG2, in October, 1984, determined that cracks existed in several locations. The results of these inspections and metallographic inspections are discussed below. This is followed by an analysis to determine the effect of enlarging the oil holes and the stress concentration around the oil hole. First, the operating history of the two engines at the time of the eddy-current inspections is discussed.

2.1 Operating History

The operating history of engines DG1 and DG2 prior to eddy-current testing is summarized in Table 2-1. It is seen that DG1 has 740 starts compared with 450 for DG2. This difference is due to the approximately 300 fast starts that TDI performed on the engine while it was at the Oakland plant. This testing on the lead engine was not repeated on DG2.

The total number of hours of operation for each engine are also shown in Table 2-1. It is not known how many of these hours were logged at full rated load of 6000 kW.

2.2 Eddy-Current Inspections

Failure Analysis Associates (FaAA) performed eddy-current examinations of the main journal oil holes in crankshafts in both DG1 and DG2 engines [2-2, 2-3]. Eddy-current examinations were performed on main journals numbers 3, 4, 8, 9, and 10 in DG1 and on main journal numbers 8, 9, and 10 in DG2.

Numerous eddy-current crack indications were discovered as shown in Tables 2-2 and 2-3. The cracks all occurred at or near 45° orientations (i.e., 45°, 135°, 225°, and 315°) indicating that they were induced by torsional stresses rather than bending stresses. The fact that cracks exist in adjoining quadrants (e.g., 45° and 135°) indicates sign reversals in the torsional stresses, which confirms that the cracks were induced by vibration rather than overload.

The cracks were removed by drilling out the holes to a larger diameter. The initial oil hole geometry is shown in Figure 2-1 along with the geometry of the $1\text{-}1/2$-inch deep holes on main journal 12. The initial diameter was $15/16$ inches, and subsequently drill sizes of $1\text{-}1/16$, $1\text{-}3/16$, $1\text{-}5/16$, $1\text{-}7/16$, and $1\text{-}1/2$ inches were used. The holes were enlarged to the extent that no recordable eddy-current indications remained. Both ends of each hole were bored to the same size that was necessary to remove the deepest indication.

The largest cracks were found in oil holes on main journal numbers 9 and 10 in DG1. The extent of these cracks may be determined from Figures 2-2 through 2-5. It is seen that several cracks extended for 3.0 inches or more. The greatest continuous depth of these long cracks was between 1/16 and 1/8 inch on main journal number 9. The deepest crack was also found on main journal number 9 and was between 1/4 and 9/32 inch.

Main journal oil hole number 9 on DG1 was drilled to a final diameter of 1 1/2 inches, and main journal oil hole number 10 on DG1 was drilled to a final diameter of 1 5/16 inches. Metal was removed from the blend radius of main journal oil hole number 8 on DG1 and main journal oil hole number 9 on DG2 by grinding and polishing.

The crankshaft fillet inspection revealed no eddy-current indications exceeding the threshold.

2.3 Metallographic Replicas

Metallographic replicas of cracked regions of the DG1 crankshaft were taken and inspected [2-4]. There is no evidence of large plastic deformation which might be associated with fatigue resulting from very few cycles. Closely spaced parallel cracks were found in a number of locations.

The fatigue cracks are primarily transgranular in nature. These fatigue cracks do not have a preferred orientation with respect to the metallurgical microstructure. In some instances the cracks lie along the approximate orientation of the material texture while in others the crack is perpendicular to the material texture.

2.4 Enlarged Oil Holes

The observed fatigue cracks, were eliminated by drilling the oil holes out to larger diameters. The effect of the larger diameter oil holes upon the stress concentration factor in the oil hole was calculated and found not to be significant.

To study the effect on the torsional stress due to enlarging the oil hole diameters in the crankshaft main bearing journals from 15/16 inch to 1 1/2 inches, the change in polar moment of inertia of the section and the stress concentration factor in the shaft due to the transverse oil hole were reviewed.

Calculations indicate that enlarging the 15/16 inch oil hole to 1 1 /2 inches in diameter will result in a 4% reduction in the polar moment of inertia of the section (2631.9 in^4 to 2527.5 in^4). The behavior of the stress concentration based upon the net section of the shaft, K_{tn}, as a function of increasing oil hole diameter is shown in Figure 2-6. The combined effect of the reduction of inertia and K_{tn} must be considered when determining the crankshaft torsional stresses.

The stress concentration factor based upon the gross section of the shaft, K_{tg}, is also shown in Figure 2-6. K_{tg} accounts for the combined effect of the reduction in polar moment of inertia and K_{tn}. K_{tg} stays essentially the same as the oil hole is increased from 15/16 inch to 1 1/2 inches in diameter, resulting in negligible changes in torsional stress.

2.5 Summary

- DG1 has had more starts than DG2 by approximately 740 to 450.
- Main journal oil holes on both DG1 and DG2 were found by eddy-current inspection to have fatigue cracks generally orientated along 45° planes.
- Cracks on DG1 were much more severe than on DG2 with oil holes on main journals 9 and 10 being the most significant.

- Cracks were removed by drilling and grinding out the oil holes to a larger diameter without significantly altering the stress concentration effect of the oil hole.

- A liquid penetrant inspection of the No. 11 main journal oil hole on DG1 was performed. Minor cracking was observed. The oil hole was ground and polished. Reinspection showed no relevant indications [2-6].

Section 2 References

2-1 Letter to Director, Office of Nuclear Reactor Regulation, J.A. Zwolinski, Chief Operating Reactors Branch No. 5, Division of Licensing, U.S. Nuclear Regulatory Commission, Washington, D.C. from M.O. Medford, Manager, Nuclear Licensing, Southern California Edison Company, October 26, 1984.

2-2 "Eddy-Current Examination, DG1 Crankshaft, San Onofre Nuclear Electric Generating Station, August 1984," for TDI Diesel Owners Group, by Failure Analysis Associates, Report FaAA-84-10-2, October 1984.

2-3 "Eddy-Current Examination, DG2 Crankshaft, San Onofre Nuclear Electric Generating Station, October 1984," for TDI Diesel Owners Group, by Failure Analysis Associates, Report FaAA-84-10-24, December 1984.

2-4 Memo to Dave Pilmer, Southern California Edison, from Harry F. Wachob, Failure Analysis Associates, October 11, 1984.

2-5 R.E. Peterson, Stress Concentration Factors, Figure 173, John Wiley and Sons, 1974.

2-6 Southern California Edison Company NDE Report No. 1PT-072-84 by G. Schmidt and NDE Report No. 1PT-086-84 by L. Thomas.

Table 2-1

Operating History of Engines Prior to Eddy-Current Inspections [2-1]

Operation	Engine	
	DG1	DG2
No. of Starts	740	450
Total Hours	725	550

Table 2-2

Eddy-Current Crack Indications Found in DG1 Prior to Rework

Oil Hole Number[1]	Crack Number	Position[2]	Magnitude[3]	Length[4]
10 Main, Left	1*	45°	200%+	From 60° to at least 3 inches.
	2	225°	200%+	From 42° to at least 3 inches.
10 Main, Right	1	45°	166%+	From 60° to 15/16 inch.
	2	225°	166%+	From 66° to 1 1/16 inch.
9 Main, Left	1	45°	200%	From 12° to at least 3 inches.
	2	135°	36%	At 0°.
	3*	225°	200%+	From 40° to at least 3 inches.
9 Main, Right	1*	126°	200%+	From 40° to 1 inch.
	2	315°	200%+	From 40° to 1 inch.
8 Main, Left	1	130°	200%	66° to 84°
	2	225°	200%	66° to 72°
8 Main, Right	1	135°	200%+	60° to 84°
	2	335°	200%+	54° to 84°

* Two closely spaced indications.

NOTES:
1. Left or right from the perspective of someone standing at the generator end facing the governor with number 9 crankpin at top dead center.
2. Measured clockwise with 0° at the governor end of the crankshaft centerline.
3. Percentage of the signal obtained from a 0.020-inch deep by 0.040-inch long crack-like defect.
4. Angular measurement in the blend radius is from 0° at the main journal surface to 90° at the junction with the bore. Linear measurement is depth from the journal surface.

Table 2-3

Eddy-Current Crack Indications Found in DG2 Prior to Rework

Oil Hole Number[1]	Crack Number	Position[2]	Magnitude[3]	Length[4]
9 Main, Right	1	315°	250%	From 66° to 1.1 inch.
	2	130°	300%	From 66° to 0.5 inch.

NOTES:

1. Left or right from the perspective of someone standing at the generator end facing the governor with number 9 crankpin at top dead center.
2. Measured clockwise with 0° at the governor end of the crankshaft centerline.
3. Percentage of the signal obtained from a 0.020-inch deep by 0.040-inch long crack-like defect.
4. Angular measurement in the blend radius is from 0° at the main journal surface to 90° at the junction with the bore. Linear measurements is depth from the journal surface.

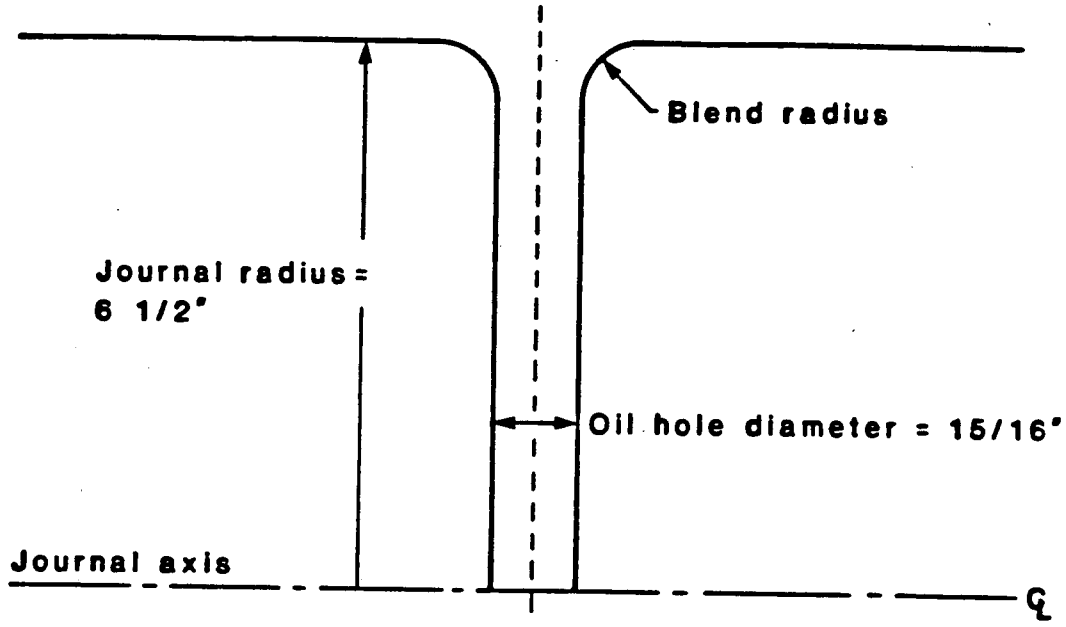

(a) Main journals 2 to 11.

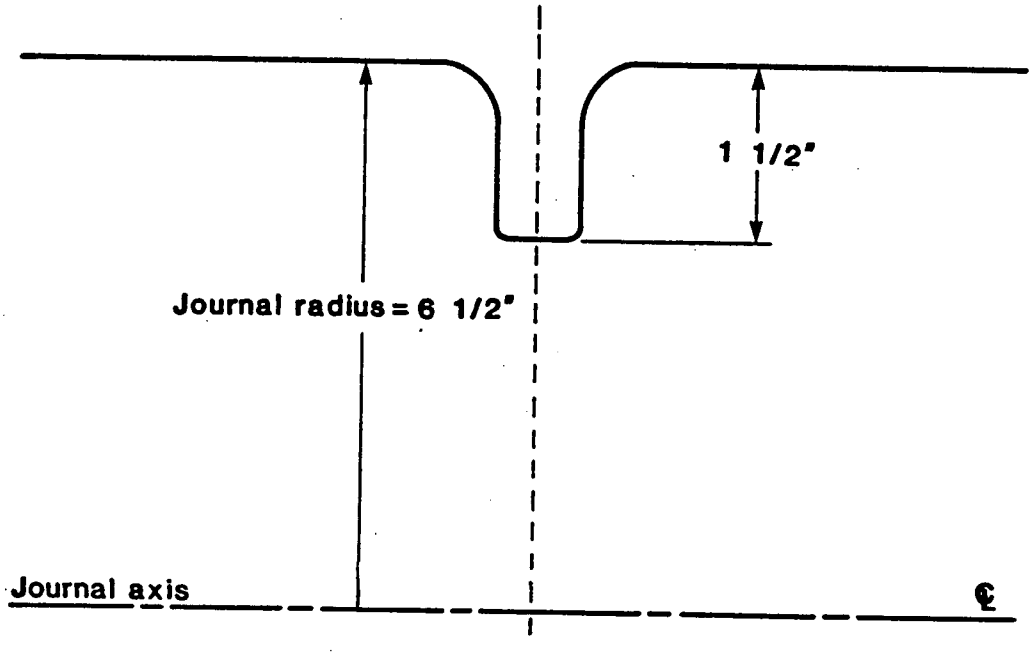

(b) Main journal 12.

Figure 2-1. Main journal oil hole geometry.

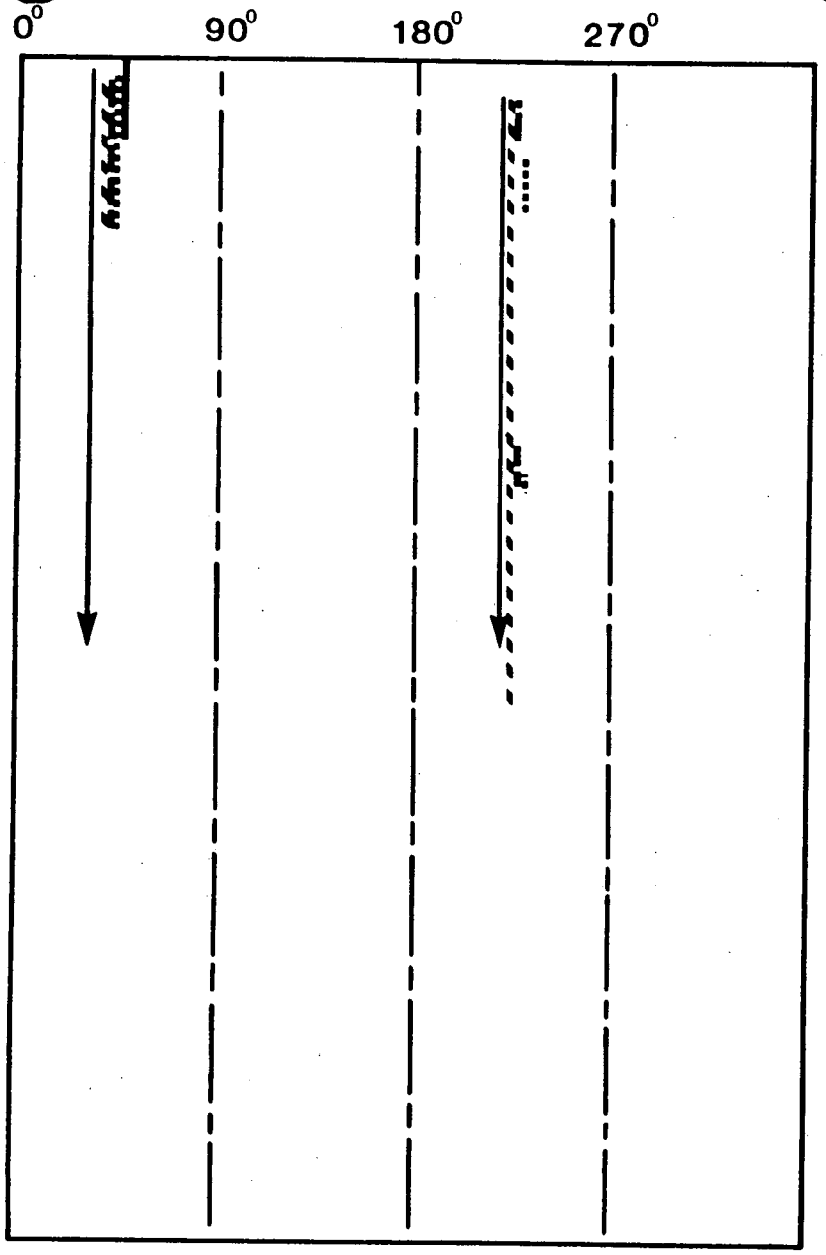

DG1 – Crankshaft main journal #9
Left oil hole

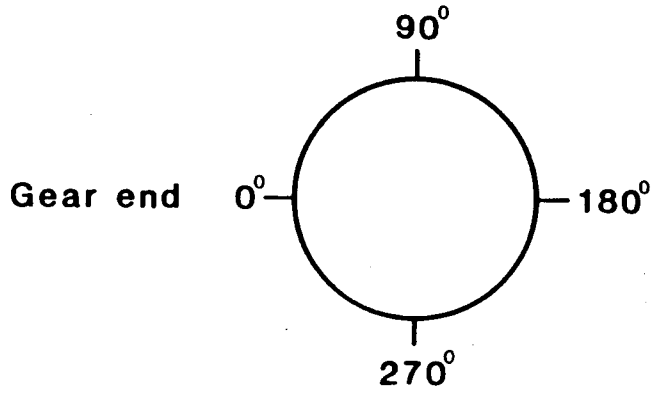

Hole diameter $1\frac{7}{16}$ in.

Hole diameter $1\frac{5}{16}$ in.

Hole diameter $1\frac{3}{16}$ in.

Hole diameter $1\frac{1}{16}$ in.

Hole diameter $\frac{15}{16}$ in.

FAA-84-12-14

Figure 2-2. Crack indication length at various locations and hole diameters. (Lengths to scale.)

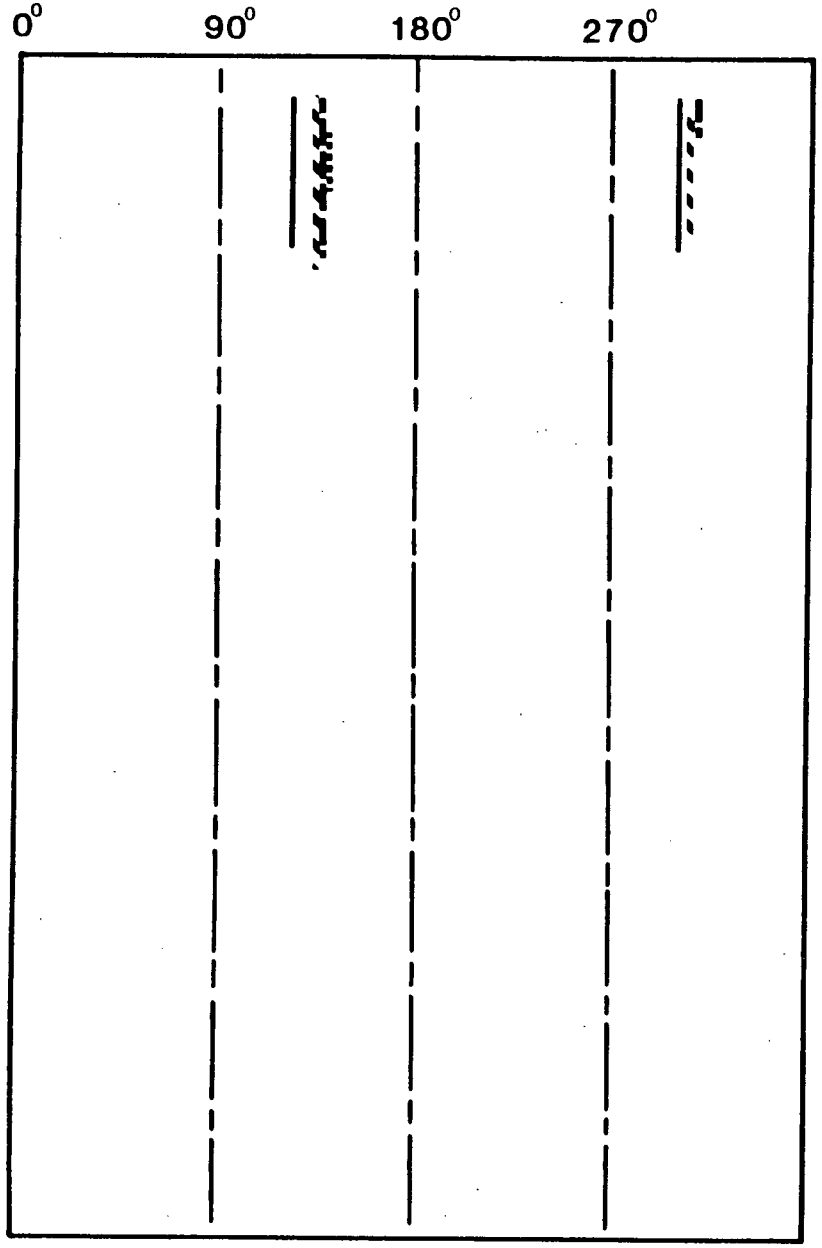

DG1 - Crankshaft main journal #9
Right oil hole

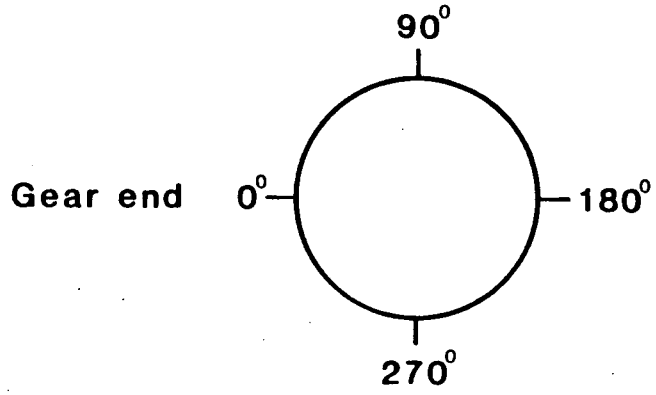

..... Hole diameter $1\frac{5}{16}$ in.

– – – Hole diameter $1\frac{3}{16}$ in.

- - - - - Hole diameter $1\frac{1}{16}$ in.

——— Hole diameter $\frac{15}{16}$ in.

FAA-84-12-14

Figure 2-3. Crack indication length at various locations and hole diameters. (Lengths to scale.)

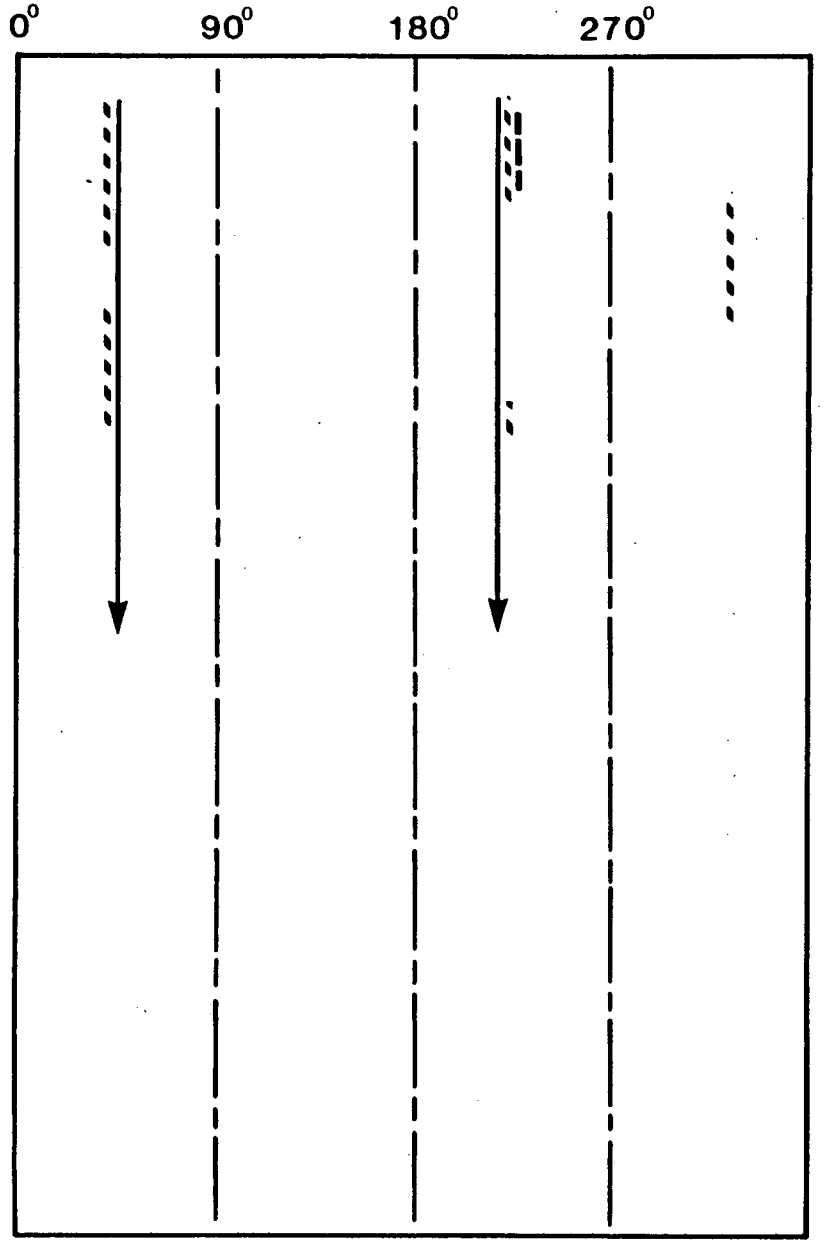

DG1 - Crankshaft main journal #10
Left oil hole

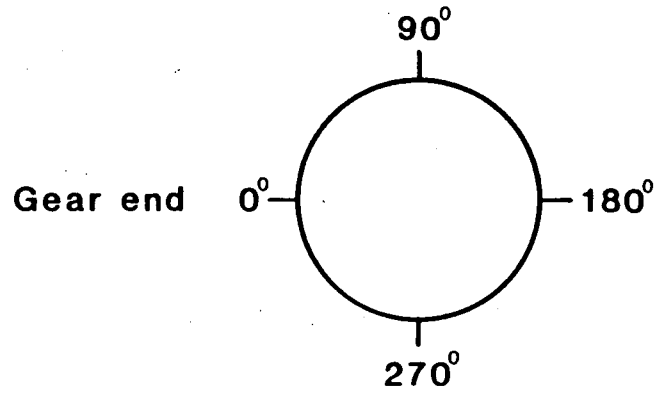

---- Hole diameter $1\frac{3}{16}$ in.

- - - - - Hole diameter $1\frac{1}{16}$ in.

——— Hole diameter $\frac{15}{16}$ in.

FAA-84-12-14

Figure 2-4. Crack indication length at various locations and hole diameters. (Lengths to scale.)

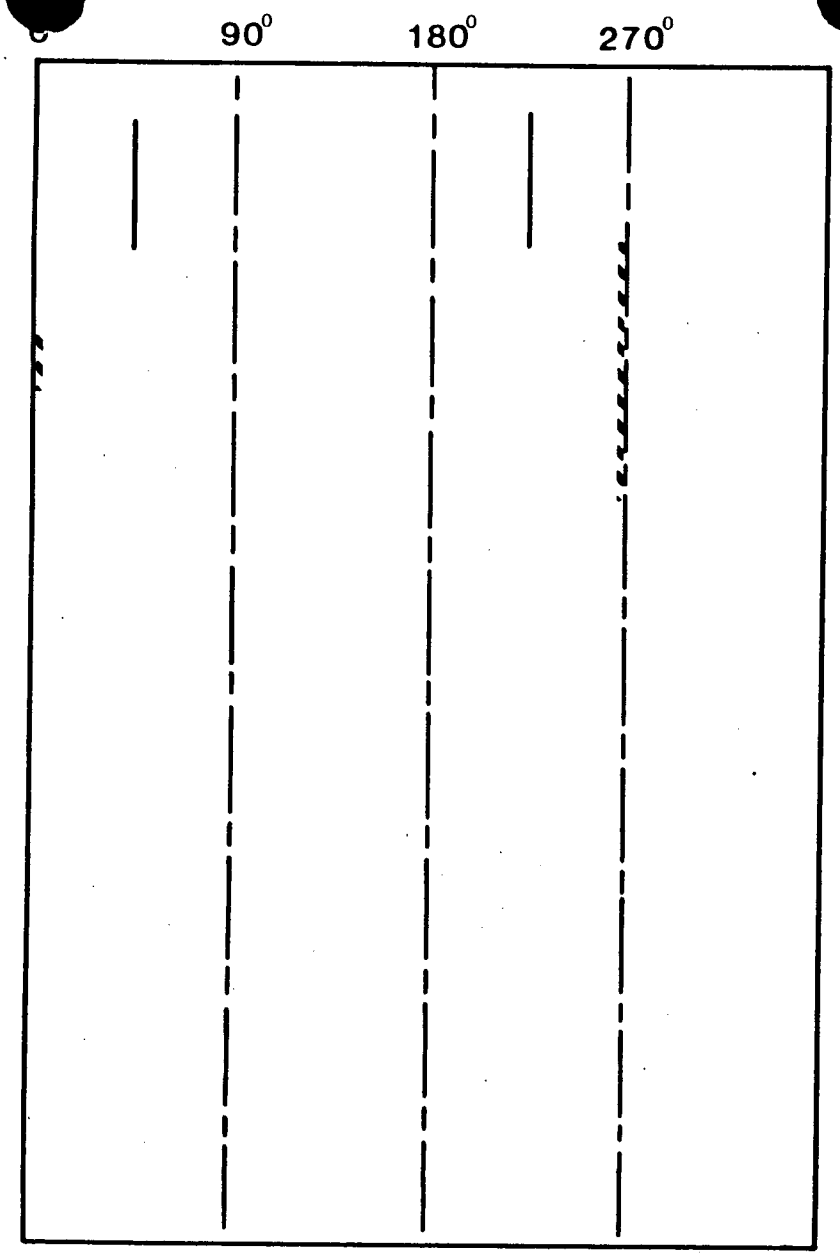

DG1 - Crankshaft main journal #10
Right oil hole

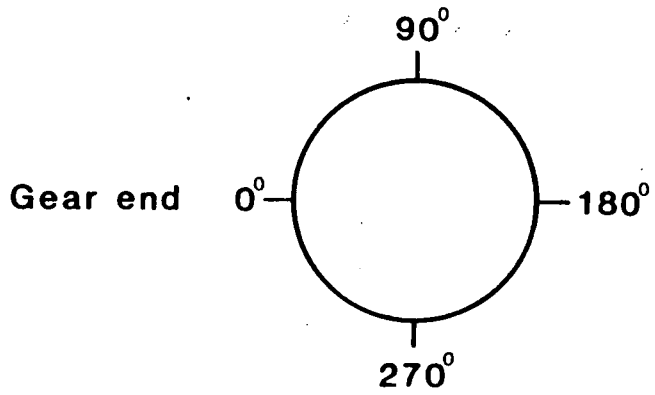

----- Hole diameter $1\frac{1}{16}$ in.

——— Hole diameter $\frac{15}{16}$ in.

FAA-84-12-14

Figure 2-5. Crack indication length at various locations and hole diameters. (Lengths to scale.)

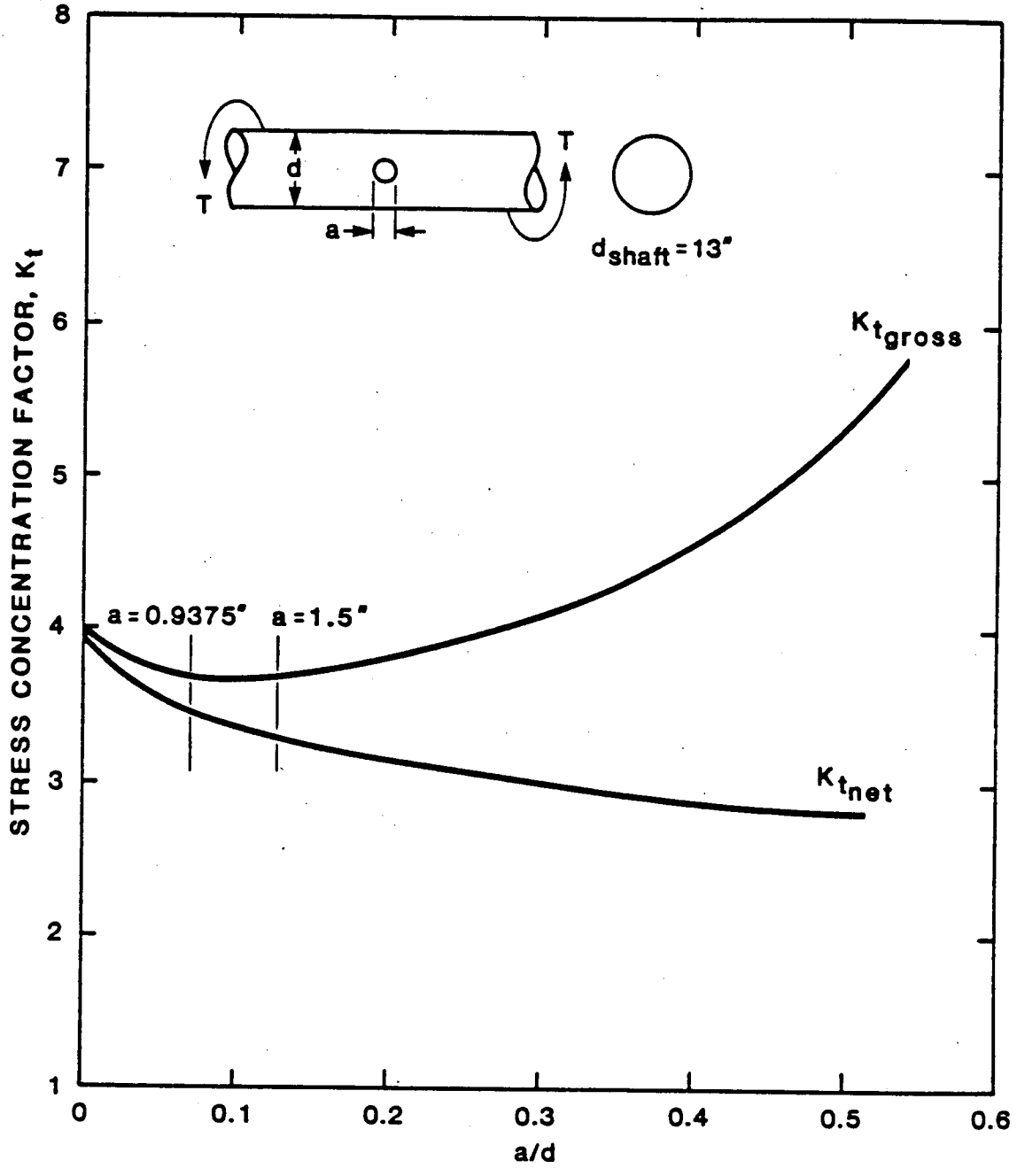

Figure 2-6. Stress concentration factor for torsion of a solid round bar with a transverse hole. Reference: "Stress Concentration Factors," R.E. Peterson, John Wiley & Sons, 1974, Figure 173.

3.0 CRANKSHAFT TESTING UNDER TRANSIENT CONDITIONS

A torsiograph test was performed on the San Onofre Emergency Standby DG1 to measure and record the angular vibration of the gear-train end of the crankshaft. Data was obtained during both steady state and transient (startup and coastdown) operation of the engine. This report deals only with the transient responses of the system. Steady state responses were addressed in a separate report [3-1].

Data was recorded during three types of transient conditions; fast start, slow start, and coastdown. The fast start and coastdown conditions monitored are the normal procedural startup and coastdowns that were in use at San Onofre. The slow start monitored was a gradual start manually controlled at the engine governor. Data was obtained for three fast starts, two slow starts, and six coastdowns.

3.1 Instrumentation and Test Set-Up

A torsiograph was mounted on the front end of the crankshaft to measure the angular vibrations of the free-end of the crankshaft as the crankshaft rotated.

During startup, the acceleration of the crankshaft causes a mean shift in the response of the torsiograph (see Figures in Appendix A). To assure that valid data would be obtained should the torsiograph exceed its limits due to this mean shift, two accelerometers were mounted on the slip ring assembly which was attached to the torsiograph. Data was obtained throughout the duration of the test. When necessary, the accelerometer data can be used to reconstruct the torsiograph signal.

Pressure transducers were mounted on the bleed ports or cylinder heads No. 8 RB and No. 8 LB to monitor pressure throughout the test [3-2].

3.2 Torsiograph Data

Torsiograph results for all transient cases monitored are presented in Appendix A.

3.2.1 Coastdown

For the coastdowns monitored, the response of the crankshaft was found to be repeatable in both shape and magnitude (see Events B, C, E, and G in Appendix A). The coastdown response is governed by three major orders as indicated in Figure 3-1 [3-3]. The three major orders and their corresponding engine speeds are shown in Table 3-1. This plot indicates that the response at the 4-1/2 and 5th order speeds is roughly the same. A plot of engine speed versus torsiograph peak-to-peak amplitude for a typical coastdown is shown in Figure 3-2. This plot verifies the speed of these critical orders.

The maximum peak-to-peak amplitude was found to be 3.2 degrees and occurs at the 4-1/2 order critical speed of 264 RPM. The approximate length of time for a coastdown is 70 seconds.

3.2.2 Slow Start

A comparison of the slow start and coastdown plots in Appendix A indicates the response during a slow start is similar to that of a coastdown (in both magnitude and peak locations). A plot of the engine speed versus torsiograph peak-to-peak amplitudes for a slow start is shown in Figure 3-3. This curve also verifies the location of the critical orders in Table 3-1. The maximum peak-to-peak amplitude is 3.4 degrees which occurs at the 5th order critical speed of 240 RPM.

The length of time for the slow start monitored is approximately 24 seconds.

3.2.3 Fast Start

The response of the crankshaft during the fast start was not repeatable. Of the three fast starts monitored, two produced similar amplitudes of 2.0 degrees peak-to-peak (Events A and F, Appendix A), while the third produced much larger amplitudes which caused the torsiograph to exceed its limits (Event D, Appendix A). The peak-to-peak amplitude for Event D was obtained from the accelerometer data and was equal to 5.0 degrees. A plot of engine

speed versus torsiograph peak-to-peak amplitudes for Event F is shown in Figure 3-4.

Two of the fast starts were performed with predetermined initial crankshaft positions. For fast start D the crankshaft starting position was with cylinder No. 8 RB at BDC exhaust stroke. For Fast start F, the crankshaft starting position was with cylinder No. 8 RB at BDC compression stroke. This represents a difference of 360 degrees of crankshaft rotation between the two starts. The ratio of the maximum peak-to-peak responses for the two cases was found to be approximately 2.5. This indicates that the response of the crankshaft is highly dependent upon the initial position of the crankshaft.

The length of time for a fast start is approximately six seconds.

3.3 Accelerometer Data

In order to obtain an independent measure of crankshaft vibration in San Onofre diesel engine tests, in addition to the torsiograph, two linear accelerometers were mounted on the free end of the crankshaft. These transducers were positioned to measure tangential acceleration of the crankshaft at a 2.75 inch radius. Their orientation was such that tangential acceleration components would be read equally, whereas any lateral vibration of the shaft would be measured as a positive amplitude on one device and a negative amplitude on the other.

Free-end displacement data was obtained from the accelerometer data by filtering, averaging and integrating.

Each accelerometer signal was independently lowpass filtered for anti-aliasing purposes. These filtered signals were then sampled at 1.5 millisecond intervals, individually scaled to account for tape channel gains and transducer gains, and then summed and divided by two to eliminate the effects of gravity and non-tangential oscillations. This signal was then high pass filtered to eliminate any DC offsets and low frequency drift. This processed acceleration data was integrated twice to obtain angular displacement and again high pass filtered to eliminate low frequency drift and initial condition effects in the integration.

3.3.1 Fast Start

An example of reconstruction of a free-end amplitude signal for fast start "F" is shown in Figure 3.5. The top trace is the torsiograph signal which has been filtered to eliminate the effect of the offset which is caused by the acceleration of the crankshaft. The bottom trace shows the accelerometer reconstruction. The correlation is good, even though the torsiograph trace is not filtered as much as the accelerometer trace. These types of comparisons were used to confirm the reconstruction technique.

The free-end amplitude for fast start "D" had to be reconstructed from accelerometer data because the torsiograph signal went beyond the range of the instrument. The reconstruction is shown in Figure 3.6 and shows a peak-to-peak amplitude of 5.0 degrees.

3.4 Pressure Data

All pressure data used were taken from cylinder 8 LB, because cylinder 8 RB produced a noisy signal.

3.4.1 Coastdown

During coastdown the pressure loading is due to cold compression. The peak pressure during coastdown was measured to be approximately 450 psi.

3.4.2 Slow Start

The peak pressure during a slow start is approximately 1100 psi initially and slowly decays until steady-state conditions are reached.

3.4.3 Fast Start

The pressure as a function of time is shown in Figures 3.7, 3.8 and 3.9 for fast starts "A", "D", and "F" respectively. The peak pressure is approximately 1340 psi. All fast starts exhibit approximately the same peak pressure envelope; however, fast start "D" does show an extended period of high pressure. This start does also produce the highest stresses.

3.5 Summary

- The coastdown and slow start transient conditions have similar responses with peak-to-peak amplitudes of approximately 3.3 degrees.

- The response during a fast start is dependent upon the initial position of the crankshaft. The peak-to-peak amplitude is 2.0 degrees with cylinder No. 8 RB at BDC compression stroke initially and 5.0 degrees with cylinder No. 8 RB at BDC exhaust stroke initially.

- The peak-to-peak steady-state response was approximately 0.34 degrees [3-1].

Section 3 References

3-1 "Torsiograph Test of Emergency Diesel Generator #1 at San Onofre Nuclear Generating Station", FaAA 84-10-9, October 12, 1984.

3-2 "Torsiograph and Pressure Test Procedure for TDI DSRV-20-4 13-inch By 13-inch Crankshaft at San Onofre Nuclear Station", September 1984, Prepared by Owners Group.

3-3 Yang, Roland, "Torsional and Lateral Critical Speed, Engine Number 75041/42 Delaval Enterprise Engine Model DSRV-20-4 6000 kW/8303BHP at 450 RPM for Southern California Edison Company; Transamerica Delaval Inc., Engine and Compressor Division, Oakland, California, October 22, 1975, Updated.

Table 3-1
Resonant Speeds for Major Orders

Engine Speed (RPM)	Order
217	5 1/2
240	5
264	4 1/2

Southern California Edison Company
#75041/42
DeLaval Enterprise DSRV-20-4
8303 BHP 6000 kw at 450 rpm 153-3 BMEP
2 CTWT (02-310-08-AJ) per crankthrow, 90x3 3/4 flywheel

I-10 Represents 1st mode resonance with 10th order loading
II-9 1/2 Represents 2nd mode resonance with 9 1/2 order loading

*Nominal stress in 13" diameter shaft between cylinder 10 and flywheel.

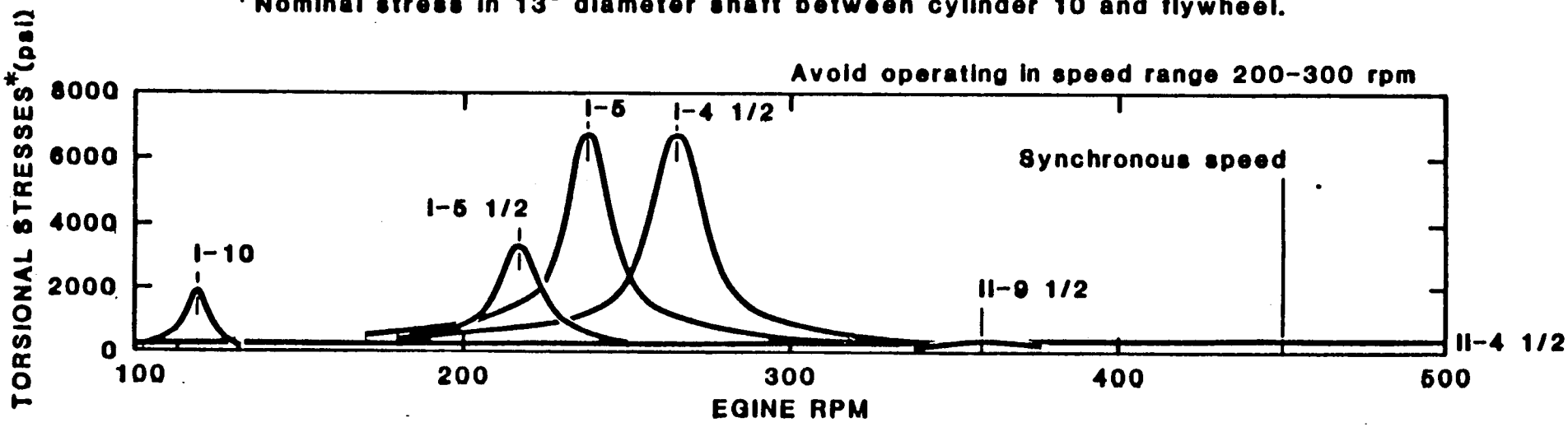

Figure 3-1. Results of TDI torsional analysis (Ref. 3-3).

FaAA-84-12-14

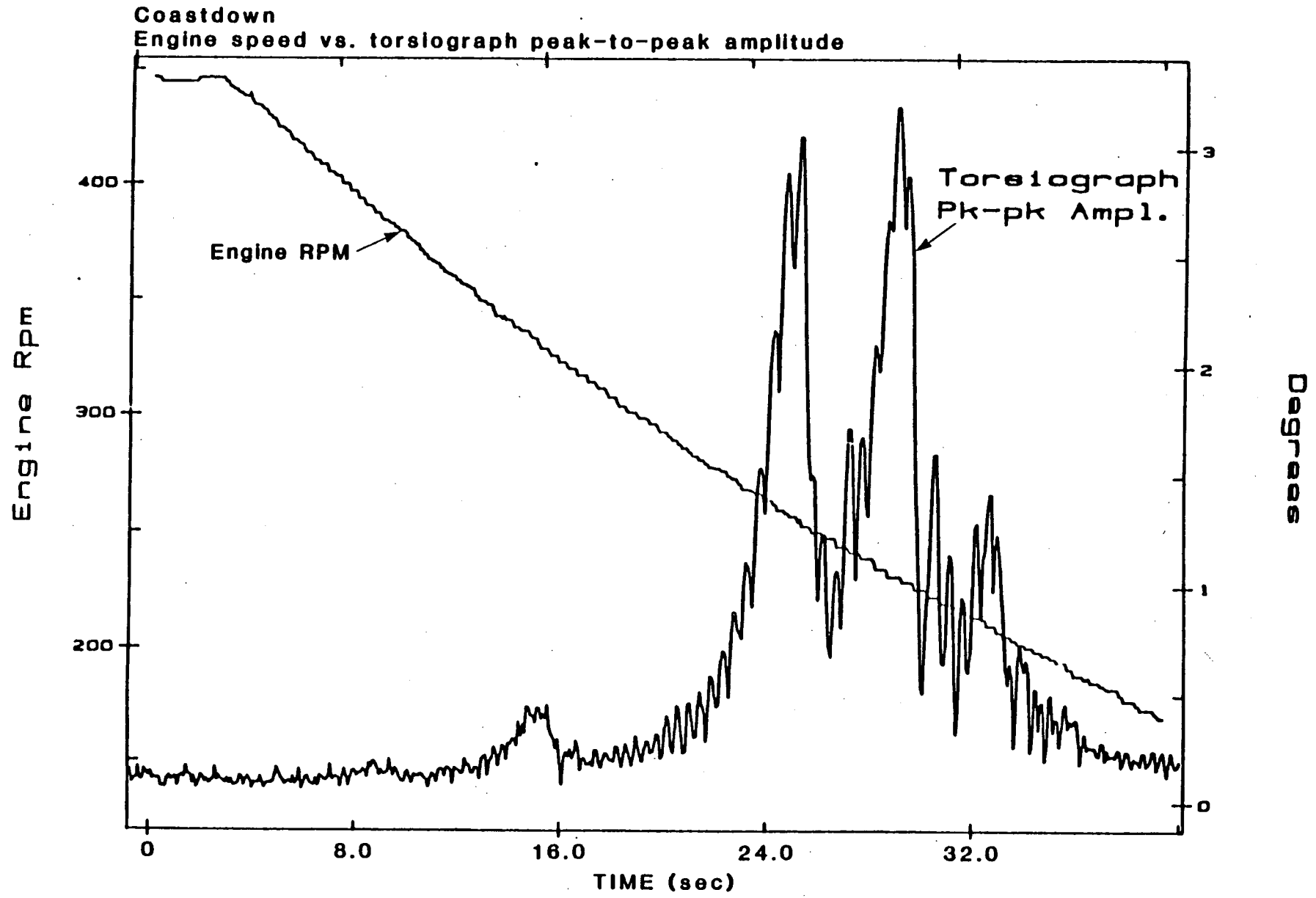

FAA-84-12-14

Figure 3-2. Typical coastdown response.

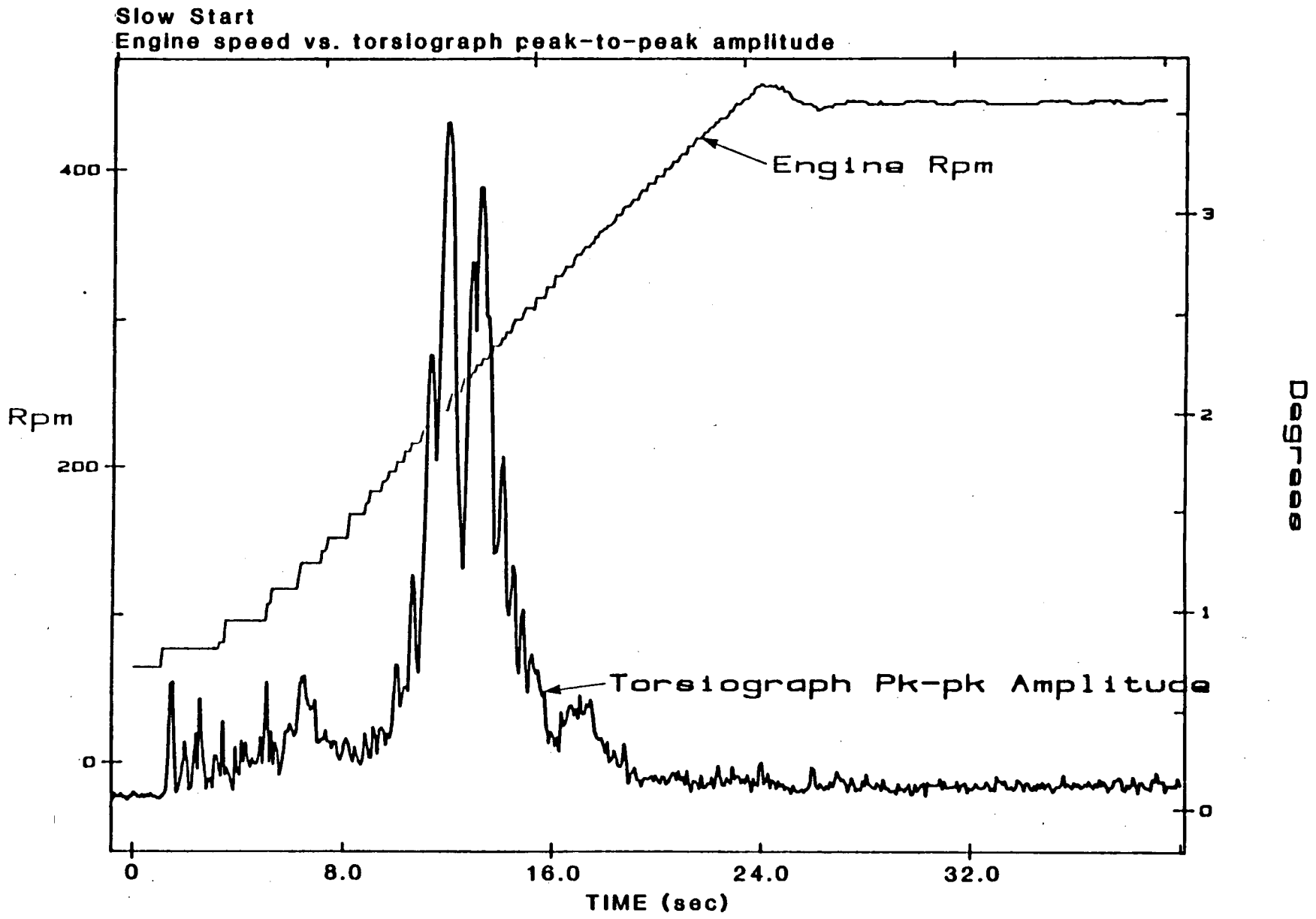

FsAA-84-12-14

Figure 3-3. Typical slow start response.

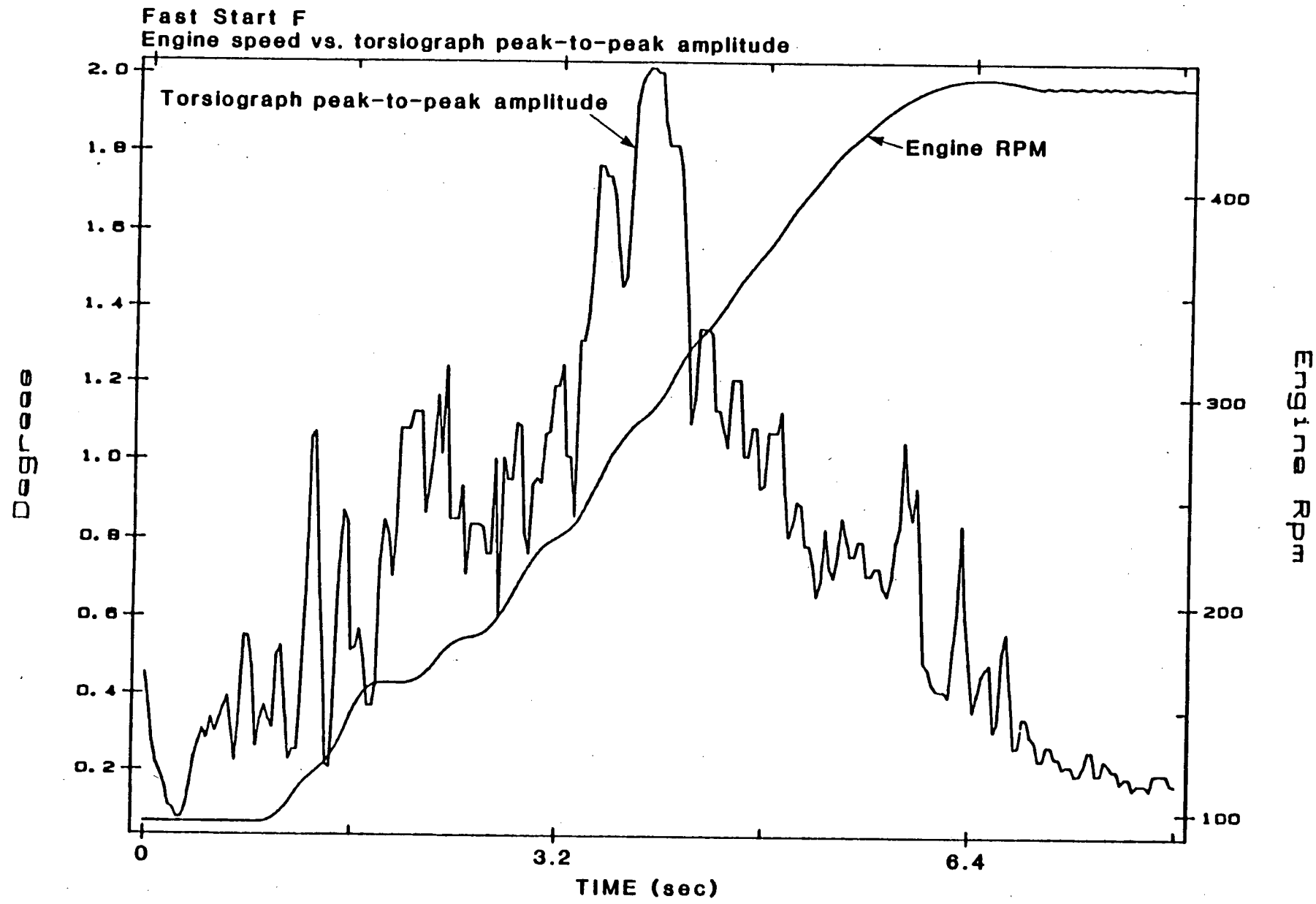

FAA-84-12-14

Figure 3-4. Fast start, initial crankshaft position with 8 RB at BDC compression.

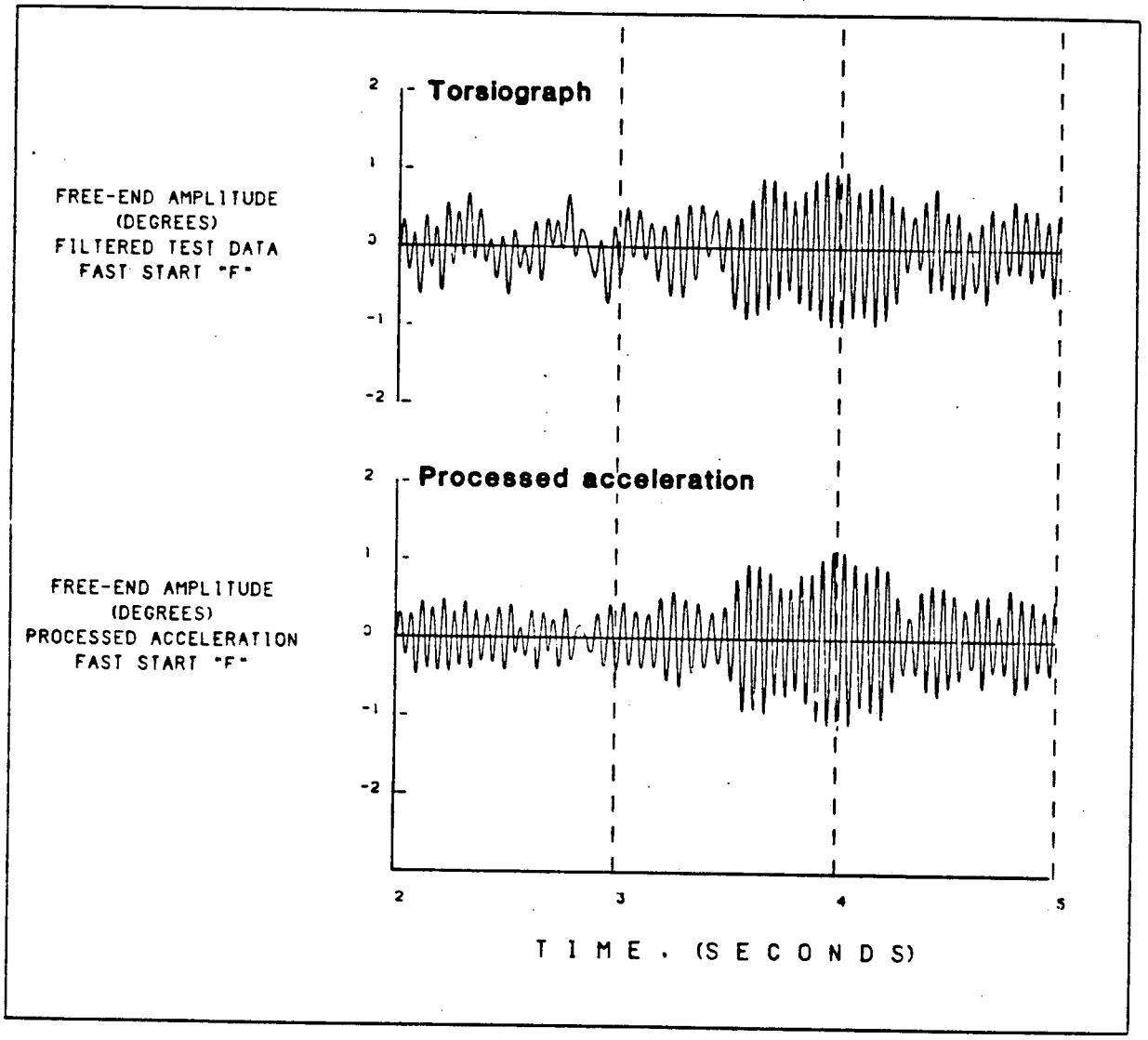

Figure 3-5. Accelerometer reconstruction of fast start "F".

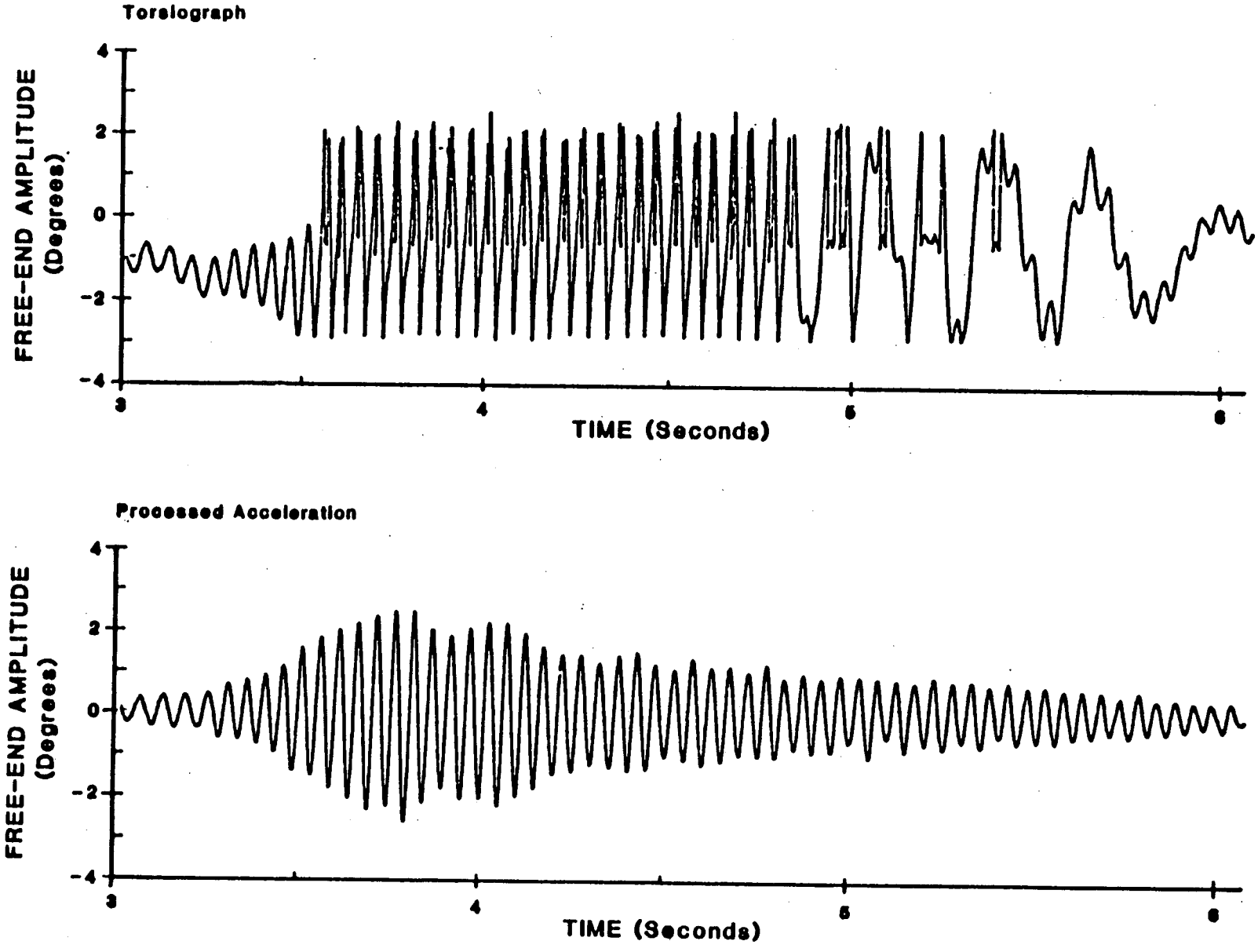

Figure 3-6. Accelerometer reconstruction of fast start "D".

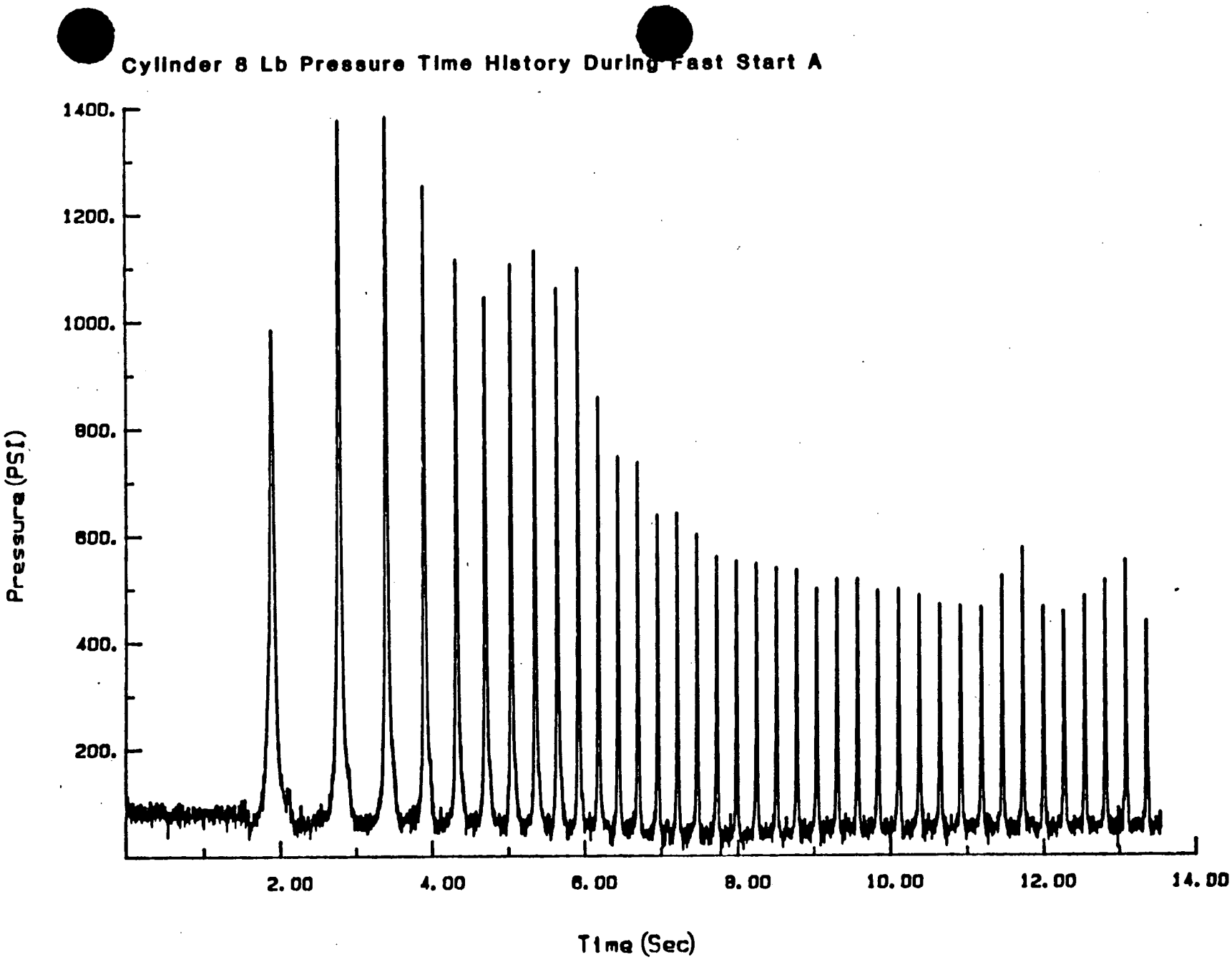

Figure 3-7. Pressure loading during fast start A.

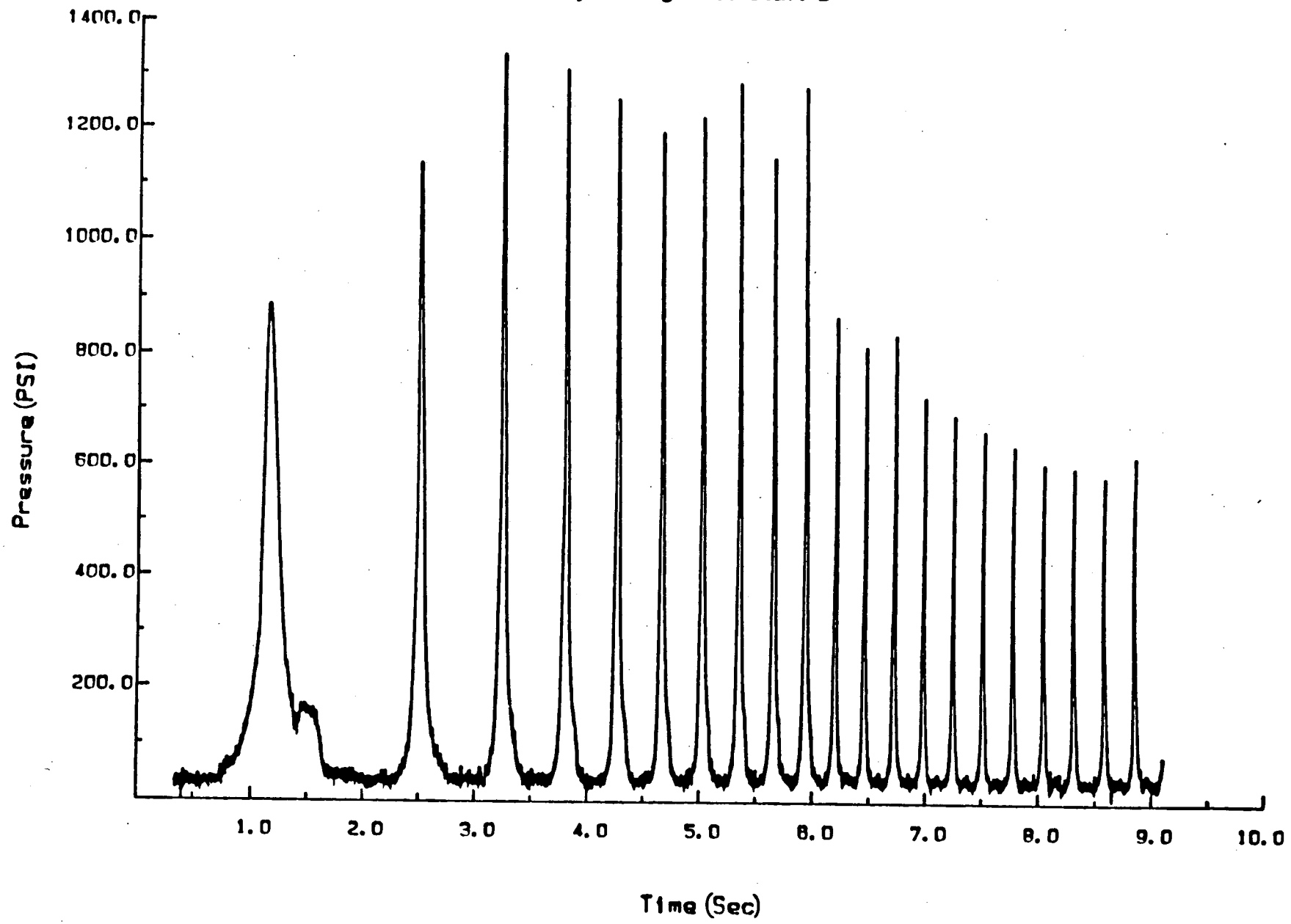

FAA-84-12-14

Figure 3-8. Pressure loading during fast start D.

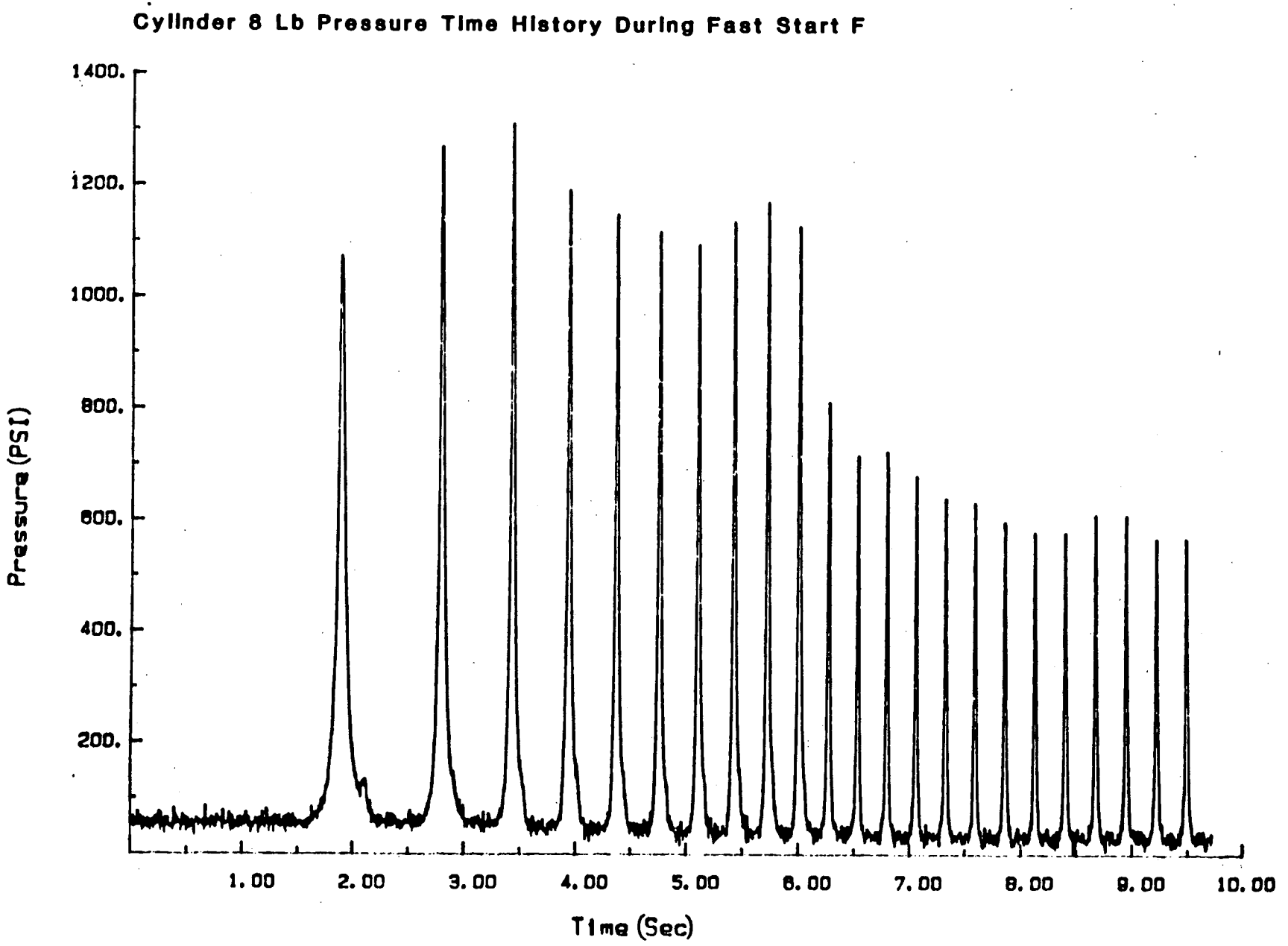

Figure 3-9. Pressure loading during fast start F.

4.0 TORSIONAL ANALYSIS OF CRANKSHAFT FOR START-UP AND COASTDOWN TRANSIENTS

The torsiograph testing of transient conditions provides the free-end rotational vibration as a function of time. To determine the nominal torsional stress at a given main journal location it is necessary to convert from free-end rotational vibration to this stress. This conversion is easily made if the shaft is responding purely in a single mode. However, single mode response is often not a good assumption, particularly for a long crankshaft such as those in a DSRV-20. This problem may be overcome by developing an analytical model which predicts the stress as a function of time at each shaft section as well as the free-end rotational vibration. This model also has the advantage that it may easily be used to predict the response for transient conditions other than those tested.

4.1 Dynamic Model for Transient Analysis

A 13 degree of freedom idealized lumped inertia and torsional spring model, shown in Figure 4-1, was used. The inertia and stiffnesses were computed by TDI [4-1] and are shown in Table 4-1.

The first step in the solution of the equations of motion is to determine the natural frequencies and modes of vibration. This was done by solving the undamped eigenvalue problem to determine the normal modes [4-2]. The natural frequencies are shown in Table 4-2 for the first three modes [4-3] and are compared with torsiograph test data for the first two modes [4-4]. This excellent comparison indicates the accuracy of the TDI inertias and stiffnesses.

The second step is to determine the time dependent response of the crankshaft. This step is performed by using modal superposition with step-by-step response calculations [4-2]. The pressure and inertia loading at each time step is calculated for each cylinder (or inertia). This loading is converted to applied torque at each cylinder. The loading is then transformed to normal (or modal) coordinates by pre-multiplying the load vector by the transpose of the eigenvector matrix.

In normal coordinates, solutions to each mode at each time step may be obtained using Duhamel's integral with linear load variation during the time

step. In this approach modal damping is employed. At each time step the response of the inertias is calculated by multiplying the normal displacements by the eigenvector matrix.† Torques in each shaft are calculated by multiplying the relative rotation across a shaft by its stiffness. Nominal torsional stresses, τ, are calculated from torques, T, by the equation $\tau = Tr/J$ where r is the journal radius and J is its polar moment of inertia.

Reciprocating inertial loads were calculated using a reciprocating mass of 820 pounds in both left and right bank cylinders. The inertial torques are calculated at each time step and depend on the current angular velocity, ω, and current crank throw orientation, θ, for each cylinder.

The pressure loads for coastdown and startup were calculated from cylinder pressure test measurements by two different approaches. In the first approach, a pressure versus crank angle curve for a given cylinder is assumed to be repeated every two crankshaft revolutions. This condition prevails for coastdown where a cold compression curve repeats itself. The pressure torques are then calculated at each time step and depend on the pressure and the crank angle.

In the second approach, a pressure trace versus time from test data in one cylinder for the duration of the transient is used directly. This condition is suitable for starts where the peak pressure does not remain uniform from cycle to cycle. The pressure at each other cylinder for each time step is interpolated from the one pressure trace provided.

4.2 Coastdown Analysis

The coastdown analysis was performed using a cold compression curve with a peak pressure of 450 psi. The coastdown was assumed to take 70 seconds and it was further assumed that the angular velocity reduced linearly from 450 rpm to 0 rpm during this time. The test data shown in Section 3 shows that this is approximately true, although a more accurate representation of rate of

---

† The eigenvector matrix is made up of columns containing mode shapes which have been normalized with respect to the mass matrix.

decay of angular velocity would be parabolic. It was found that with a damping of 0.6 percent of critical modal damping in each mode, the amplitude of response was in good agreement with test measurements. This damping represents a dynamic magnification factor of 83. The time step algorithm was executed using a step size of three degrees rotation of the crankshaft.

The time history of free-end response, cylinder pressure, and nominal torsional stress on each main journal is shown in the fold out print in Appendix B. The maximum free-end response is found to have a range of 3.25 degrees peak-to-peak. The portions that show resonance with the 5.5, 5.0 and 4.5 orders of loading and first mode of the crankshaft are clearly visible. By counting the number of cycles per second one may determine that the shaft is vibrating at approximately 20 cycles per second, which indicates a largely first mode response.

The nominal torsional stress ranges for each main journal location are shown in Table 4-3. The maximum amplitude of nominal torsional stress is 11.86 ksi in main journal number 10. The stresses in main journals 8 through 11 are very nearly as high.

A comparison of the predicted and measured free-end amplitude time histories is shown in Figure 4-2. The good comparison of dynamic features is readily apparent in these plots. The time of occurrence of some features are shifted in the analysis due to the assumed change of angular velocity with time. There is close correspondence of these features between test and analysis with respect to angular velocity.

4.3 Startup Analysis

The startup analysis was performed using the pressure-time data recorded in 8 LB during fast start D. The pressure at other cylinders was obtained by interpolation from the recorded pressure-time trace. A conservative damping value of 0.6 percent of critical modal damping in each mode was used. This damping represents a dynamic magnification factor of 83. A uniform time step of 0.00074 seconds was used for the numerical integration procedure.

4.3.1 Fast Starts A and F

The initial starting position of the crankshaft was varied to represent the different fast start conditions measured. Fast starts "A" and "F" occurred with cylinder 3RB at BDC of its exhaust stroke. The free-end vibration obtained from the analytical model is compared to the test data in Figure 4.3. The first two traces in the figure contain test data which has been high pass filtered to eliminate the offset caused by torsiograph distortion due to acceleration of the crankshaft. There is closer agreement between the model and fast start "F" than there is with fast start "A". However, all three traces produce peak-to-peak vibrations of approximately the same magnitude.

The time history of free-end response, cylinder pressure, and nominal torsional stress on each main journal is shown in the fold-out print in Appendix C. The maximum free-end response is calculated to have a range of 2.0 degrees peak-to-peak which is the same as the peak-to-peak value obtained from the test data.

The nominal torsional stress ranges for each main journal location are shown in Table 4-4. The maximum amplitude of nominal torsional stress is 9.17 ksi in main journals number 9 and 10. The stresses in main journals 8, 11, and 12 are very nearly as high.

4.3.2 Fast Start D

This fast start was modeled with cylinder 8 RB at BDC of its exhaust stroke. The free-end vibration obtained from the analytical model is compared to the test data in Figure 4.4. The two traces in the figure show excellent agreement with the analysis calculating a peak-to-peak vibration of 5.1 degrees and the accelerometer data showing 5.0 degrees. The mean value of vibration angle was filtered out of the test data by high pass filtering to eliminate low frequencies associated with the crankshaft acceleration during startup.

4.3.3 Effect of Initial Crankshaft Position on Response

Ten fast start analyses were performed with the crankshaft's initial position altered by 72 degrees each time, thereby covering two revolutions (720 degrees) of the crankshaft. The peak-to-peak vibration from each of these conditions is shown in Figure 4.5. It is seen that the start with the lowest vibration occurs when startup occurs with cylinder 3 RB at BDC during its exhaust stroke. This condition has been measured twice and was previously referred to as fast starts "A" and "F".

Fast start "D" produces a high level of vibration and is modeled by having cylinder 8 RB start at BDC in its exhaust stroke.

The highest level of vibration (5.6 degrees peak-to-peak) is obtained with cylinder 10 RB starting at BDC in its exhaust stroke. The time history of free-end response, cylinder pressure, and nominal torsional stress on each main journal is shown in the fold-out print in Appendix D.

The nominal torsional stress ranges for each main journal location are shown in Table 4-5. The maximum amplitude of nominal torsional stress is 20.79 ksi in main journal number 10. The stresses in main journals 8 through 12 are very nearly as high.

4.3.4 Effect of Duration of Fast Start on Response

The analytical model of the crankshaft was used to determine the effect of varying the duration of the fast start on the response. Since pressure data for different length starts was not available, a single full load pressure curve was used and timed so that a linear increase in speed from 0 to 450 RPM was obtained. The analysis was repeated for 10 initial crankshaft positions for each of three start durations (5, 6 and 7 seconds). Figure 4-6 shows the response for over 30 cases analyzed. The absolute value of peak-to-peak vibration is not meaningful, since a full load pressure curve is not used during startup, so only relative peak-to-peak vibrations are shown in the figure. The figure shows that the highest peak-to-peak vibration is independent of startup duration for the range of startup durations considered.

However, the initial crankshaft starting position which produces the highest vibration is highly dependent on the startup duration. In fact, with cylinder 3 RB starts at BDC of its exhaust stroke, the response is a minimum for a 6 second start but a maximum for a 5 or 7 second start.

When cylinder 10 RB starts at BDC of its exhaust stroke, the effect of length of start on response is shown in Figure 4.7. Figures 4.6 and 4.7 show that the duration of start must be kept within ±0.5 seconds in order to control fast start response when an initial starting position is chosen.

4.4 Summary

- The transient analysis model can be used to adequately predict response of the crankshaft during startup and coastdown.
- Nominal torsional stresses during coastdown have a maximum amplitude of 11.86 ksi.
- Response of crankshaft during startup is dependent on the initial crankshaft position and duration of fast start.
- Nominal torsional stresses during a fast start have a maximum amplitude of between 9.17 ksi and 20.79 ksi depending on the initial crankshaft position.

Section 4 References

4-1 Yang, Roland, "Torsional and Lateral Critical Speed Analysis, Engine Numbers 75041/41 Delaval Enterprise Engine Model DSRV-20-4, 6000 KW/8303 BHP at 450 RPM", for Southern California Edison Company, Delaval Engine and Compressor Division, Oakland, California, October 22, 1975.

4-2 Timoshenko, S., Young, D. H., and Weaver, W. Jr., Vibration Problems in Engineering, 4th Edition, John Wiley and Sons, 1974.

4-3 "Evaluation of Emergency Diesel Generator Crankshafts at Midland and San Onofre Nuclear Generating Stations," Failure Analysis Associates, Report FaAA-84-6-54, June 1984.

4-4 "Steady-State Torsiograph Test of Emergency Diesel Generator #1 at San Onofre Nuclear Generating Station," Failure Analysis Associates, Report FaAA-84-10-9, October 1984.

Table 4-1

Stiffness and Inertias for Torsional Dynamic Analysis
of DSRV-20-4 13-Inch By 13-Inch Crankshaft at San Onofre

Inertia Location	Inertia (lb. ft. sec^2)	Stiffness (ft. lb./rad)
Front Gear	11.8	53.2×10^6
Cylinder No. 1	143.1	101.9×10^6
Cylinder No. 2	141.6	101.9×10^6
Cylinder No. 3	141.6	101.9×10^6
Cylinder No. 4	141.6	101.9×10^6
Cylinder No. 5	141.6	101.9×10^6
Cylinder No. 6	141.6	101.9×10^6
Cylinder No. 7	141.6	101.9×10^6
Cylinder No. 8	141.6	101.9×10^6
Cylinder No. 9	141.6	101.9×10^6
Cylinder No. 10	144.5	72.7×10^6
Flywheel	1503.9	485.6×10^6
Generator	11114.3	

Table 4-2

Torsional Natural Frequencies of DSRV-20-4
13-Inch by 13-Inch Crankshaft at San Onofre

Mode	Natural Frequency (Hz)	
	Torsiograph Test	Dynamic Analysis
1	19.7	19.9
2	56.4	56.7
3	--	90.0

Table 4-3

Nominal Torsional Stresses During Coastdown

Main Journal		Nominal torsional Stress (ksi)	
Location	Designation	Maximum	Minimum
Between Cylinder 1 and Cylinder 2	2	2.35	-2.34
Between Cylinder 2 and Cylinder 3	3	4.31	-4.52
Between Cylinder 3 and Cylinder 4	4	6.15	-6.07
Between Cylinder 4 and Cylinder 5	5	7.31	-7.37
Between Cylinder 5 and Cylinder 6	6	8.65	-8.34
Between Cylinder 6 and Cylinder 7	7	9.90	-9.68
Between Cylinder 7 and Cylinder 8	8	10.98	-10.97
Between Cylinder 8 and Cylinder 9	9	11.47	-11.72
Between Cylinder 9 and Cylinder 10	10	11.66	-12.06
Between Cylinder 10 and the Flywheel	11-12	11.70	-11.91

Table 4-4

Nominal Torsional Stresses During Fast Start
With 3 RB Initial Position at BDC Exhaust Stroke

Main Journal Location	Main Journal Designation	Nominal torsional Stress (ksi) Maximum	Nominal torsional Stress (ksi) Minimum
Between Cylinder 1 and Cylinder 2	2	3.90	-2.25
Between Cylinder 2 and Cylinder 3	3	5.68	-3.63
Between Cylinder 3 and Cylinder 4	4	6.80	-4.70
Between Cylinder 4 and Cylinder 5	5	6.62	-4.47
Between Cylinder 5 and Cylinder 6	6	7.47	-3.79
Between Cylinder 6 and Cylinder 7	7	9.22	-4.65
Between Cylinder 7 and Cylinder 8	8	10.29	-5.14
Between Cylinder 8 and Cylinder 9	9	11.74	-6.60
Between Cylinder 9 and Cylinder 10	10	11.91	-6.43
Between Cylinder 10 and the Flywheel	11-12	11.63	-4.31

Table 4-5

Nominal Torsional Stresses During Fast Start
With 10 RB Initial Position at BDC Exhaust Stroke

Main Journal		Nominal torsional Stress (ksi)	
Location	Designation	Maximum	Minimum
Between Cylinder 1 and Cylinder 2	2	5.73	-4.05
Between Cylinder 2 and Cylinder 3	3	9.41	-7.63
Between Cylinder 3 and Cylinder 4	4	12.43	-9.38
Between Cylinder 4 and Cylinder 5	5	14.40	-12.22
Between Cylinder 5 and Cylinder 6	6	15.67	-13.16
Between Cylinder 6 and Cylinder 7	7	18.87	-14.22
Between Cylinder 7 and Cylinder 8	8	21.57	-16.73
Between Cylinder 8 and Cylinder 9	9	22.83	-18.54
Between Cylinder 9 and Cylinder 10	10	23.17	-18.42
Between Cylinder 10 and the Flywheel	11-12	23.82	-16.74

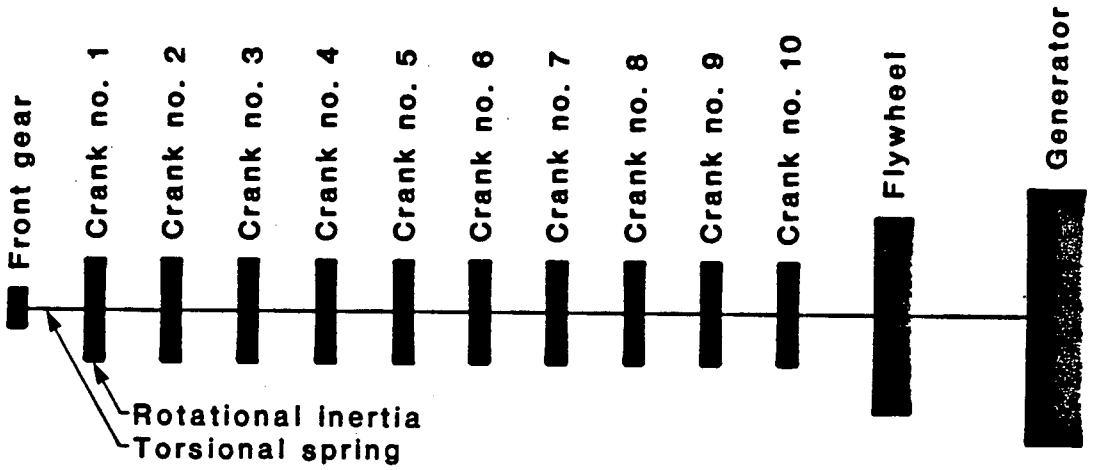

Figure 4-1. Dynamic model of DSRV-20-4 13-inch by 13-inch crankshaft at San Onofre.

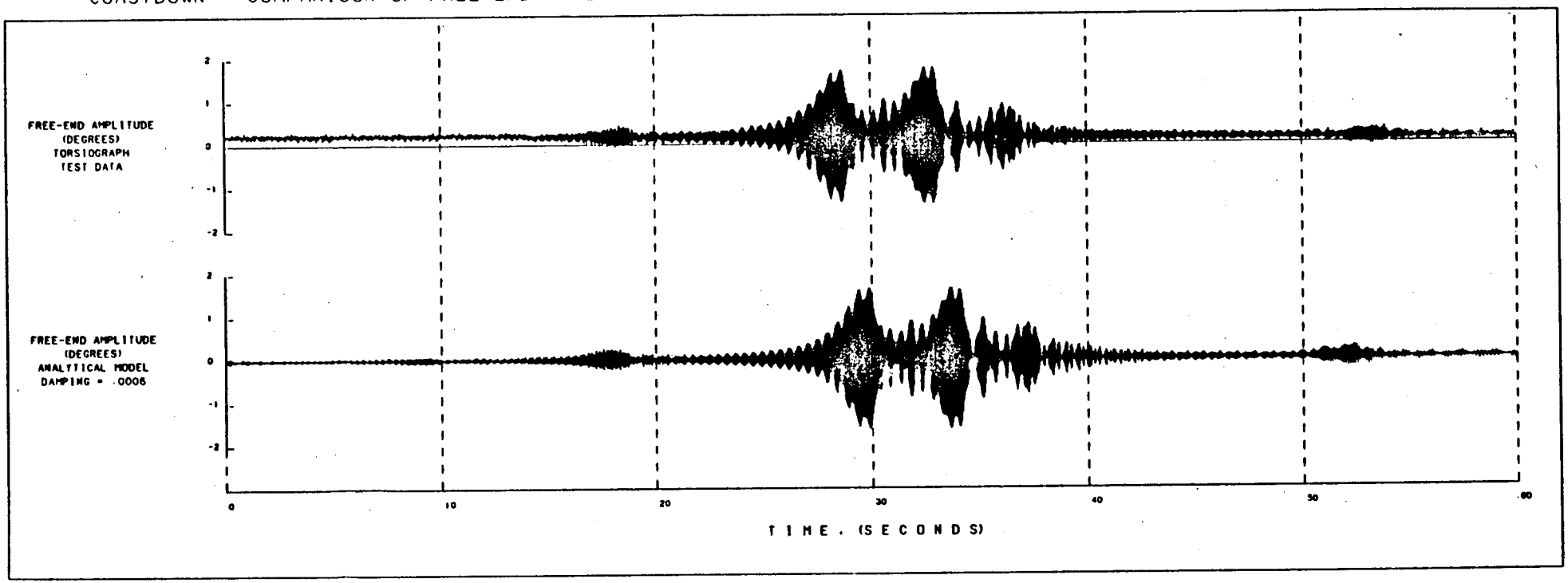

Figure 4-2. Comparison of test data and analytical model results for coastdown.

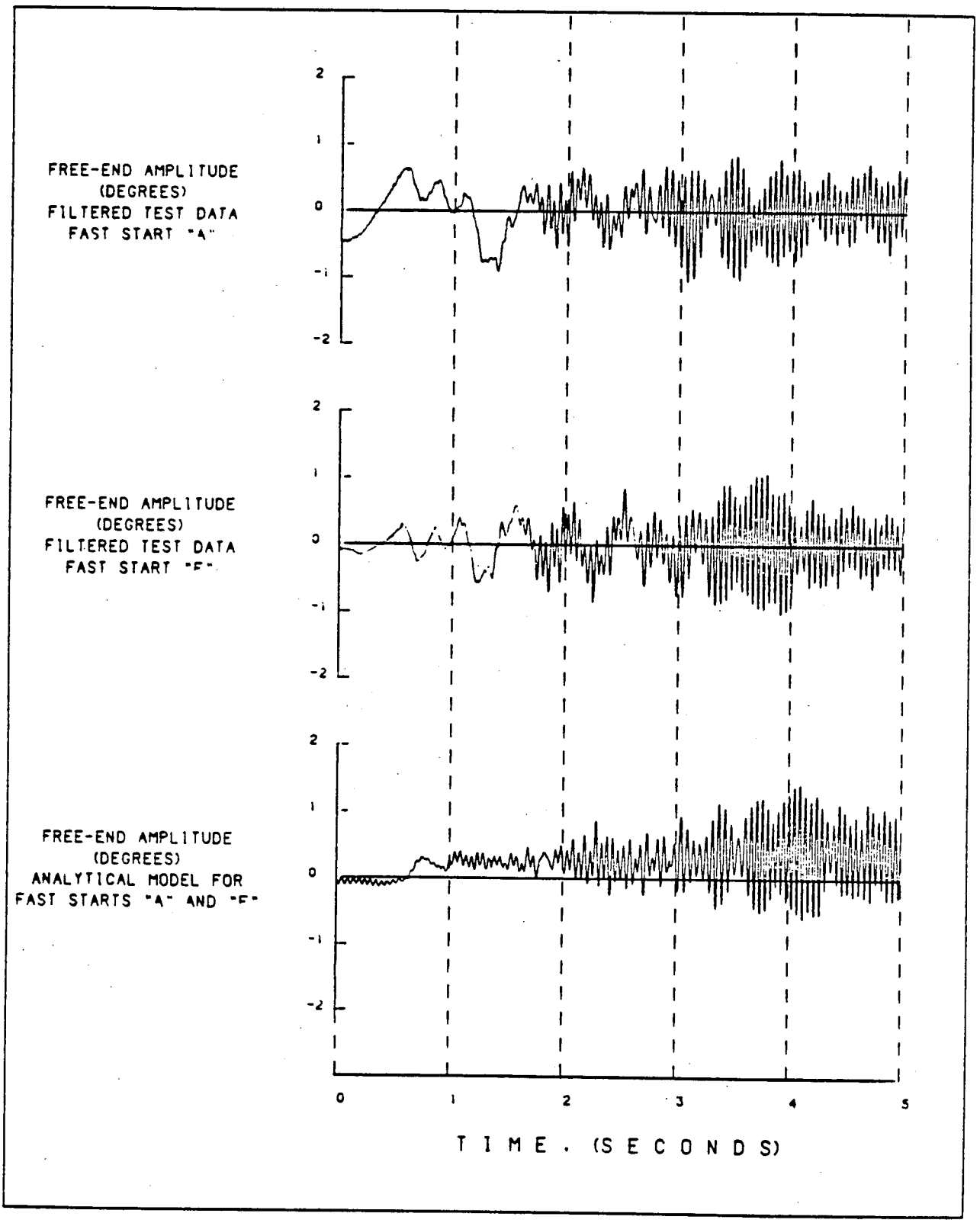

Figure 4-3. Comparison of test data and analytical model results for fast starts "A" and "F".

SOUTHERN CALIFORNIA EDISON - SAN ONOFRE - START-UP
COMPARISON FREE-END AMPLITUDES

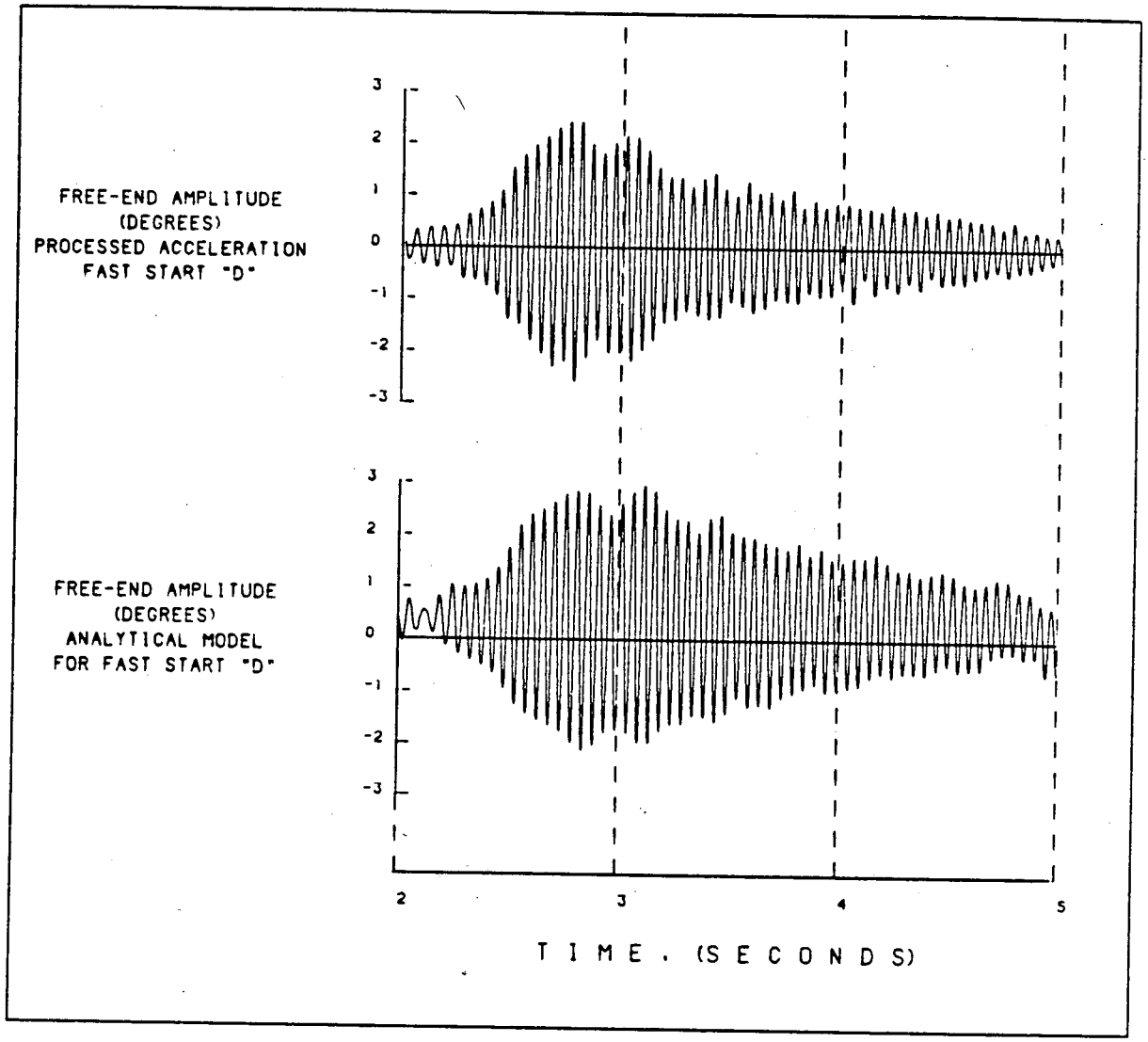

Figure 4-4. Comparison of test data and analytical model results for fast start "D".

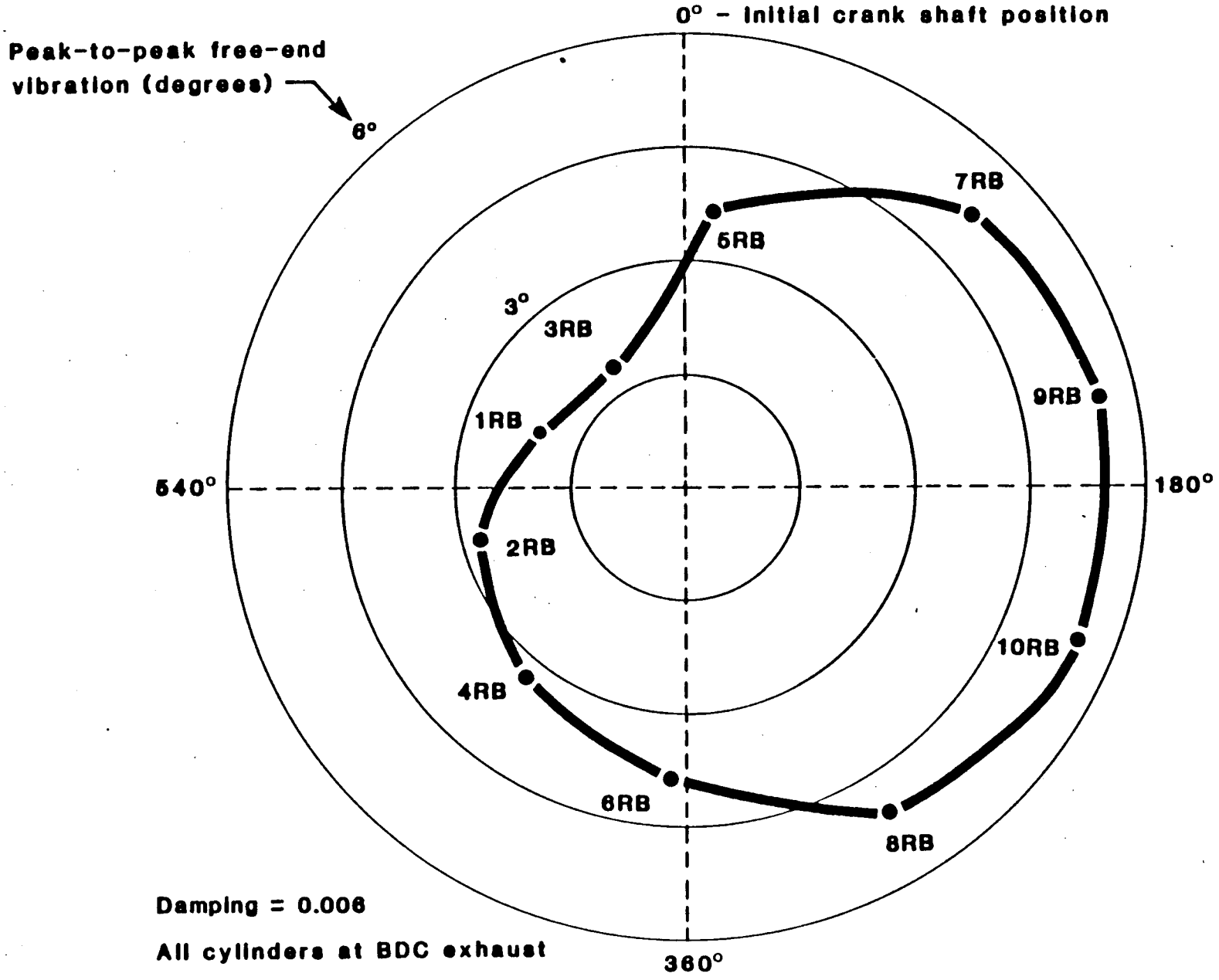

FaAA-84-12-14

Figure 4-5. Effect of initial crankshaft position on free-end vibration during a fast start.

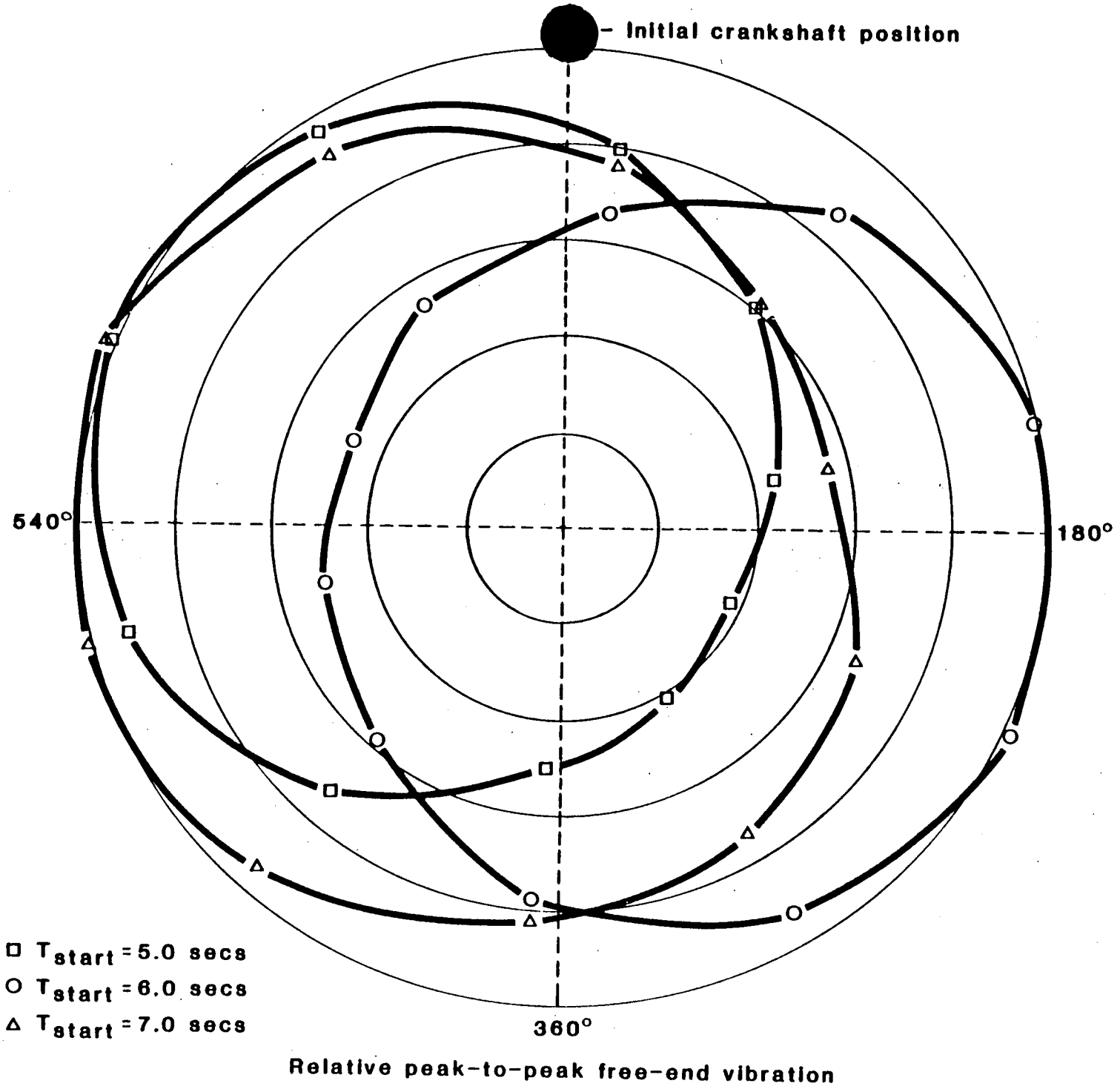

FAA-84-12-14

Figure 4-6. Effect of initial crankshaft and length of fast start on free-end vibration during a fast start.

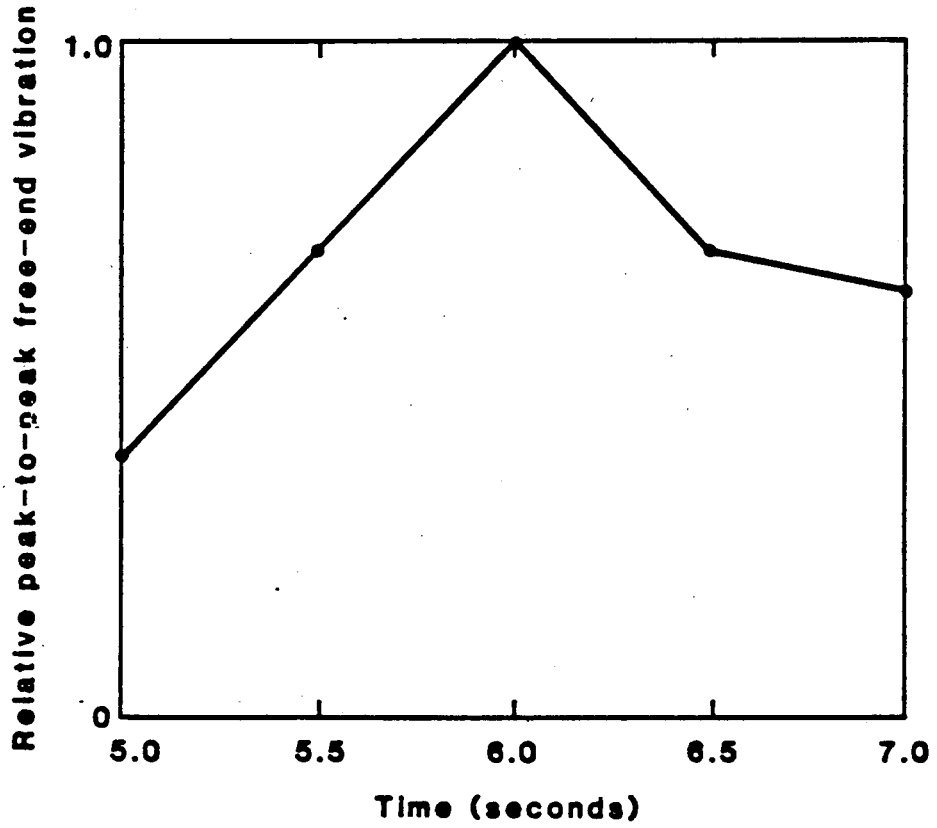

Figure 4-7. Effect of length of fast start on free-end vibration for 10RB initial position at BDC exhaust stroke.

5.0 FRACTURE MECHANICS ANALYSIS

In this section the nominal torsional stresses calculated in Section 4 will be used to estimate crack growth rates. The influence of changes in the crack model, crack growth law, and residual stresses on crack growth rates will be determined. By comparing the results of this analysis with San Onofre field experience, estimates of life and recommendations of inspection intervals will be made.

5.1 Stress Distribution Around Oil Holes

The nominal torsional stresses calculated in Section 4 must be multiplied by a stress concentration factor k_t, to obtain the actual stresses near the hole. A contour plot showing the distribution of k_t, for main journal oil holes 2 through 11, as a function of depth from the journal surface and distance from the oil hole centerline is shown in Figure 5.1. The distribution of k_t on the surface was obtained from a finite element model of this geometry with axial symmetry about the oil hole centerline. An axisymmetric tensile stress was applied at a distance of 3 inches from the centerline of the oil hole. This stress increased from zero at the journal centerline to unity at the journal surface. The distribution of k_t on the surface was calculated from the axisymmetric k_t by multiplying by 2 to account for the difference in k_t between a plate with a hole in biaxial tension (axisymmetric tension) and a plate with a hole in shear. The distribution of k_t at depth x from the journal surface and distance y from the oil hole centerline is then given by

$$k_t(x,y) = \left(1 + \frac{3\ r^4}{y^4}\right)\left(\frac{k_t(x)}{4}\right) \quad \text{for } 0 < x < 0.7 \text{ inches}$$

$$k_t(x,y) = \left(1 + \frac{3\ r^4}{y^4}\right)\left(\frac{R - x}{R}\right) \quad \text{for } 0.7 < x < R$$

where r is the oil hole radius

R is the main journal radius

$k_t(x)$ is obtained on the surface from the finite element model.

The first term in these equations gives the radial decay of hoop stress for a plate with a hole in shear. The second term represents the nominal stress as a function of depth from the surface. Thus, the maximum principal stress is approximately 4 times the nominal shear stress on the oil hole surface in the blend radius. This stress decays approximately linearly with depth from the journal surface.

The distribution of k_t on the surface of the holes in main journal 12 was also obtained from a finite element analysis. The maximum k_t for these holes is approximately equal to the maximum k_t for main journal oil holes 2 through 11. Thus, crack initiation and propagation studies will not distinguish between the geometries of main journals 2 through 11 and that of main journal 12.

5.2 Crack Initiation

The existence of many different cracks on the San Onofre crankshafts aligned on planes with maximum principal stresses under torsional loading indicates that the cracks initiated rather than grew out of material discontinuities. The stress cycles under the most severe fast start and under coastdown are shown in Figure 5-2 and compared with the 10^7 cycle endurance limit [5-2] for the material on a Goodman diagram. Many stress cycles during each start-stop are well beyond the endurance limit. This shows that initiation will occur, but does not indicate how many starts are required.

Low cycle fatigue data for materials similar to the San Onofre crankshaft material are shown in Figure 5-3. Based on the [5-2] curve for normalized and tempered material which has a k_t of 1 and multiplying nominal torsional stresses by a k_t of 4, a conservative estimate of initiation life may be obtained using linear cumulative damage. A cumulative damage of 0.8 was calculated to be caused by 95 start-stops on main journal number 10.

There is much scatter in low cycle fatigue data so that, while initiation is likely to occur in the more highly stressed journals, the number of start-stops required to initiate is not known with a high degree of certainty.

5.3 Crack Propagation

In Section 5.2 it was shown that crack initiation could occur under certain startup and coastdown conditions. This section uses the BIGIF fracture mechanics code [5-1] to calculate crack propagation rates. Crack propagation rates will be determined as a function of the number of starts and stops rather than calendar time.

5.3.1 Crack Growth Models

Two geometric models were used in the prediction of crack growth rates. The geometry for the first model is shown in Figure 5.4. This geometric model includes the journal surface, oil hole surface and blend radius. A three degree of freedom (3 DOF) elliptical-shaped crack can be introduced at any point on the surface. The three crack shape parameters, a_1, a_2 and a_3 have freedom to grow independently. A bivariate stress field can be used to describe the stresses in the journal near the oil hole. A 10-mil deep crack was introduced at the junction of the blend radius and oil hole surface. This model was investigated because this is the type of crack growth that might be expected in the stress field of Figure 5-1.

The second model is shown in Figure 5.5. This model just includes the oil hole surface. A one degree of freedom (1 DOF) edge crack is modelled. The crack size, a, has freedom to grow under a univariate stress field. The stress field chosen consists of k_t of 4 on the oil hole surface, which decays to unity with increasing distance from the oil hole surface in the same manner as the bivariate stress field. A 5-mil deep crack was introduced at the oil hole surface. This model is more conservative than the first model since it will predict higher propagation rates. It was used because the appearance of long cracks in the San Onofre oil holes suggested that a univariate stress field would represent a realistic model.

5.3.2 Crack Growth Analysis

Four types of loading histories were considered and are summarized in Table 5.1. Each load history consists of a block which is repeated. The block contains a start, some steady-state operation and a coastdown. In the

best case, the fast start which produces the least vibration (cylinder 3 RB starts at BDC of its exhaust stroke) is used. In the worst case, the fast start which produces the most vibration (cylinder 10 RB starts at BDC of its exhaust stroke) is used. In the average case all ten fast starts analyzed in Section 4 are averaged. In the slow start case, the startup is assumed to consist of the same stress cycles as a coastdown.

All four load histories assume two hours of full load (6000 kW) operation between startup and coastdown. The number of hours chosen is not important for this analysis, since it will be shown that, once a crack is large enough for steady-state stresses to contribute to its growth, the crack propagates at a rapid rate. Thus, it is assumed that operation is safe when cracks are smaller than those which would propagate under steady-state stresses.

Figures 5.6 and 5.7 show the crack size as a function of number of load blocks (starts and stops) for main journal number 10. The figures also show the crack size when steady-state stresses contribute to growth. For the 3 DOF crack model, this occurs at a depth of 50 mils, while for the 1 DOF model steady-state stresses contribute to crack growth at a depth of 18 mils. The figures also show that the best case fast start is less damaging than a slow start. Crack size versus load history produced by the 1 DOF model with average loading correlates well with field experience at San Onofre.

The effect of excluding the effect of steady-state stresses on crack growth is shown in Figure 5.8.

Most of the remaining analyses will be performed on main journal 10 with worst case loading. This condition shows the shortest life of all models and load cases considered in Figures 5.6 and 5.7.

The crack growth for main journals 6 through 12 is shown in Figure 5.9 for the worst case start using the 1 DOF model. It is seen that the fastest growth occurs in main journals 9, 10, 11, and 12. The field experience at San Onofre indicates that main journals 9 and 10 have the largest cracks, although main journal 11 on DG2 and main journal 12 on DG1 and DG2 have not been inspected.

5.3.3 Effect of Range of Stress Intensity Factor Threshold on Crack Growth

The effect of reducing the value of $\Delta K_{threshold}$ from 5.5 ksi$\sqrt{in}$ to 4.5 ksi$\sqrt{in}$ is shown in Figure 5.10. The difference is relatively small on crack growth rates except that steady-state stresses would contribute earlier to growth for the smaller threshold value.

5.3.4 Effect of Residual Stresses and Martensite on Growth

The aspect ratio (surface length of crack divided by crack depth) of the growing crack using the 3 DOF crack model generally remained constant at about 2. Field experience indicates that long shallow cracks exist. The effect of the possible existence of residual stresses and/or martensite on crack shape and growth rate was explored.

Although the forgings for TDI crankshafts are normalized and annealed, there is still a possibility that tensile residual stresses can exist on the outer surfaces. Such stresses could arise due to the volume change accompanying the transformation from austenite to ferrite and pearlite upon cooling from the normalizing temperature. The outside would transform first, and then at a lower temperature be put into tension by the expansion of the transforming core.

The magnitude of the residual stress developed would be bounded by the yield stress of the steel at a temperature just below the transformation range. A literature review of the elevated temperature properties of medium-carbon steel [5-4 to 5-7] showed that the yield strength at that temperature is about 10 ksi. Therefore, it is possible that biaxial tensile residual stresses of less than 10 ksi are present in a finished crankshaft. They would be highest at the surface, and would then become compressive within a few inches of the center. This tensile stress would be concentrated when the oil hole was drilled, resulting in tensile residual stresses of up to 20 ksi. Polishing of the oil holes could produce higher residual stresses over a very thin layer near the surface of the oil hole.

A bounding model with yield level residual stresses to a depth of 25 mils was analyzed. The results of this analysis for 3 DOF and 1 DOF crack

models are shown in Figures 5.11 and 5.12, respectively. The results indicate faster growth; however the aspect ratio did not differ appreciably from the value of 2 obtained in previous analyses.

If grinding took place in the oil hole at elevated temperatures, it may be possible that a thin layer (perhaps 5 mils deep) of martensite would form. This material has poorer crack growth properties than the ferrite and pearlite. Figures 5.11 and 5.12 show the effect on crack growth rate when this material is used in the crack growth law. It was not possible to model the finite size of the martensite layer in the BIGIF computer code. However, by comparing the crack growth laws for martensite with the underlying material, one can conclude that aspect ratios of up to 6 : 1 could be explained if martensite was found to exist.

5.4 Summary and Recommendations

- Stress cycles during startup and coastdown are above the endurance limit.
- It is safe to operate the engine with cracks up to 18 mils deep based on the 1 DOF crack model.
- If the oil hole regions are inspected so that 10 mil deep cracks can be detected, then the number of start-stops to propagate a crack from 10 mils to 18 mils deep represents the effective life of the crankshaft.
- Based on a conservative analysis, inspections should be performed at outages so that the inspection interval is approximately 50 start-stops.
- When cracks are detected they should be removed.
- Initially, main journals 4 through 12 should be inspected, although during future inspections a smaller number could be inspected as long as no cracks are found.

Section 5 References

5-1 "BIGIF - Fracture Mechanics Code for Structures," Manuals 1-3, Failure Analysis Associates (April 1981).

5-2 "Structural Alloys Handbook," 1984 Edition, Battelle's Columbus Laboratories, Volume 1.

5-3 "SAE Handbook," Society of Automotive Engineers, 1976, Volume 1.

5-4 Early, J. G., "Elevated-Temperature Mechanical Behavior of a Carbon-Manganese Pressure Vessel Steel," Journal of Engineering Materials and Technology, October 1977, pp. 359-365.

5-5 Miller, R. F., "The Strength of Carbon Steels for Elevated-Temperature Applications," American Society for Testing and Materials Proceedings, Vol. 54 (1954) pp. 964-986.

5-6 Smith, G. V., Elevated Temperature Static Properties of Wrought Carbon Steels, American Society for Testing and Materials STP 503 (1972).

5-7 White, A. E., Clark, C. L. and Wilson, R. L., "The Fracture of Carbon Steels at Elevated Temperatures," Transactions American Society for Metals, Vol. 25 (1937) pp. 863-888.

Table 5-1

Description of Load Cases

Load Case	Load Description
Best Case	3 RB fast start 2 hours full load Coastdown
Worst Case	10 RB fast start 2 hours full load Coastdown
Average	Average of all fast starts 2 hours full load Coastdown
Slow Start	Slow Start 2 hours full load Coastdown

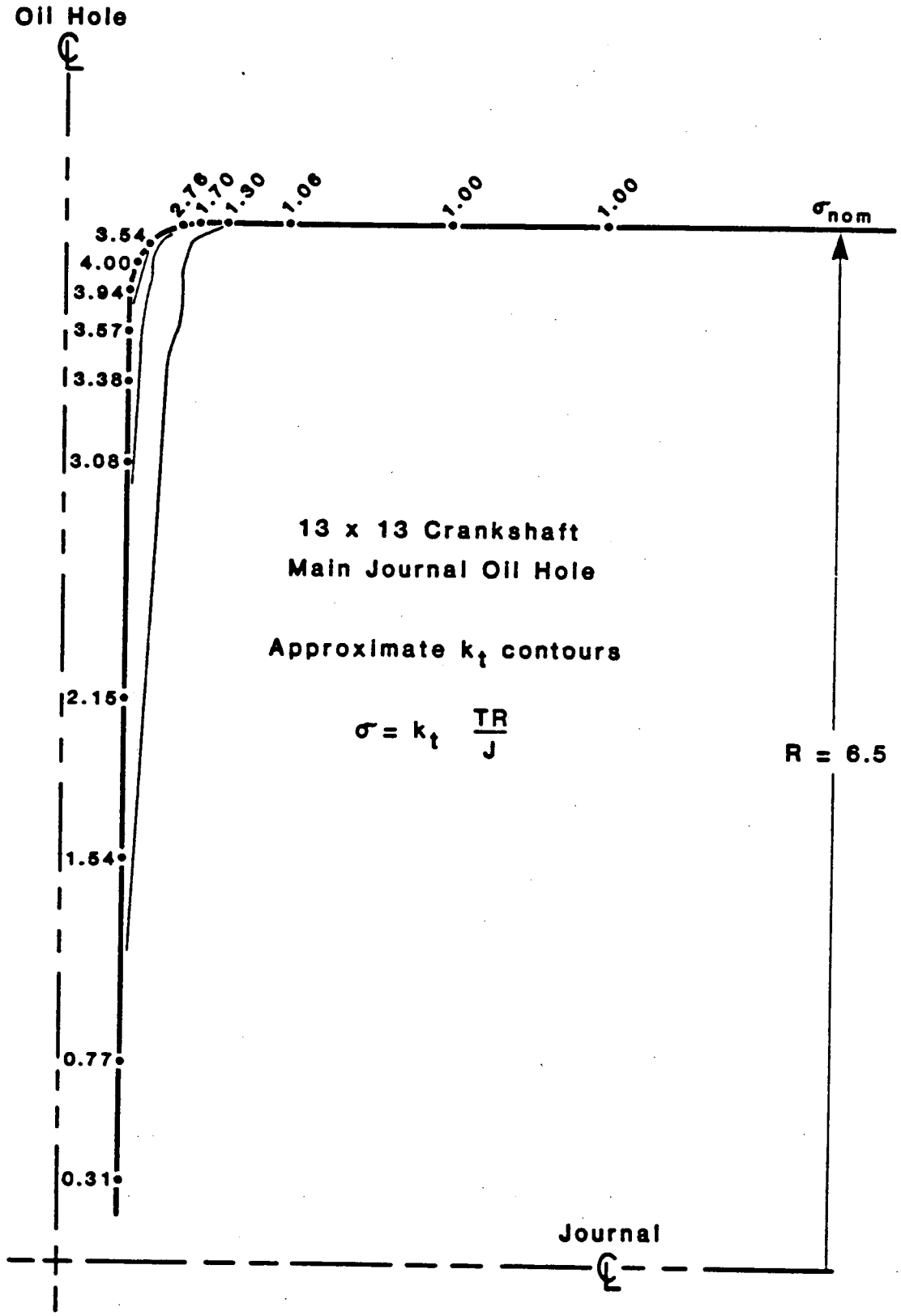

Figure 5-1. Distribution of stress concentration factor around an oil hole.

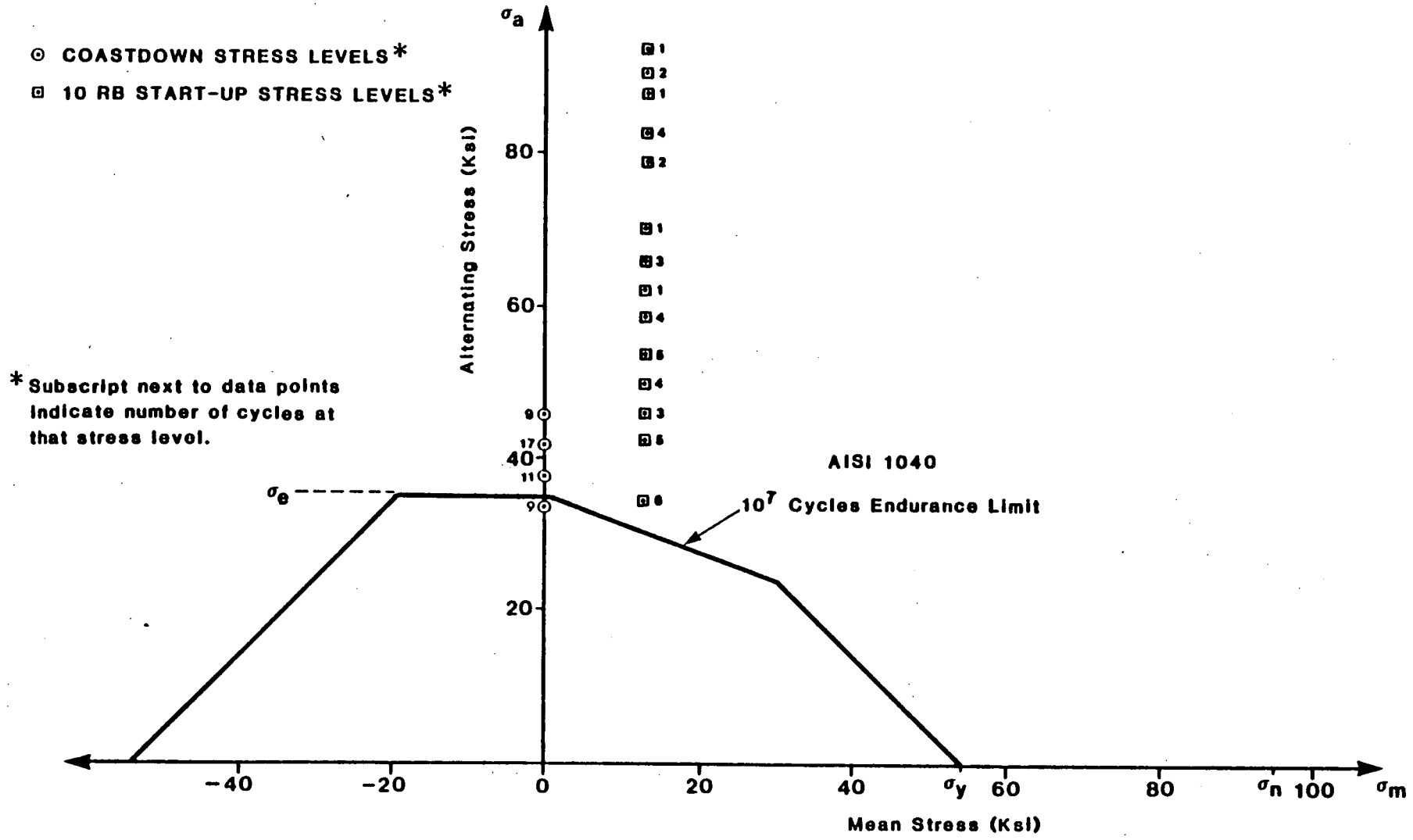

FaAA-84-12-14

Figure 5-2. Comparison of endurance limit with stress cycles during startup and coastdown.

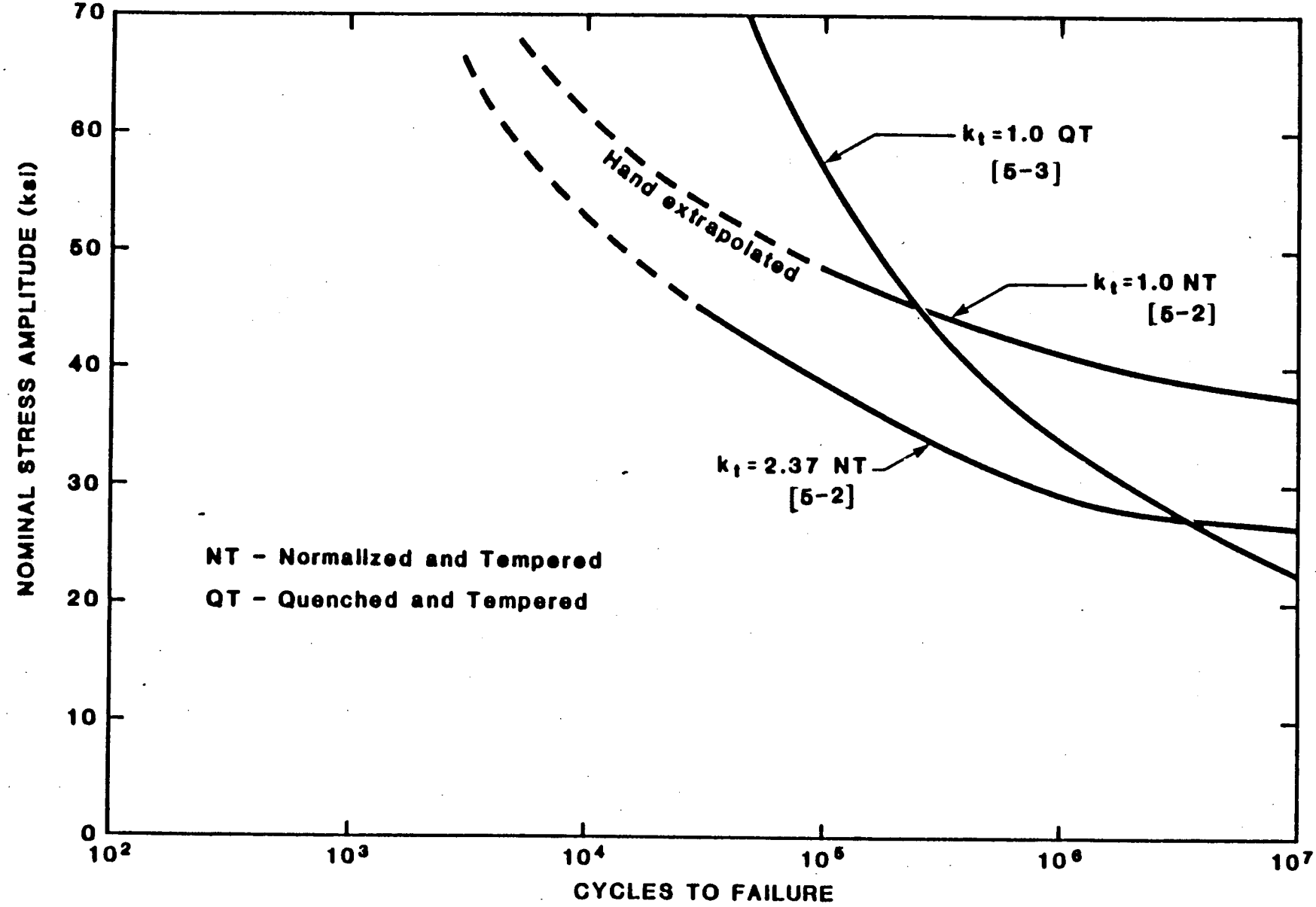

FAA-84-12-14

Figure 5-3. Fatigue life data for 1040 steel.

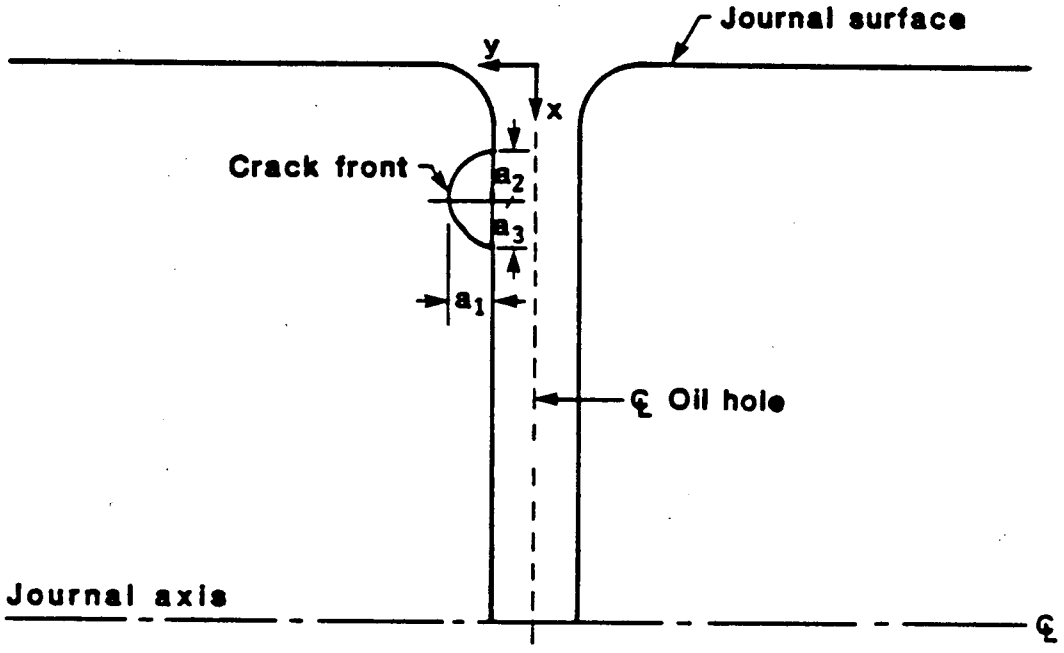

Figure 5-4. Three degree of freedom crack model.

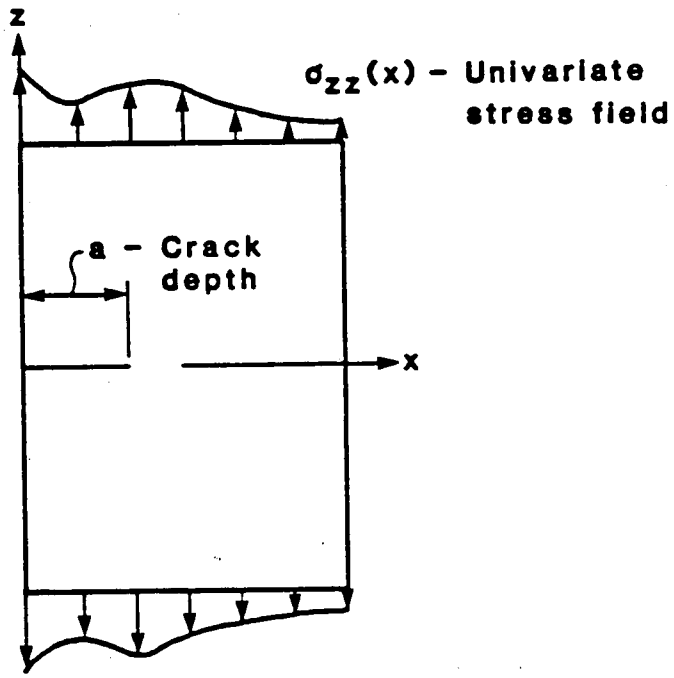

Figure 5-5. Single degree of freedom crack model.

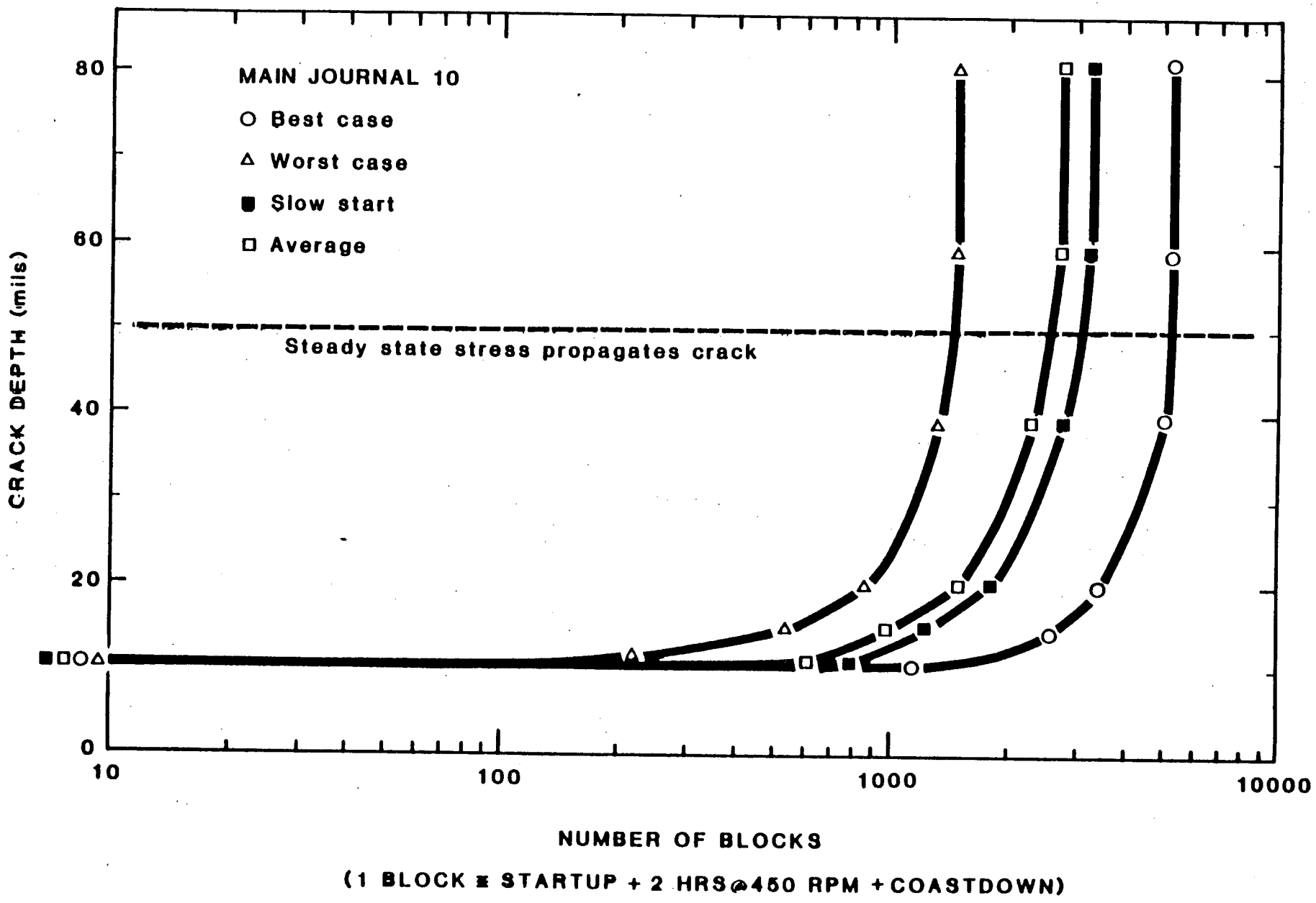

FEAA-84-12-14

Figure 5-6. Effect of load history on crack growth using 3 DOF crack.

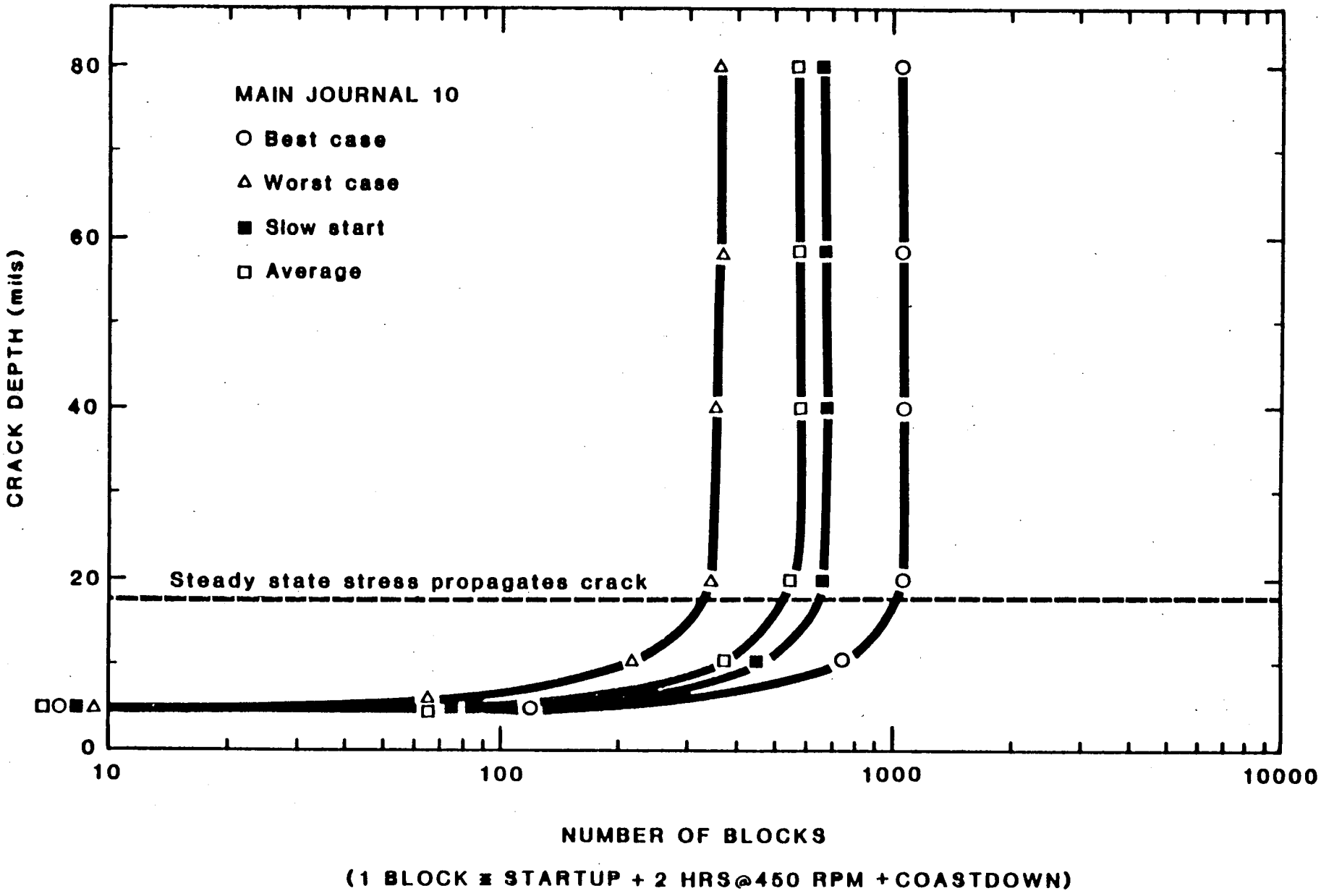

FaAA-84-12-14

Figure 5-7. Effect of load history on crack growth using 1 DOF crack.

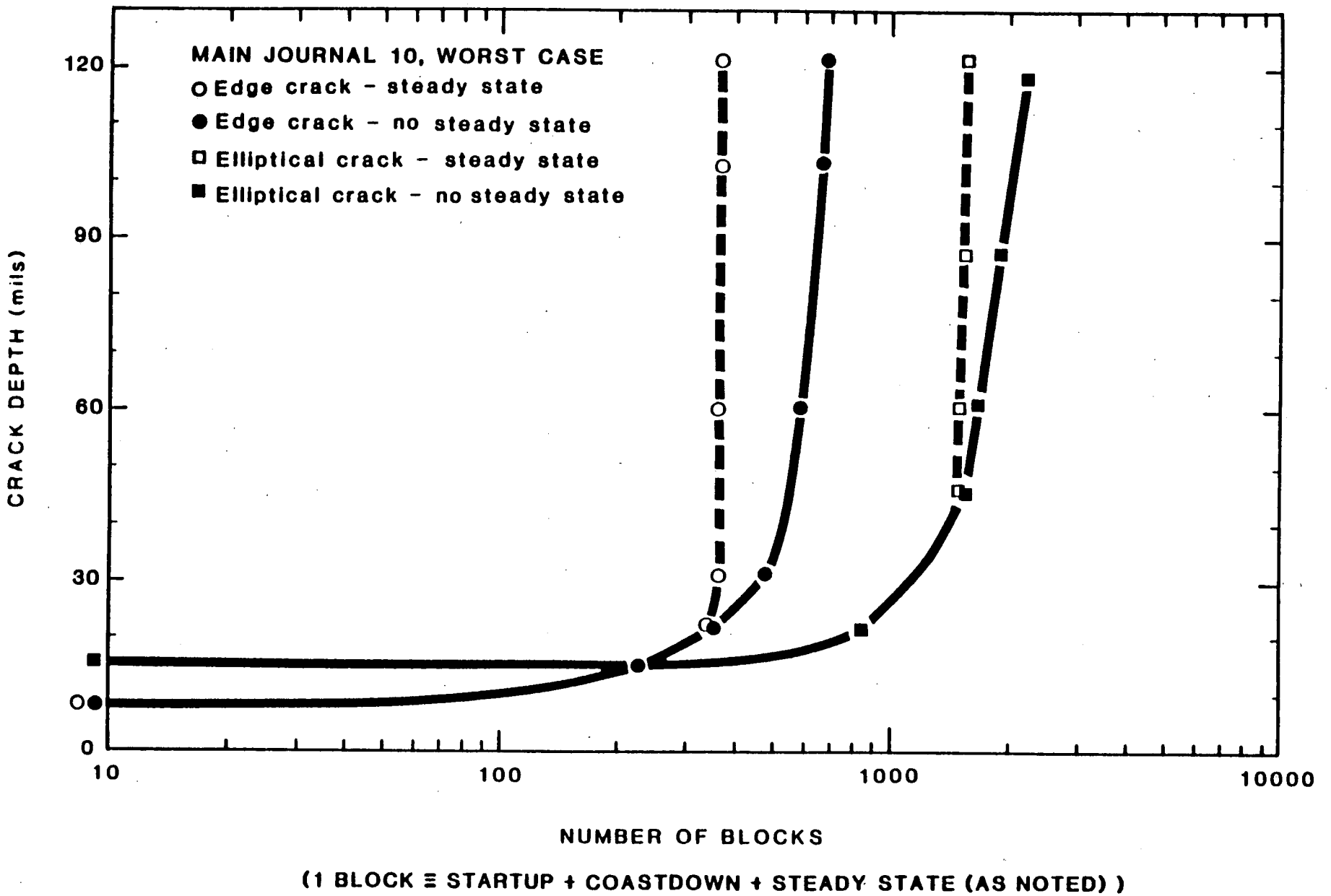

FaAA-84-12-14

Figure 5-8. Effect of steady-state stresses on crack growth.

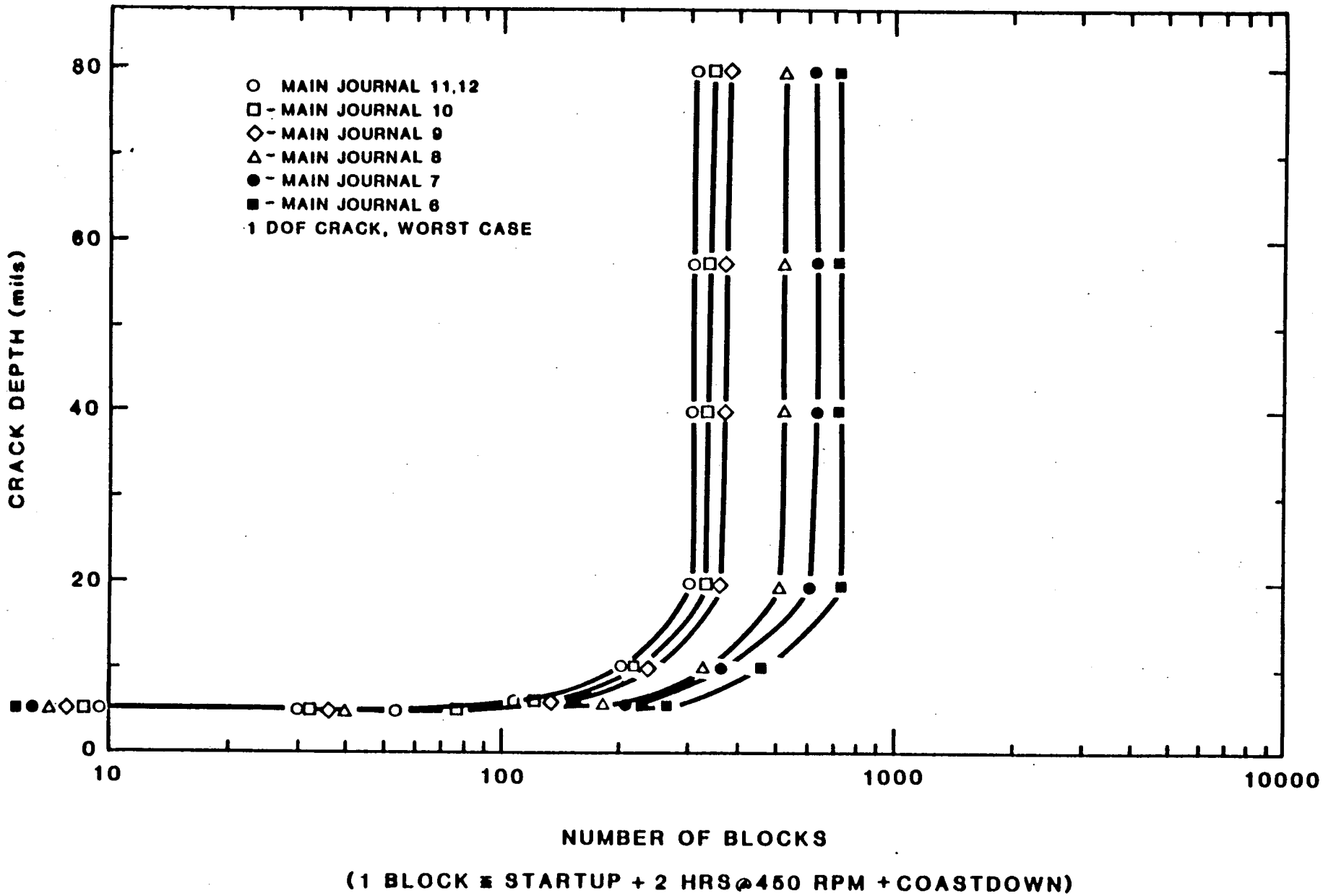

F&A-84-12-14

Figure 5-9. Effect of location of oil hole on crack growth rate.

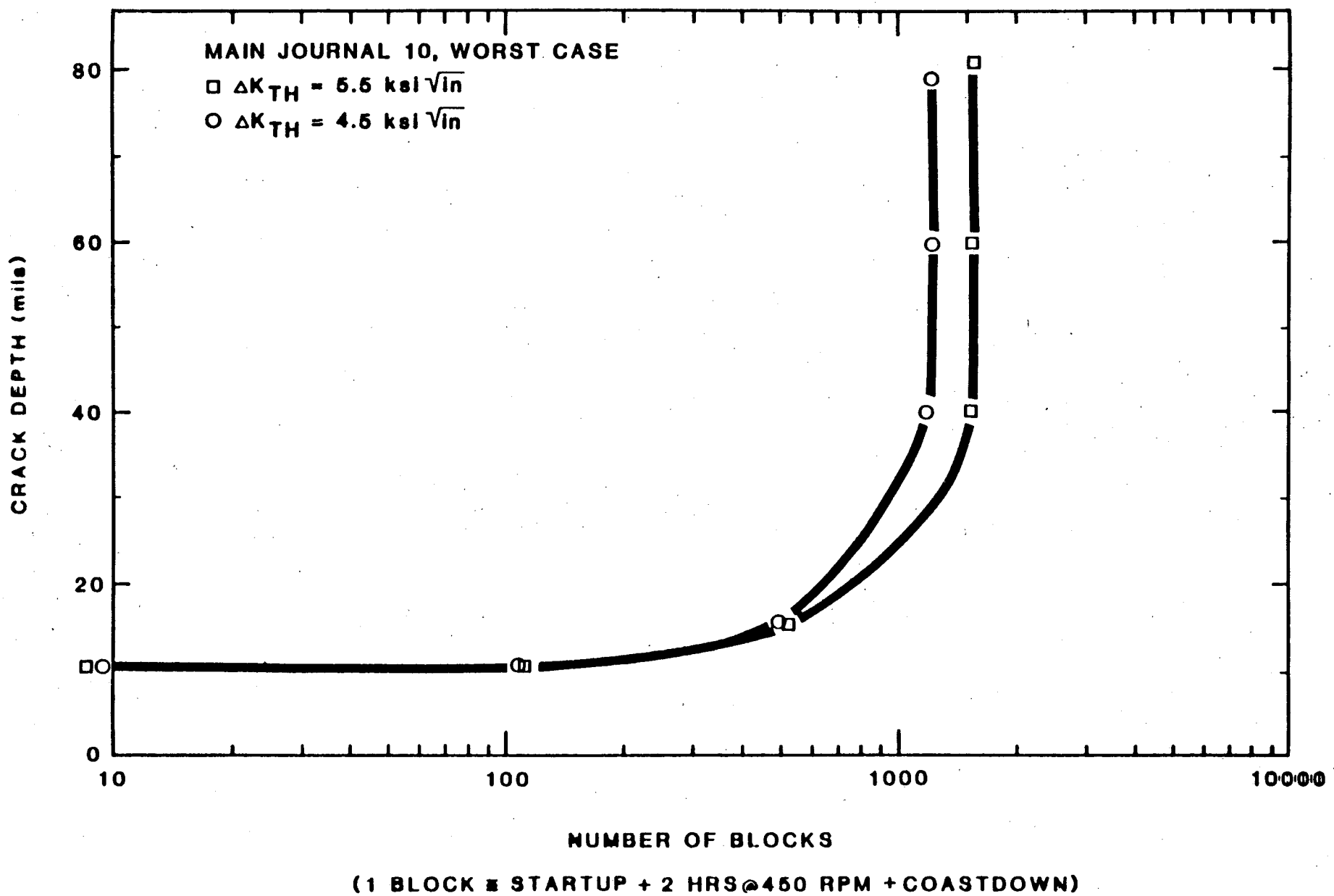

FaAA-84-12-14

Figure 5-10. Effect of ΔK threshold on crack growth using 3 DOF crack.

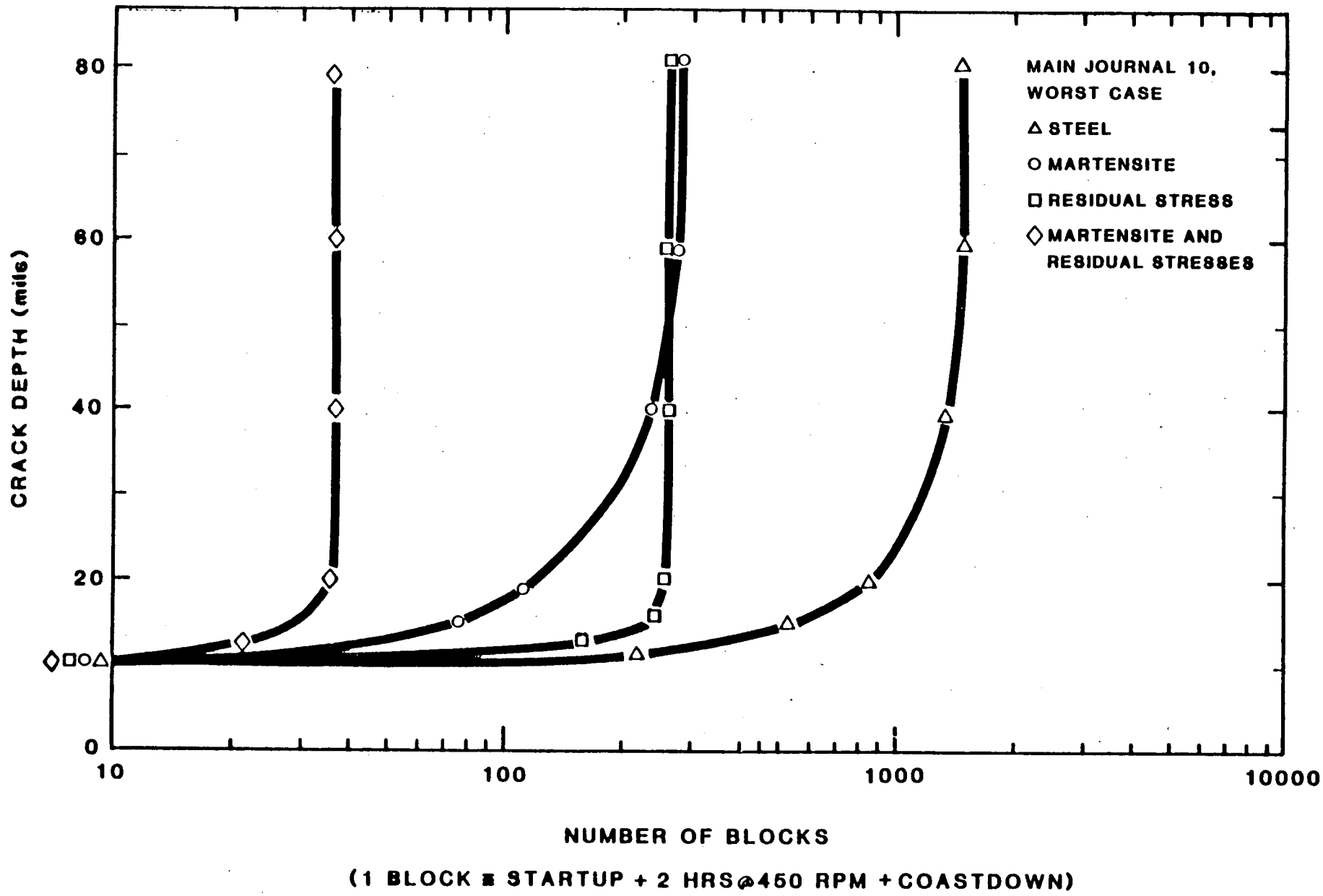

FAA-84-12-14

Figure 5-11. Effect of residual stress and martensite on crack growth using 3 DOF crack.

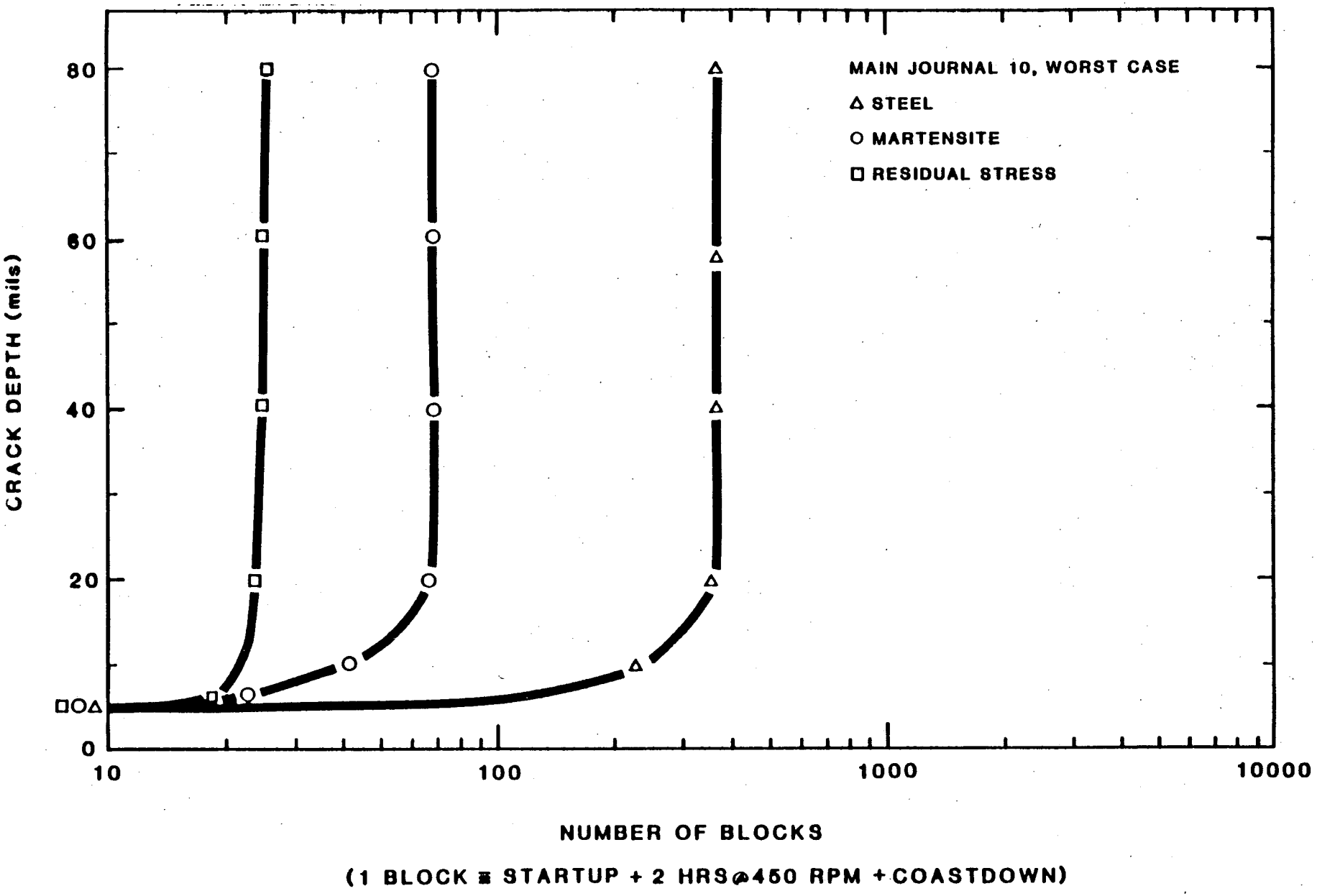

FSAA-84-12-14

Figure 5-12. Effect of residual stress and martensite on crack growth using 1 DOF crack.

Appendix A

Torsiograph Test Data

APPENDIX

CALIBRATION

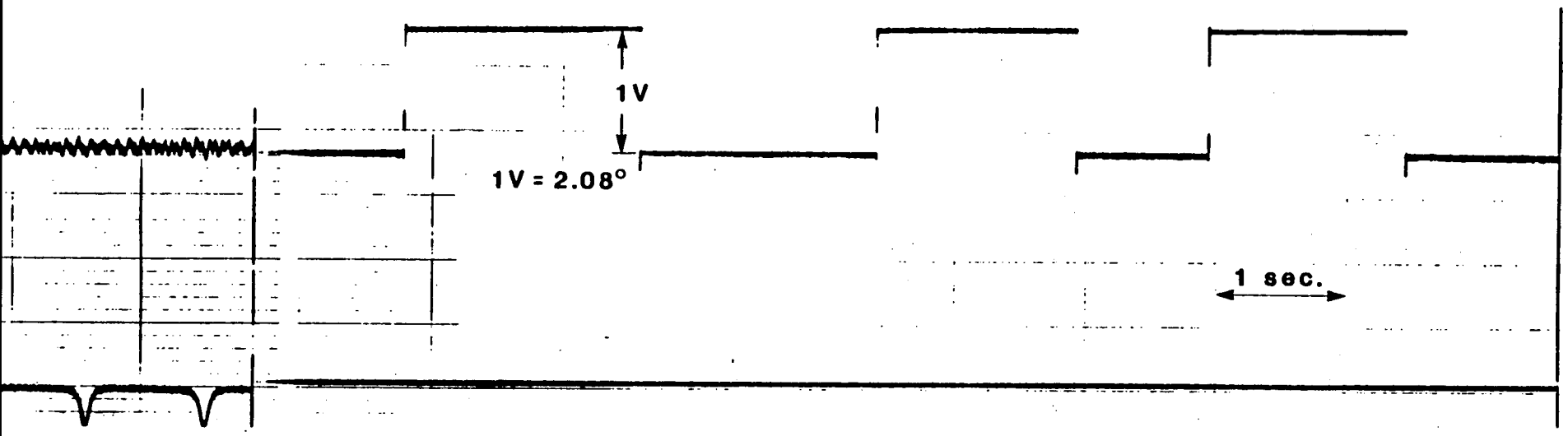

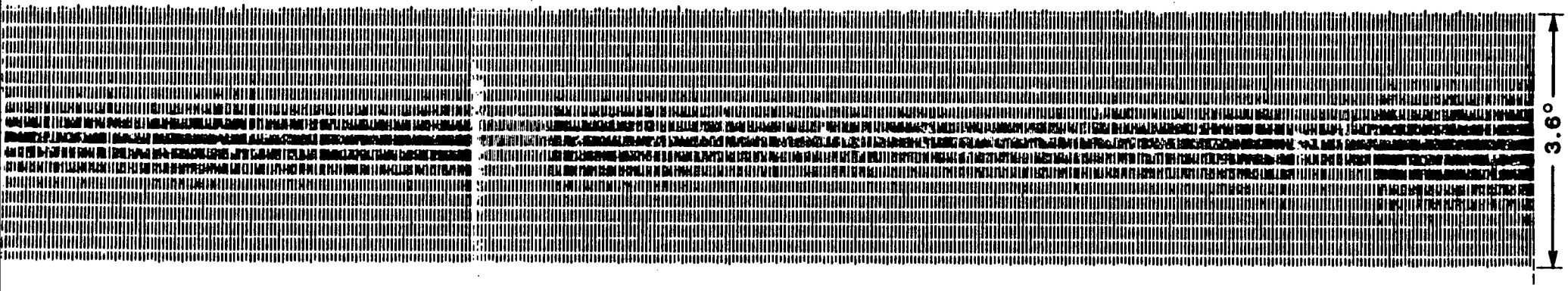

San Onofre torsiograph test 9/26/84

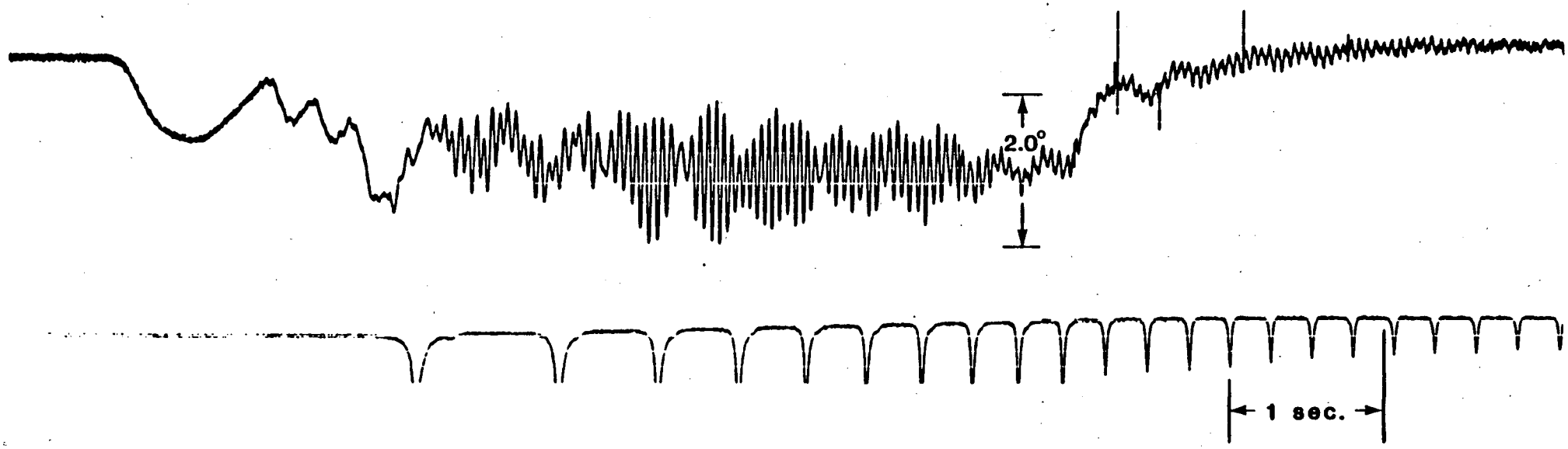

APPENDIX A

EVENT "A" - Fast Start

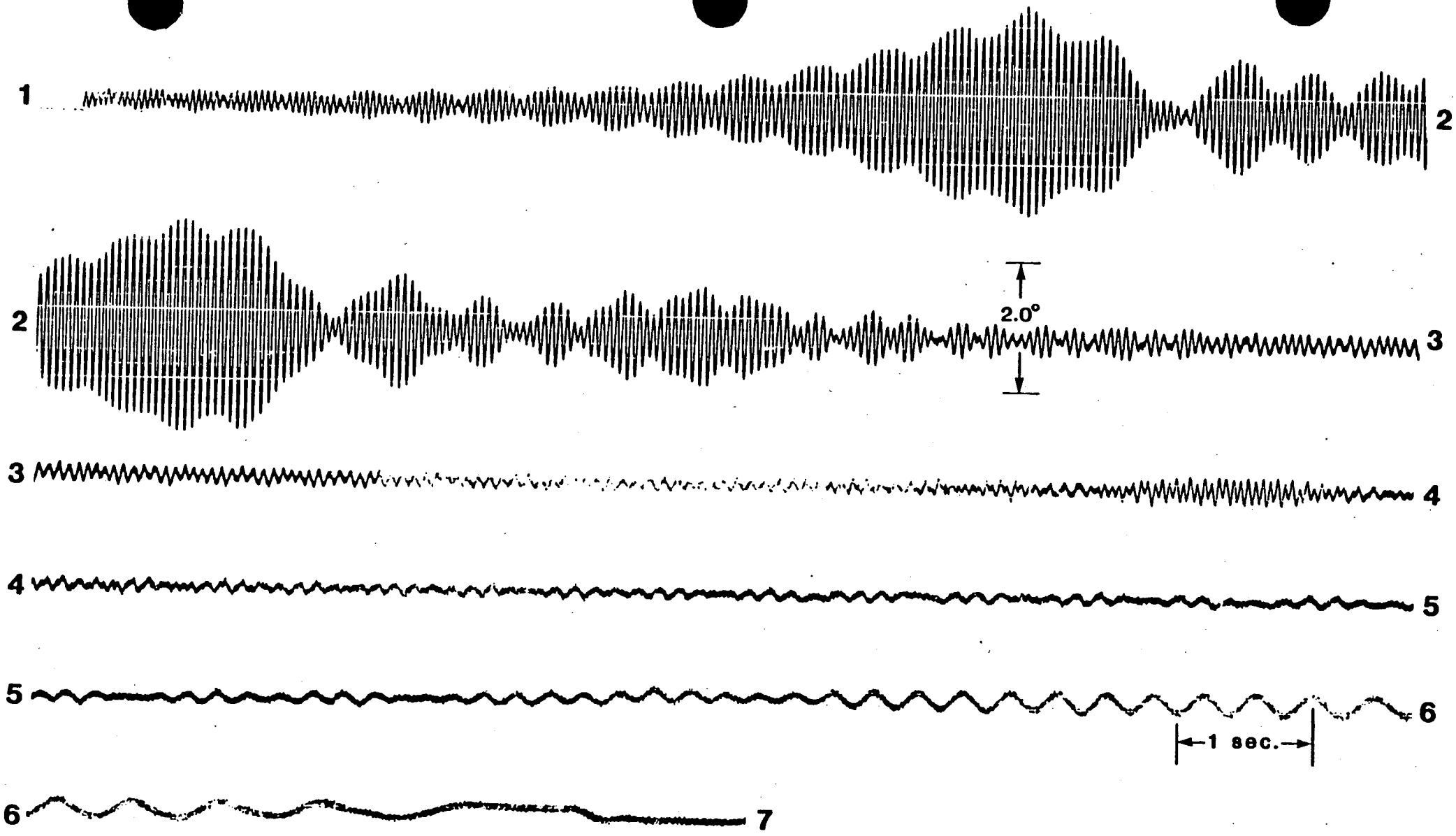

APPENDIX A

EVENT "B" - Coast Down

FAA-84-12-14

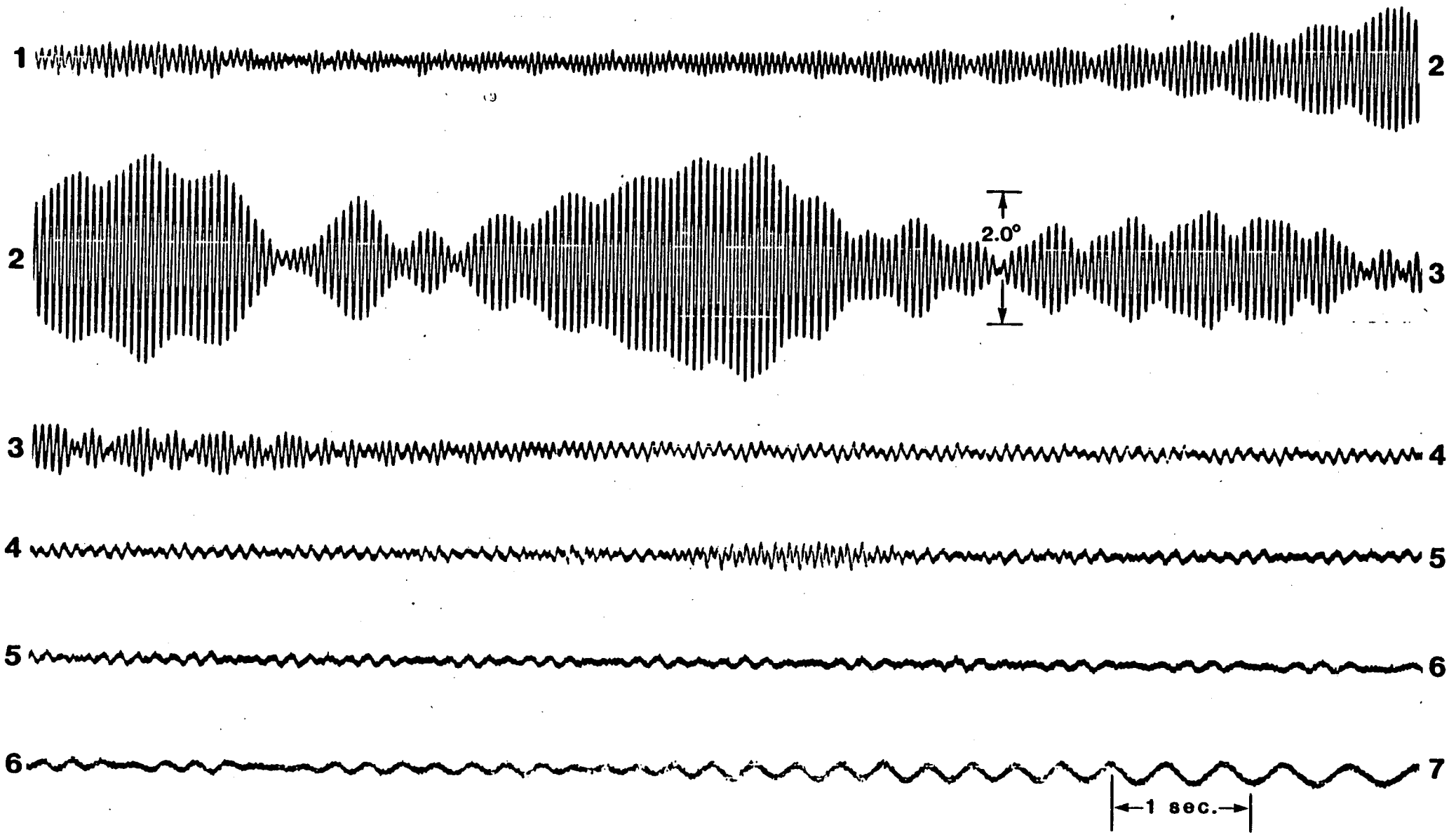

APPENDIX A

EVENT "C" - Coast Down

FaAA-84-12-14

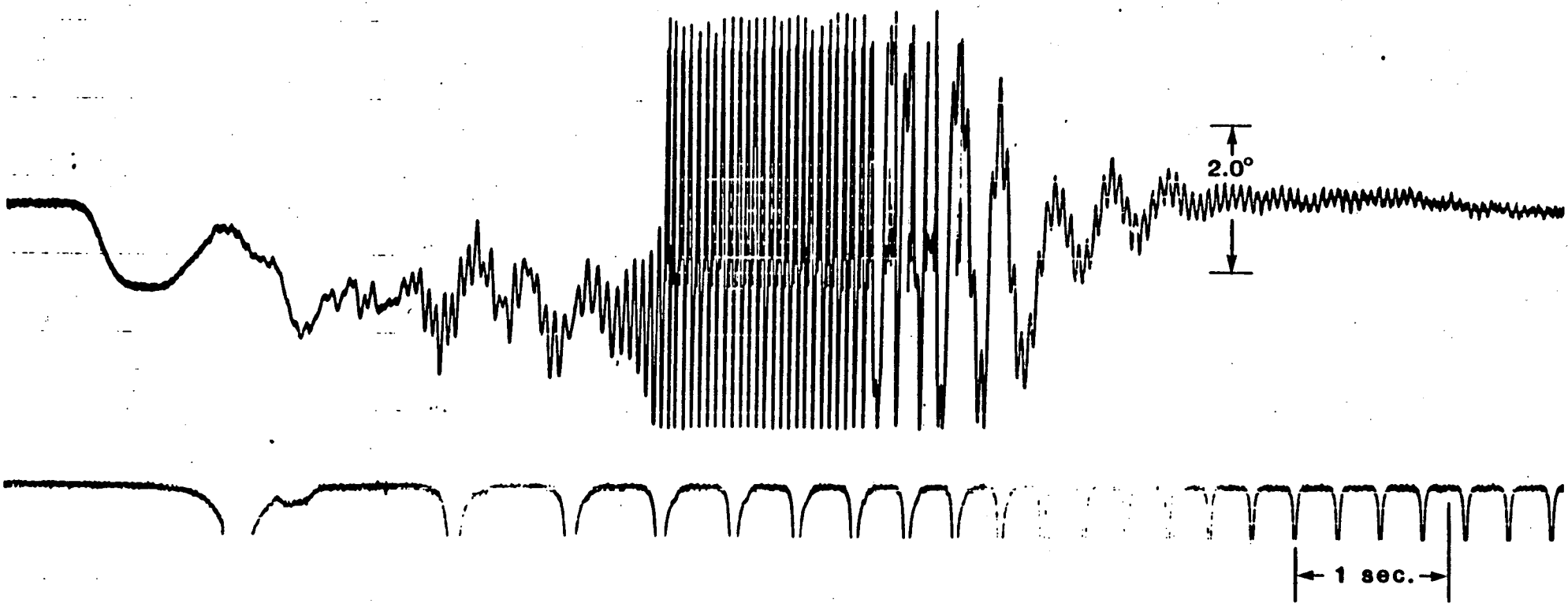

APPENDIX A

EVENT "D" - Fast Start (Cylinder 8 RB at BDC Exhaust)

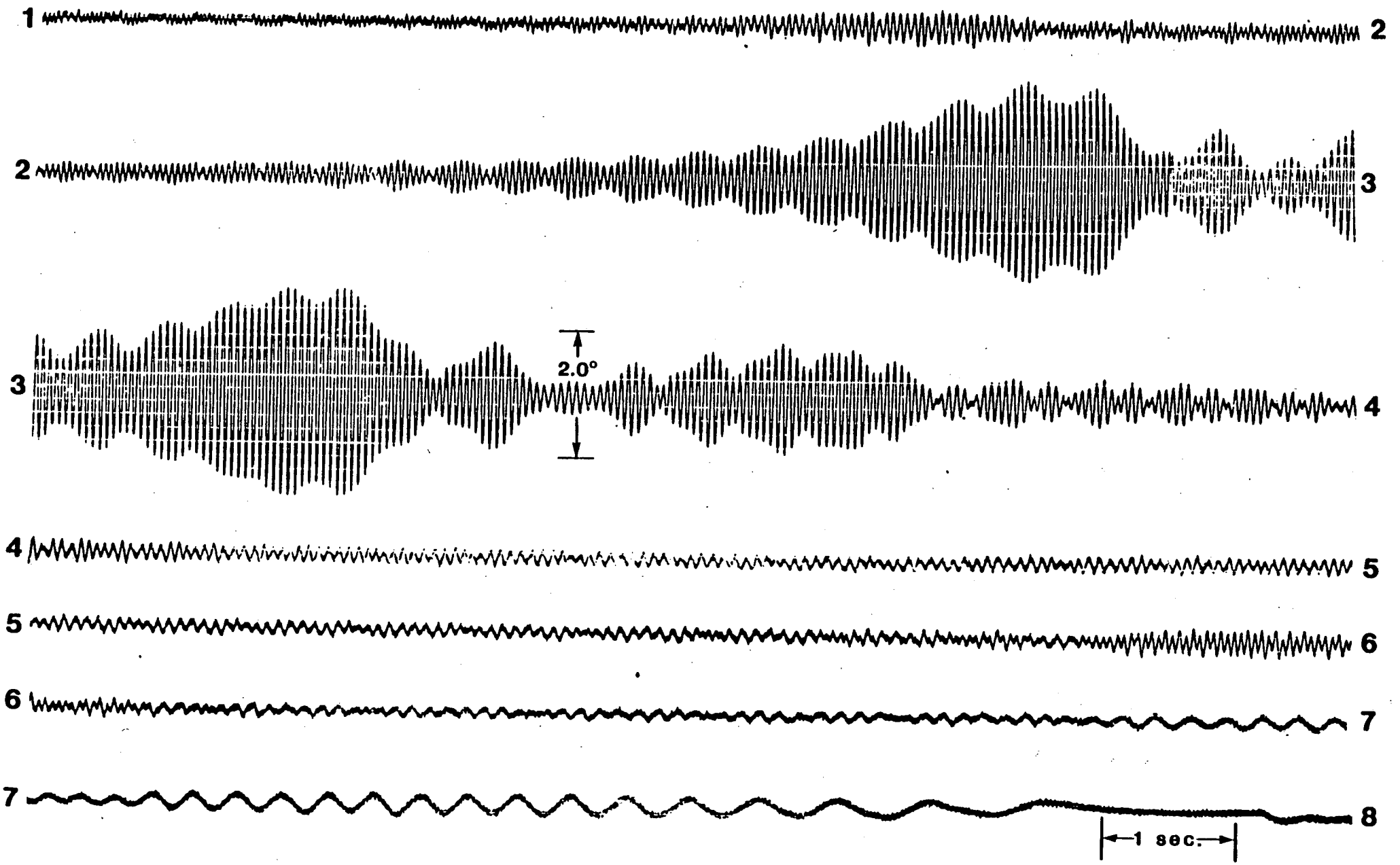

APPENDIX A

EVENT "E" - Coast Down

FaAA-84-12-14

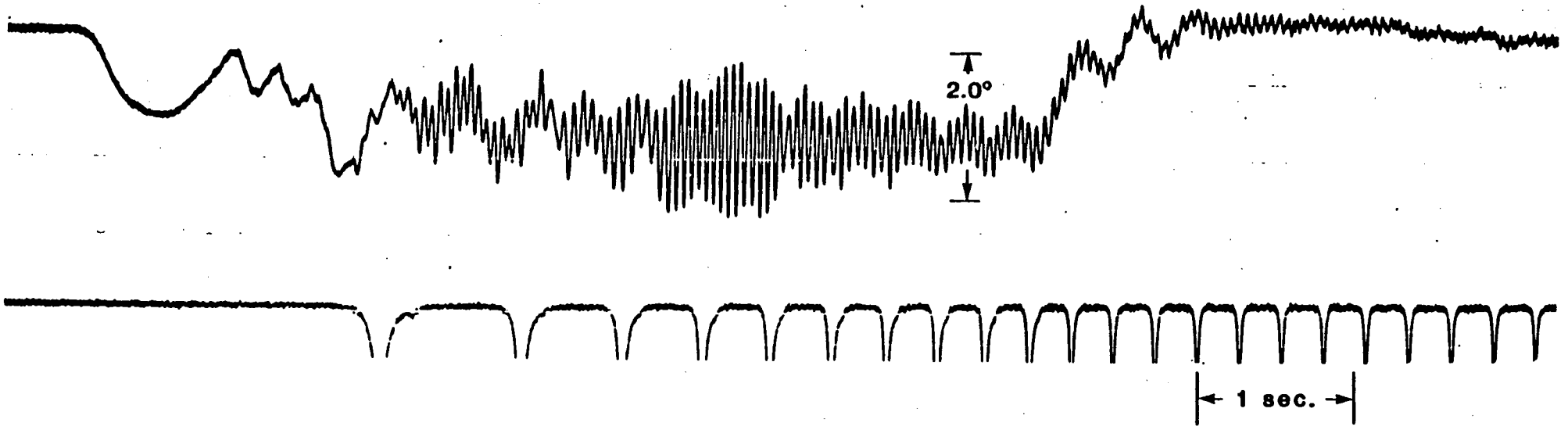

APPENDIX A

EVENT "F" - Fast Start (Cylinder 8 RB at BDC Compression)

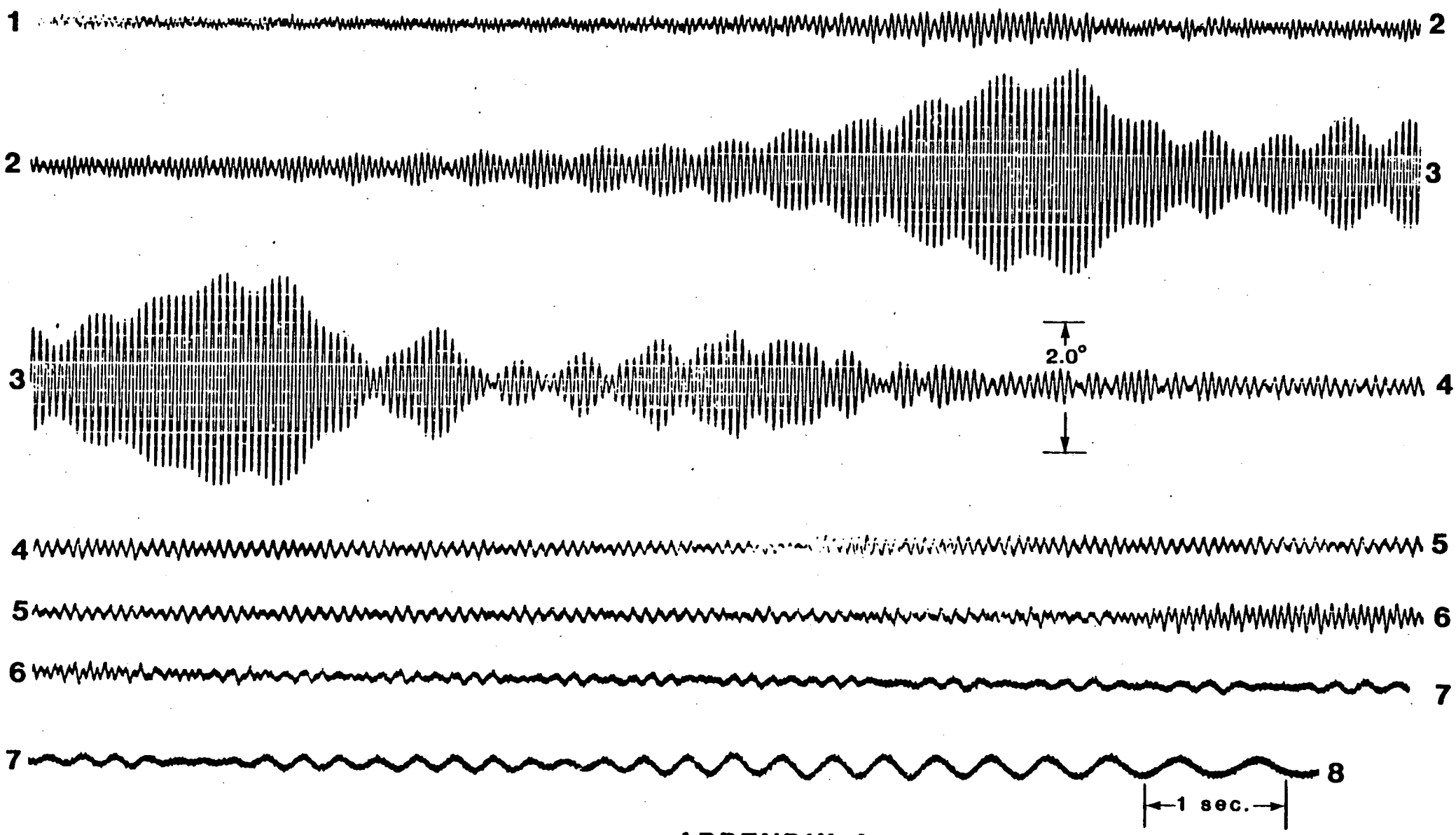

APPENDIX A

EVENT "G" - Coast Down

FaAA-84-12-14

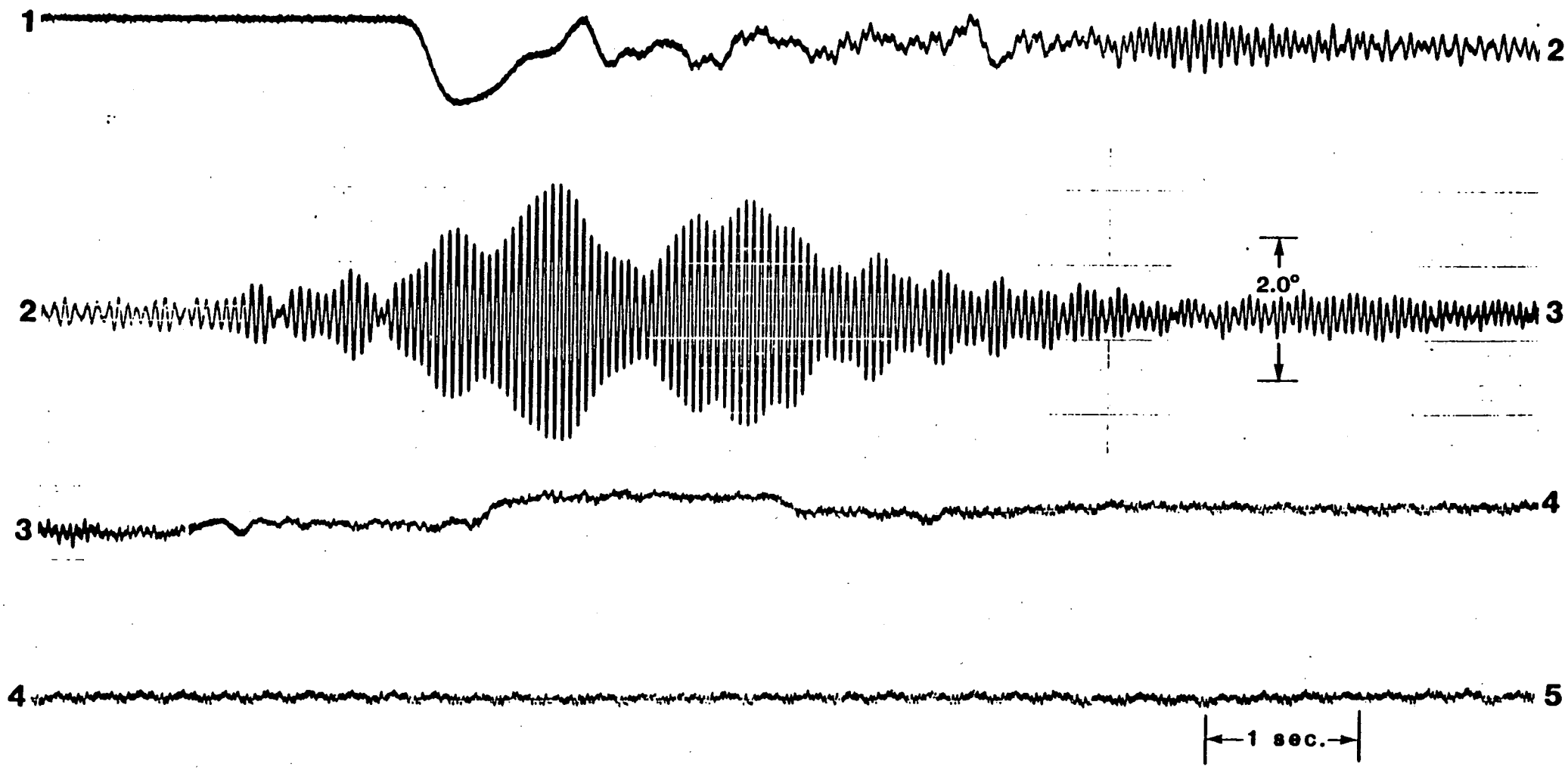

APPENDIX A

EVENT "H" - Slow Start

FaAA-84-12-14

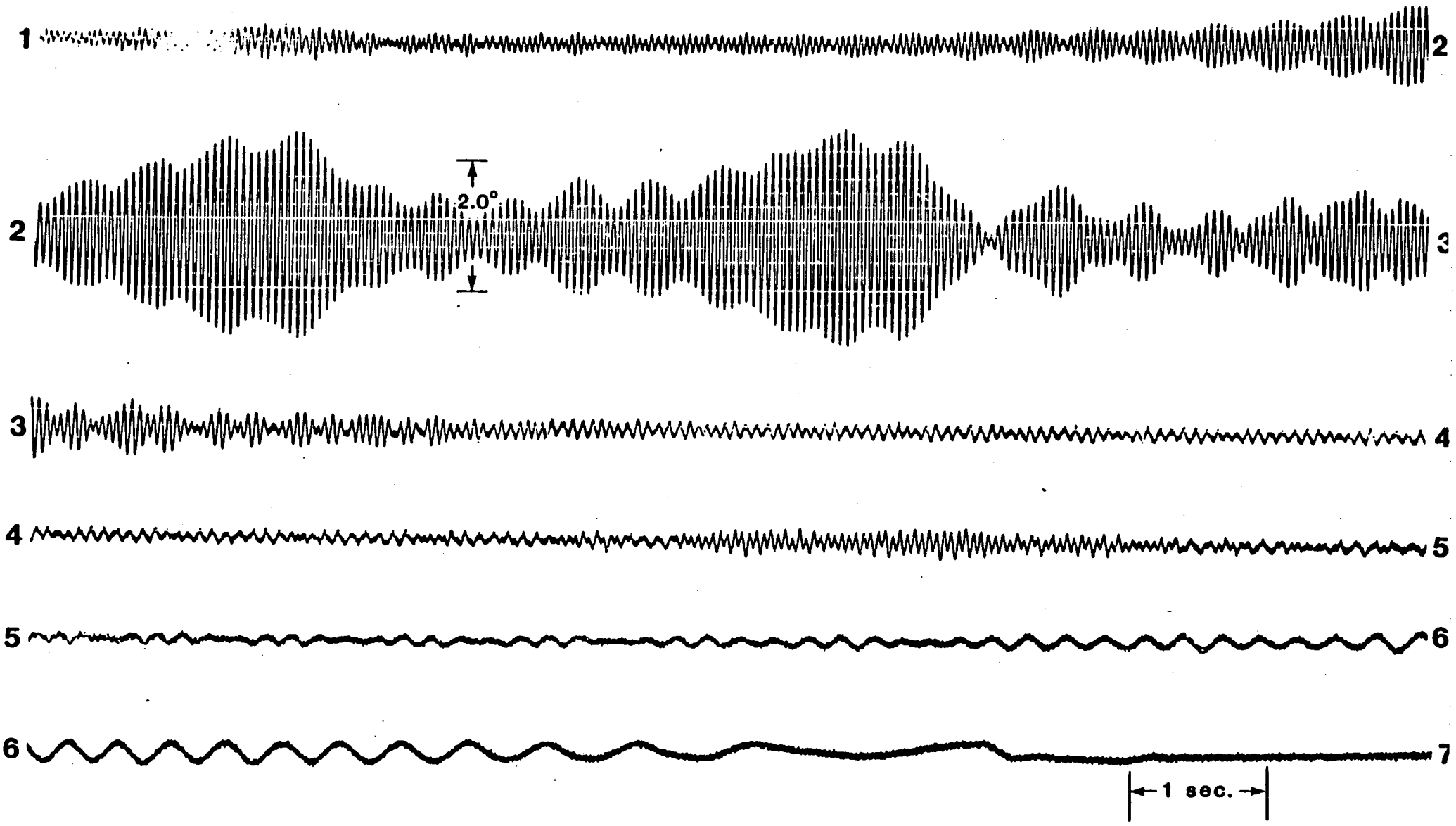

APPENDIX A

EVENT "I" - Coast Down

FaAA-84-12-14

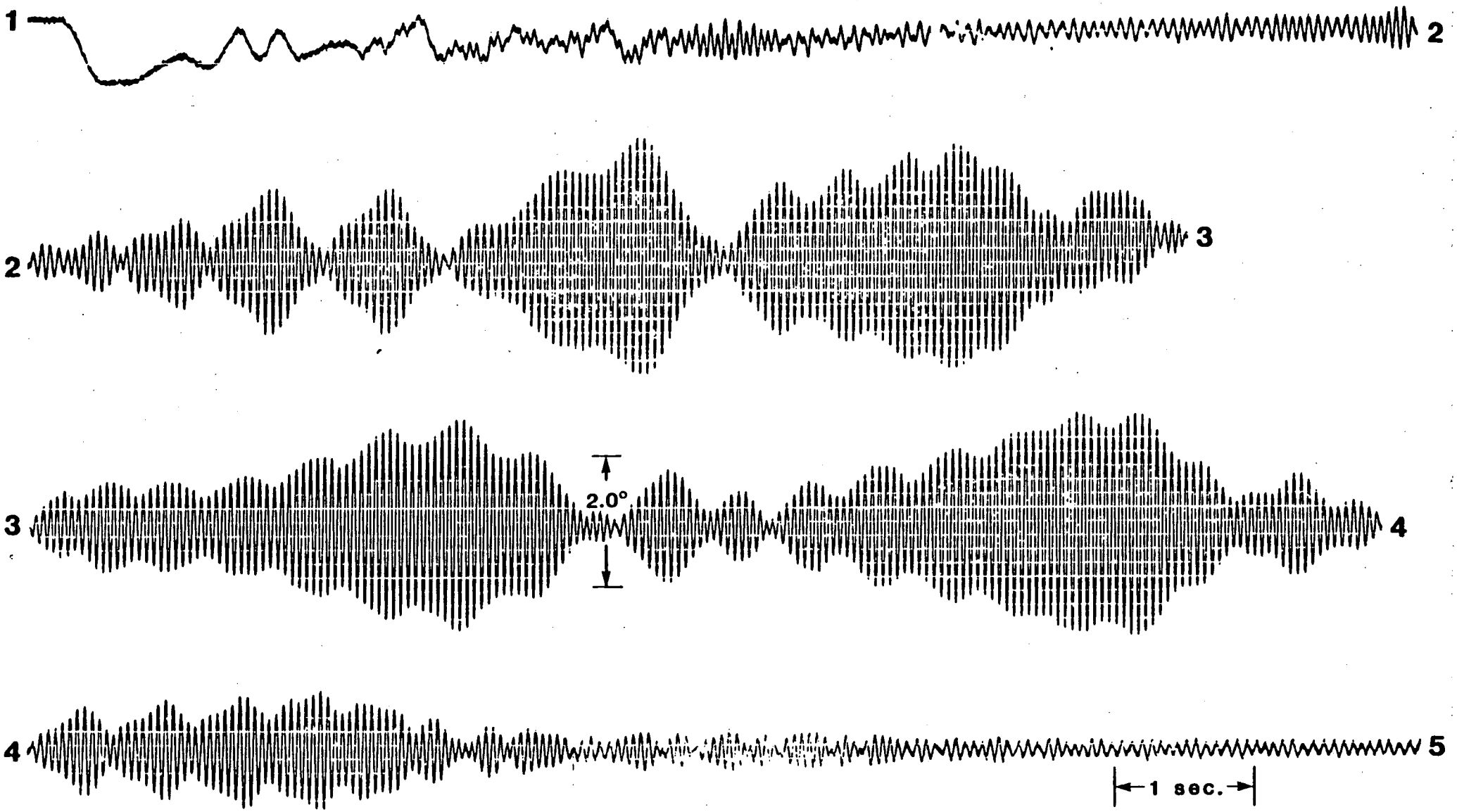

APPENDIX A

EVENT "J-K" - Slow Start and Coast Down

FaAA-84-12-14

Appendix B

Coastdown Analysis

Appendix C

3 RB Fast Start Analysis

Appendix D

10 RB Fast Start Analysis